Non-invasive near infrared spectroscopy: a tool for measuring cerebral oxygenation and metabolism in patients with traumatic brain injury

Martin M Tisdall, MBBS MA MRCS

Department of Brain Repair and Rehabilitation
The Institute of Neurology
University College London

Supervisors:
Dr Martin Smith
Dr Clare E Elwell

Thesis submitted for the degree of Doctor of Medicine (MD) at the University of London

ProQuest LLC
789 East Eisenhower Parkway
P.O. Box 1346
Ann Arbor, MI 48106-1346

Declaration

I hereby declare that the work presented in this thesis is my own.

Martin M Tisdall

Abstract

Traumatic brain injury (TBI) causes significant morbidity and mortality. Modern neurocritical care management utilises several monitoring techniques to identify or predict secondary insults but many of these techniques have significant limitations. The ideal cerebral monitor would be a non-invasive system able to provide realtime quantitative haemodynamic and metabolic information at multiple sites with high temporal and spatial resolution.

Near infrared spectroscopy (NIRS) fulfils many of these requirements and has great potential as a cerebral monitoring tool. In addition to measurements of oxy- and deoxy-haemoglobin concentration, NIRS can monitor changes in mitochondrial redox state by measuring changes in oxidised cytochrome c oxidase (oxCCO) concentration. This is an attractive monitoring target as it is intimately involved in adenosine triphosphate synthesis and cellular homeostasis, yet few studies exist which investigate oxCCO concentration changes in either the normal or injured adult human brain.

This thesis explores the use of NIRS, and in particular measurement of oxCCO concentration changes, for monitoring patients with TBI. Cerebral metabolism in both health and TBI is described and current monitoring tools and treatment strategies used in TBI are discussed. Studies investigating NIRS measurements in the brains of healthy volunteers during changes in arterial oxygen and carbon dioxide tension are described in order to determine the ability of NIRS to detect these physiological perturbations and to characterise the resulting metabolic changes. Spectroscopic data are analysed to investigate the methodology used to calculate oxCCO concentration changes. NIRS is used to monitor patients with TBI during normobaric hyperoxygenation and non-invasively measured NIRS variables are compared with those acquired using invasive cerebral monitoring devices. Correlations are shown between non-invasive measures of mitochondrial redox state and invasive measures of cellular redox state.

NIRS can monitor changes in cerebral physiology after TBI and has the potential to guide neuroprotective strategies on the neurocritical care unit.

Acknowledgements

Firstly I would like to thank Dr Martin Smith and Dr Clare Elwell for the inspirational supervision and guidance they have provided through the course of my studies. Both have given unstintingly of their time and expertise and have thus enabled me to acquire the requisite tools to complete this thesis. Over the last two years they have become friends as well as mentors and have provided scientific, emotional and financial support aplenty.

I am extremely grateful to Mr Neil Kitchen for his surgical mentorship and guidance. I would like to thank Dr Ilias Tachtsidis, for the invaluable help he gave me whilst performing the healthy volunteer studies described in this thesis and for his tutorship in analytical technique, and Dr Terence Leung for many stimulating discussions and insightful comments.

I owe a huge debt of gratitude to the doctors and nurses of The National hospital for Neurology and Neurosurgery. The consultant staff has been constantly supportive to me while the nursing staff of the Surgical Intensive Care Unit have proved invaluable during the recruitment and data collection phases of the clinical studies.

Special thanks go to my girlfriend, Lucie, for the love she has shown me over the last nine years and to my family for their constant and ongoing support.

I would like to thank The Wellcome Trust for providing me with the clinical research fellowship which allowed me to undertake this course of study.

Publications arising from this work

Investigation of in-vivo measurement of cerebral cytochrome c oxidase redox changes using near-infrared spectroscopy in patients with orthostatic hypotension.
Tachtsidis I, **Tisdall M**, Leung TS, Cooper CE, Delpy DT, Smith M, Elwell CE.
Physiol Meas 2007;28:199-211.

Cerebral microdialysis: research technique or clinical tool.
Tisdall MM, Smith M.
Br J Anaesth 2006;97:18-25.

Theoretical investigation of measuring cerebral blood flow in the adult human head using bolus Indocyanine Green injection and near-infrared spectroscopy.
Leung TS, Tachtsidis I, **Tisdall M**, Smith M, Delpy DT, Elwell CE.
Appl Opt 2007;46:1604-1614.

Near infrared spectroscopic quantification of changes in the concentration of oxidized cytochrome oxidase in the healthy human brain during hypoxemia.
Tisdall M, Tachtsidis I, Leung TS, Elwell CE, Smith M.
J Biomed Opt 2007;12:1-7.

Multimodal monitoring in traumatic brain injury: current status and future directions.
Tisdall MM, Smith M.
Br J Anaesth 2007;99:61-67.

Measurement of cerebral tissue oxygenation in young healthy volunteers during acetazolamide provocation: a transcranial Doppler and near-infrared spectroscopy investigation.
Tachtsidis I, **Tisdall M**, Delpy DT, Smith M, Elwell CE.
Adv Exp Med Biol 2008;614:389-396.

Changes in the attenuation of near infrared spectra during hypoxaemia by the healthy adult brain cannot be accounted for solely by changes in the concentrations of oxy- and deoxy-haemoglobin.
Tisdall M, Tachtsidis I, Leung TS, Elwell CE, Smith M.
Adv Exp Med Biol 2008;614:217-225.

Investigation of frontal cortex, motor cortex and systemic haemodynamic changes during anagram solving.
Tachtsidis I, Leung TS, **Tisdall M**, Davendra P, Smith M, Delpy DT, Elwell CE.
Adv Exp Med Biol 2008;614:21-28.

Cerebral tissue oxygen saturation calculated using low frequency haemoglobin oscillations measured by near infrared spectroscopy in adult ventilated patients.
Leung TS, **Tisdall M**, Tachtsidis I, Smith M, Delpy DT, Elwell CE.
Adv Exp Med Biol 2008;614:235-244.

Normobaric hyperoxia increases cerebral aerobic metabolism after traumatic brain injury.
Tisdall M, Tachtsidis I, Leung TS, Elwell CE, Smith M.
J Neurosurg 2008;109:424-432.

Conference Presentations

Investigation of the cerebral haemoglobin and cytochrome signals using four wavelength non-invasive near infrared spectroscopy on patients with orthostatic hypotension.

Tisdall M, Tachtsidis I, Bleasdale-Barr K, Mathias CJ, Delpy DT, Elwell CE, Smith M.

Poster, Brain05, Amsterdam, Netherlands 2005.

Non-invasive monitoring of carbon dioxide reactivity: spatially resolved near infrared spectroscopy and transcranial Doppler.

Tisdall M, Tachtsidis I, Elwell CE, Smith M.

Poster, EuroNeuro, Cambridge, UK 2005.

Measurement of cerebral tissue oxygenation and flow in young healthy volunteers during acetazolamide provocation: a transcranial Doppler and near infrared spectroscopy investigation.

Tachtsidis I, **Tisdall M**, Delpy DT, Smith M, Elwell CE.

Oral Presentation, ISOTT, Brisbane, Australia 2005.

Multimodal modelling simulation of hypercapnoeic challenge in acutely brain injured adult patient.

Tisdall M, Tachtsidis I, Banaji M, Delpy DT, Elwell CE, Smith M.

Poster, MIAS-IRC Plenary, Manchester, UK 2005.

Modelling of indocyanine green bolus with a finite element model of the adult human head and the Fick principle.

Leung TS, Tachtsidis I, **Tisdall M**, Smith M, Arridge S, Elwell CE, Delpy DT.

Oral Presentation, Optical Society of America, Florida, USA 2006.

Cerebral blood flow assessment with indocyanine green bolus transit detection by near infrared spectroscopy before and after acetazolamide challenge in humans.

Tachtsidis I, Leung TS, **Tisdall M**, Delpy DT, Smith M, Elwell CE.

Poster, Optical Society of America, Florida, USA 2006.

Changes in concentrations of oxidised cytochrome oxidase measured using both broadband and four wavelength near infrared spectroscopy reflect changes in oxygen delivery during hypoxaemia in healthy volunteers.
Tisdall M, Tachtsidis I, Elwell CE, Smith M.
Poster, Optical Society of America, Florida, USA 2006.

Near infrared spectroscopy can detect reduced cerebral oxygen utilisation during hypoxaemia in healthy volunteers.
Tisdall M, Tachtsidis I, Elwell CE, Kitchen N, Smith M.
Oral and Poster Presentation, SBNS, London, UK 2006.

Changes in cerebral tissue oxygen saturation measured by near infrared spectroscopy do not only reflect changes in oxygenation.
Tisdall M, Tachtsidis I, Leung T, Elwell CE, Smith M.
Poster, NASGBI, Brighton, UK 2006.

Measurement of cerebral blood flow with indocyanine green and NIRS, before and after the administration of acetazolamide
Leung TS, Tachtsidis I, **Tisdall M**, Smith M, Elwell CE, Delpy DT.
Oral presentation, 8th International Conference on Xenon CT and related Cerebral Blood Flow Techniques, Cambridge, UK, 2006.

Changes in the attenuation of near infrared spectra during hypoxaemia by the healthy adult brain cannot be accounted for solely by changes in the concentrations of oxy- and deoxy-haemoglobin.
Tisdall M, Tachtsidis I, Leung TS, Elwell CE, Smith M.
Oral and Poster presentation, ISOTT, Louisville, USA, 2006.

Investigation of frontal cortex, motor cortex and systemic haemodynamic changes during anagram solving.
Tachtsidis I, Leung TS, **Tisdall M**, Davendra P, Smith M, Delpy DT, Elwell CE.
Oral and Poster presentation, ISOTT, Louisville, USA, 2006.

Oxygen saturation calculated using oscillations in oxy- and deoxyhaemoglobin signals measured by near infrared spectroscopy in adult ventilated patients.
Leung TS, **Tisdall M**, Tachtsidis I, Smith M, Delpy DT, Elwell CE.
Oral and Poster presentation, ISOTT, Louisville, USA, 2006.

The application of a model of human brain circulation to head trauma patients: a computational systems biology approach.
Tachtsidis I, Banaji M, **Tisdall M**, Smith M, Baigent S, Elwell CE, Delpy DT.
Poster, Gordon Research Conference, Brain Energy Metabolism and Blood Flow, Oxford, UK, 2006.

Non-invasive measurement of changes in cerebral mitochondrial oxygenation in human volunteers.
Tisdall M, Tachtsidis I, Leung TS, Elwell CE, Smith M.
Poster presentation, SNACC, Chicago, USA, 2006.

Oxidation in cerebral cellular and mitochondrial compartments induced by normobaric hyperoxia after traumatic brain injury.
Tisdall M, Tachtsidis I, Leung TS, Kitchen N, Elwell CE, Smith M.
Oral presentation, CNS, San Diego, USA, 2007.

Prizes arising from this work

Oral presentation prize runner-up Neuroanaesthesia Society of Great Britain and Ireland 2005
Runner-up, Institute of Neurology Symposium 2006/2007
Duane Bruley Award International Society for Oxygen Transport to Tissue 2006
Synthes Award for Resident Research on Brain and Cranio-facial Injury Congress of Neurological Surgeons 2007

Contents

List of Figures

List of Tables

Abbreviations

ΔA[Gluc]	change in arterial glucose concentration
ΔCBV	change in cerebral blood volume
ΔCBVinj	change in cerebral blood volume measured over most injured cerebral hemisphere
ΔCBVuninj	change in cerebral blood volume measured over least injured cerebral hemisphere
ΔCPP	change in cerebral perfusion pressure
$\Delta ecDO_2$	percentage change in estimated cerebral oxygen delivery
Δ[Hbdiff]	change in haemoglobin difference concentration
$\Delta[HbO_2]$	change in oxy-haemoglobin concentration
Δ[HbT]	change in total haemoglobin concentration
Δ[HHb]	change in deoxy-haemoglobin concentration
ΔICP	change in intracranial pressure
ΔMD[Gluc]	change in microdialysate glucose concentration
ΔMD[Lac]	change in microdialysate lactate concentration
ΔMD LPR	change in microdialysate lactate:pyruvate ratio
Δ[oxCCO]	change in oxidised cytochrome c oxidase concentration
$\Delta[oxCCO]_{meas}$	measured change in oxidised cytochrome c oxidase concentration
$\Delta[oxCCO]_{pred}$	predicted change in oxidised cytochrome c oxidase concentration
ΔPaO_2	change in arterial oxygen tension
$\Delta PaCO_2$	change in arterial carbon dioxide tension
$\Delta PbrO_2$	change in brain tissue oxygen tension
ΔPL	change in optical pathlength
ΔTOI	change in tissue oxygenation index
ΔTOIinj	change in tissue oxygenation index measured over most injured cerebral hemisphere
ΔTOIuninj	change in tissue oxygenation index measured over least injured cerebral hemisphere
ΔSaO_2	change in arterial oxyhaemoglobin saturation
ΔVMCA	change in middle cerebral artery mean blood flow velocity
μ_a	absorption coefficient
μ_s	scattering coefficient

μ_{st}	transport scattering coefficient
ρ	brain density
a	specific absorption coefficient
ABG	arterial blood gas sampling
ADP	adenosine diphosphate
AMP	adenosine monophosphate
AMPA	amino-3-hydroxy-5-methyl-4-isoxazolepropionate
ANLSH	astrocyte-neurone lactate shuttle
ANOVA	analysis of variance
ARDS	acute respiratory distress syndrome
ASDH	acute subdural haematoma
ATP	adenosine triphosphate
BBS	broadband spectroscopy
BL	baseline
CaO_2	arterial oxygen content
CBF	cerebral blood flow
CBV	cerebral blood volume
CCO	cytochrome c oxidase
cDO_2	cerebral oxygen delivery
$CMRO_2$	cerebral metabolic rate for oxygen
CO_2	carbon dioxide
CPP	cerebral perfusion pressure
CSF	cerebrospinal fluid
CSLVH	cerebral small vessel to large systemic vessel haematocrit
CT	computed tomography
DPF	differential pathlength factor
e	specific extinction coefficient
$ecDO_2$	estimated cerebral oxygen delivery
ECF	extracellular fluid
EDH	extradural haematoma
EEG	electroencephalography
Eqn	equation
$EtCO_2$	end tidal carbon dioxide tension
F	female
$FADH_2$	flavin adenine dinucleotide
FDS	frequency domain spectroscopy
FGF	fresh gas flow

FiO_2	inspired oxygen percentage
G	light attenuation due to scattering
g	anisotropy factor
GCS	Glasgow Coma Score
[Hb]	haemoglobin concentration
HbO_2	oxy-haemoglobin
$[HbO_2]$	oxy-haemoglobin concentration
HHb	deoxyhaemoglobin
[HHb]	deoxyhaemoglobin concentration
HR	heart rate
I_0	initial intensity
ICH	intracerebral haematoma
ICP	intracranial pressure
IQR	interquartile range
k	extinction coefficient
LDH	lactate dehydrogenase
LDH1/ LDH5	isoforms of lactate dehydrogenase
LPR	lactate:pyruvate ratio
M	male
MAP	invasively measured mean arterial pressure
MBLL	modified Beer-Lambert Law
MBP	non-invasively measured mean arterial pressure
MD	cerebral microdialysis
MD[Gluc]	microdialysate glucose concentration
MD[Lac]	microdialysate lactate concentation
MD LPR	microdialysate lactate:pyruvate ratio
MRI	magnetic resonance imaging
MRS	magnetic resonance spectroscopy
MWHb	molecular weight of haemoglobin
NADH	nicotinamide adenine dinucleotide
NBH	normobaric hyperoxia
NCU	neurocritical care unit
NIR	near infrared
NIRS	near infrared spectroscopy
NMDA	N-methyl-D-aspartate
NO	nitric oxide
O_2	oxygen

O_2^-	superoxide radical
oxCCO	oxidised cytochrome c oxidase
$PaCO_2$	arterial carbon dioxide tension
PaO_2	arterial oxygen tension
$PbrO_2$	tissue oxygen tension
PC	personal computer
PET	positron emission tomography
Pi	phosphate
PL	optical pathlength
redCCO	reduced cytochrome c oxidase
RTA	road traffic accident
SAH	subarachnoid haemorrhage
SaO_2	arterial oxyhaemoglobin saturation
$SjvO_2$	jugular venous oxyhaemoglobin saturation
SPECT	single photon emission computed tomography
SRS	spatially resolved spectroscopy
TBI	traumatic brain injury
TCD	transcranial Doppler ultrasonography
TOI	tissue oxygenation index
TOIinj	tissue oxygenation index measured over most injured cerebral hemisphere
TOIuninj	tissue oxygenation index measured over least injured cerebral hemisphere
TRS	time resolved spectroscopy
VIF	variable inflation factors
VMCA	mean basal middle cerebral artery blood flow velocity

Motivations and Objectives

TBI remains a significant cause of morbidity and mortality and as it predominantly affects young people, carries a huge cost to society. The last three decades have seen great advances in the care of patients with TBI but despite several promising animal studies, no pharmacological agents have been identified which improve outcome in human studies: a process which has been hampered by the lack of validated surrogate markers for outcome after TBI. Current management strategies generally make use of strictly protocolised management guidelines which are directed towards providing an optimal physiological environment in order to minimise secondary insults and maximise the body's own regenerative processes.

There is however, a potential flaw in the use of strictly protocolised management guidelines. There exists a wide heterogeneity in TBI, both between patients, and within patients across time and space. Minimising secondary injury to the brain after TBI requires the tailoring of metabolite supply to demand, but an 'adequate supply' may vary substantially between periods of hypermetabolism and periods of deep sedation or extensive mitochondrial dysfunction. Strictly protocolised management strategies attempt to address adequate metabolite demand for an average TBI patient but make no allowance for individual variation.

Most current protocols for the management of patients with TBI are based on avoiding raised ICP and maintaining adequate CPP. Gross changes in these variables are however likely to be preceded by biochemical changes within the injured brain. Identification of these biochemical changes might allow early intervention and potentially reduce secondary insults and improve patient outcome.

The ideal cerebral monitor for use after TBI would be a non-invasive system able to provide realtime quantitative haemodynamic and metabolic information at multiple sites with high temporal and spatial resolution. The development of cerebral monitoring tools able to detect biochemical changes in the injured brain has the potential to contribute to the treatment of TBI in three ways. Firstly

monitoring of cerebral biochemistry might allow tailoring of treatment strategies to the individual. Secondly identification of biochemical changes which precede changes in ICP and CPP might allow for earlier treatment intervention and hence reduction of secondary injury. Thirdly the discovery of surrogate markers of TBI pathobiology might aid the identification of effective pharmacological treatments.

NIRS fulfils almost all of the requirements of the ideal cerebral monitor. In addition to measurements of haemoglobin oxygenation, NIRS is able to monitor changes in mitochondrial redox state by measuring changes in the concentration of oxCCO: an attractive monitoring target as it is intimately involved in driving ATP synthesis and thus the maintenance of cellular homeostasis. Measurement of oxCCO concentration changes might allow assessment of the adequacy of mitochondrial oxygen delivery and therefore facilitate the identification of ischaemic thresholds specific to a given individual at a given time.

However despite early enthusiasm, NIRS measurements of changes in the concentration of oxCCO have proved to be technically difficult and the relationship between mitochondrial oxygen delivery and oxCCO concentration changes continues to be debated. These points have contributed to a relative paucity of studies investigating changes in oxCCO concentrations in the adult human brain. Recently, the use of broadband spectroscopy systems in animals has addressed some of these issues and has laid the foundation to readdress this technique in the context of the human brain.

This thesis aims to assess the use of NIRS measurements of cerebral oxygenation and oxCCO concentration to monitor the injured human brain. Responses of NIRS variables to physiological perturbations in the healthy brain are not well established and so it is important to measure initially changes in NIRS variables that occur during well controlled changes in cerebral oxygenation and blood flow in healthy volunteers. This allows identification of normal values and determination of the sensitivity of the NIRS variable responses. Studies are then carried out on patients suffering from TBI on the

neurocritical care unit. Non-invasive NIRS variables are compared with those acquired using invasive cerebral monitoring devices and in particular comparisons are made between non-invasively measured oxCCO concentration changes, a marker of mitochondrial redox state, and invasively measured brain extracellular fluid lactate pyruvate ratio, a marker of cellular redox state.

Thesis Overview

Chapter 1 provides an overview of the primary mechanisms of ATP production essential for maintaining cerebral cellular integrity. This chapter concentrates on the physiology of the healthy brain. This is an essential prequel to understanding the alterations in cerebral metabolism which occur after TBI.

Chapter 2 describes the epidemiology and pathophysiology of TBI. The available range of neurocritical care monitoring modalities is introduced and their strengths and limitations are discussed. Finally the need for novel monitoring techniques able to overcome these limitations is discussed.

Chapter 3 provide an introduction to NIRS. Specifically the theoretical bases of NIRS and the various techniques used in this thesis are discussed. Particular mention is made of the main chromophores and optical properties of biological tissue. Continuous wave spectroscopy is introduced first and then followed by a description of spatially resolved and frequency domain spectroscopy, and techniques for measuring optical pathlength.

Chapter 4 describes an experimental study using NIRS to measure changes in TOI and CBV in the brains of healthy adult volunteers during alterations in the composition of inspired gases. The physiological challenges consist of isocapnoeic hypoxia and hyperoxia, and normoxic hypocapnoea and hypercapnoea. Responses to these four challenges are described individually and the results are then combined in order to relate changes in TOI to changes in SaO_2, $EtCO_2$, CBV, CBF, heart rate and MAP.

Chapter 5 describes an experimental study using the same physiological challenges as chapter 4 but using BBS to measure changes in HbO_2, HHb and oxCCO concentrations in the brains of healthy adult volunteers. A five hour phantom study to test the stability of the BBS system is presented.

Chapter 6 describes two analytical approaches to investigate the relationship between the haemoglobin and CCO signals measured during the healthy volunteer studies. It has been previously suggested that NIRS measured

changes in oxCCO concentration might be merely an artefact of the measurement algorithm but the analyses described in this chapter suggest that this is not the case.

Chapter 7 describes a study to investigate changes in cerebral metabolism during normobaric hyperoxia in patients with TBI. Data from a wide range of invasive and non-invasive monitoring modalities including BBS, brain tissue oxygen tension measurement and cerebral microdialysis are presented and compared.

Chapter 8 provides a summary of the thesis and details promising future avenues of investigation.

Personal Statement

I have been intimately involved in all aspects of the work described in this thesis. Prior to the commencement of the course of study I applied for funding through a competitive process and successfully acquired a Wellcome clinical research fellowship. I devised the experimental protocols and drafted the ethics committee applications. Studies on the healthy volunteers were carried out in association with Ilias Tachtsidis whereas I was solely responsible for the studies on the brain injured patients. I analysed the experimental data, carried out the statistical analysis and have presented the findings at several international conferences.

Nevertheless the experimental protocols and analytical techniques I employed were developed from previous studies carried out by the staff of the Medical Physics Department of University College London and I am indebted to them for laying the foundations for the work I present in this thesis.

Chapter 1
Physiology of Normal Cerebral Cellular Metabolism

This thesis describes the use of NIRS to monitor cerebral haemodynamic and metabolic variables in both healthy adult volunteers and patients with TBI. Metabolic data from invasive cerebral microdialysis monitoring will also be presented. In order to interpret these data it is essential to understand the cellular metabolic pathways in which the monitored variables are involved. This chapter provides an overview of the primary mechanisms of ATP synthesis essential for maintaining cerebral cellular integrity. This initial chapter concentrates mainly on the situation found in the healthy brain.

1.1 Cellular Metabolism

Cell survival relies on the ability to maintain ionic gradients across membranes, and this is primarily achieved through the action of the Na/K/ATPase pump[1]. Neuronal depolarisation depletes these gradients and increased ATP synthesis is then required in order to provide the substrate required to replenish them[2]. This accounts, in part, for the high metabolic requirements of the brain, as demonstrated by the fact that it constitutes only 2% of total body mass, but has a normal blood flow of 45-60 ml/100g/min (15% of total cardiac output) and uses 3.5 ml/100g/min of oxygen (20% of total basal body oxygen consumption)[3]. In health, cerebral ATP requirements are traditionally thought to be met by the aerobic metabolism of glucose.

The overall cellular metabolism of glucose is shown in equation 1.1. This process consists of two parts: an anaerobic part termed glycolysis which takes place in the cell cytoplasm and derives pyruvate from glucose, and a second aerobic step which takes place in the mitochondria, and produces a proton gradient across the inner mitochondrial membrane which consequently drives the bulk of ATP synthesis.

$$C_6H_{12}O_6 + 6O_2 + 38ADP + 38Pi \Rightarrow 6CO_2 + 6H_2O + 38ATP \qquad Eqn\ 1.1$$

Oxygen is transported from the lungs to the mitochondria via the circulatory system facilitated by cardiac pumping of blood, and diffusion gradients which exist between the alveoli and the pulmonary vasculature, and capillaries and mitochondria. The vast majority of O_2 transport in blood occurs through the reversible binding of oxygen to hemoglobin. In addition, a small amount of oxygen is carried dissolved in plasma. Under normal atmospheric conditions, arterial blood carries approximately 20.1 ml of O_2/100ml of blood bound to hemoglobin and 0.3 ml O_2/100 ml of blood (1.5% of the total) in solution. However when FiO_2 is increased to 100% at atmospheric pressure the dissolved oxygen quantity can increase to 1.5 ml O_2/100 ml blood[4].

The cerebral metabolism of glucose commences with the transport of glucose from the capillary into the cell. Glucose is first transferred across the blood brain barrier into the brain extracellular fluid by the action of the glucose transporter GLUT-1. Uptake into cells is then facilitated by the action of GLUT-1 in astrocytes and GLUT-3 in neurones[3].

1.2 Glycolysis

Glycolysis is a multistep process in which one molecule of glucose is converted into two molecules of pyruvate: simultaneously a net two molecules of ATP and two molecules of NADH are synthesised. The first step in the glycolytic pathway requires the breakdown of two ATP molecules and derives two phosphorylated 3-carbon intermediates from glucose[1]. Further reactions occur to convert these intermediates to two pyruvate molecules and synthesise four ATP molecules and two NADH molecules (figure 1.1). The net process of glycolysis can therefore be written as in equation 1.2.

$$C_6H_{12}O_6 + 2ADP + 2Pi + 2NAD^+ \Rightarrow 2CH_3COCOOH + 2ATP + 2NADH + 2H^+$$

Eqn 1.2

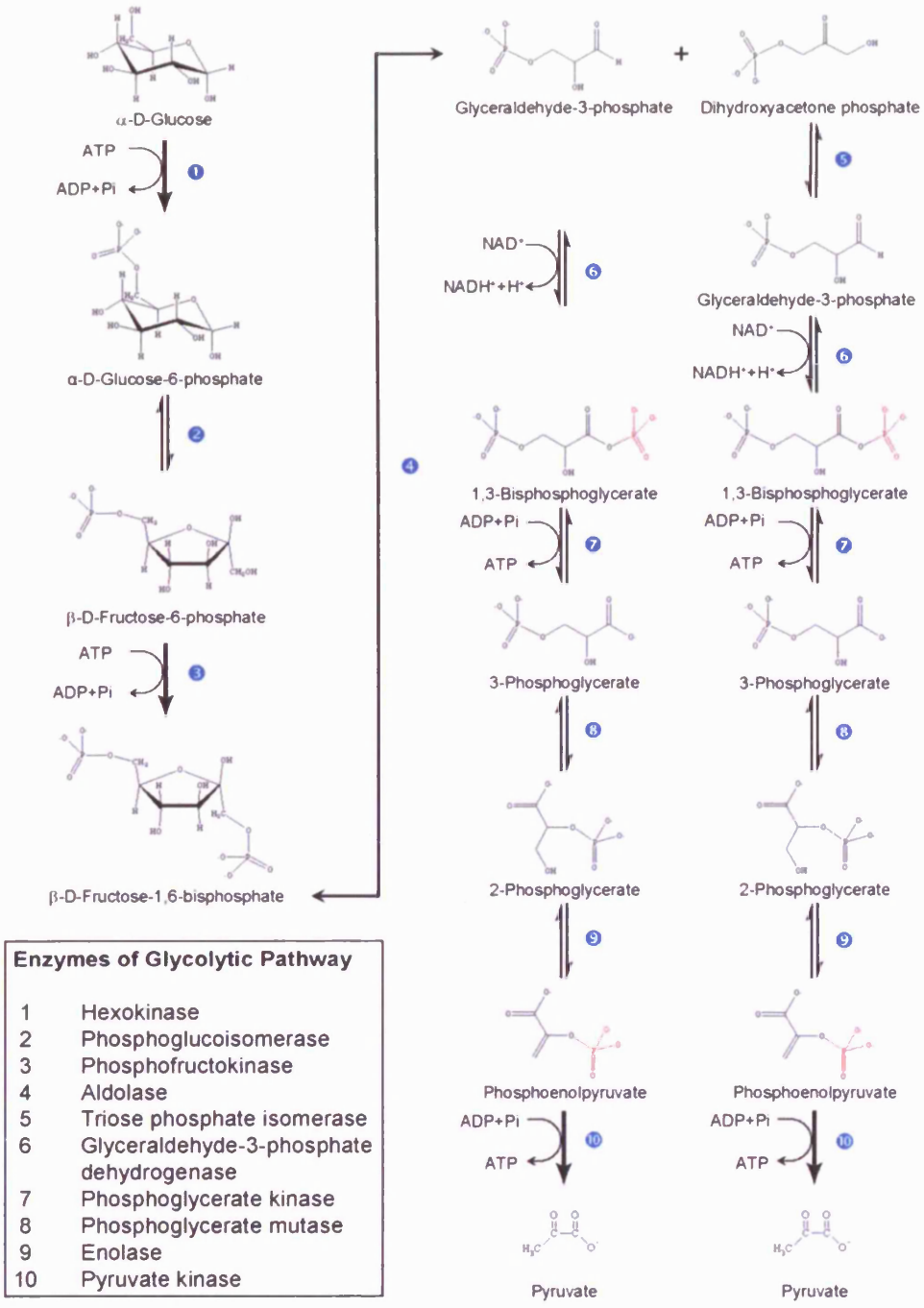

Figure 1.1: Classical model of Glycolysis.

The rate of glycolysis is tightly coupled to the ATP requirements of the cell and this is primarily achieved through modulation of the enzyme phosphofructokinase-1 which catalyses the conversion of fructose-6-phosphate to fructose-1,6-bisphosphate[3]. This is an irreversible process and ATP acts as an allosteric inhibitor thus reducing the rate of glycolysis when ATP levels in the cell are high.

Conventional wisdom states that the pyruvate produced by glycolysis can then be metabolised through three routes. It can enter the citric acid cycle, through conversion to either acetyl coenzyme A or oxaloacetate, and thereby undergo aerobic metabolism, be converted to lactate by the action of lactate dehydrogenase or be converted into the amino acid alanine. In the presence of adequate mitochondrial oxygen tension, and given the tight coupling of glycolysis to cellular ATP requirements, the majority of pyruvate will enter the citric acid cycle to take part in highly efficient aerobic synthesis of ATP[2]. However, during cellular ischaemia when there is inadequate oxygen for aerobic metabolism, pyruvate will be converted to lactate and lactate levels will rise. In the resting human 5-10% of consumed glucose is released as lactate into the blood[2].

Lactate was traditionally thought to be a waste product of anaerobic metabolism and by inducing tissue acidosis was implicated in muscle fatigue and exacerbation of cerebral ischaemia. However recent work has challenged these assumptions[5,6]. An increasing body of evidence suggests that lactate, far from being harmful, is instead a source of neuronal fuel. The traditional role of lactate as a deleterious compound has been questioned by work suggesting that lactate accumulation does not cause muscle fatigue[7]. Research involving the cerebral utilisation of lactate has shown that astrocytes can convert glycogen to lactate[8] and that lactate can be used as a neuronal fuel[9,10]. Contrary to the traditional view, *in vitro* experimentation has shown that not only is lactate neuroprotective after hypoxic insult[9] but that it may be an essential fuel for neurones and preferred to glucose[11]. Studies in humans have also shown that lactate produced through muscle exercise is metabolised by the brain[12]. In response to some of these findings, Magistretti proposed the hypothesis of the astrocyte-neurone lactate shuttle (ANLSH), which suggests that astrocytes produce lactate from glucose anaerobically through glycolysis, and that lactate can then be shuttled, via monocarboxylase transporters found in both astrocytic and neuronal membranes, to the neuronal cytoplasm where it undergoes aerobic metabolism through the citric acid cycle (figure 1.2).

Figure 1.2: Schematic showing the Magistretti model of coupled lactate-pyruvate metabolism (taken from[3]).

A more radical hypothesis has been suggested by Schurr, who proposes that, as the conversion of pyruvate to lactate releases free energy, it makes thermodynamic and chemical sense for glycolysis to proceed naturally to lactate production, and that the step from pyruvate to lactate in the cytoplasm would occur in preference to pyruvate entering the mitochondria, even during aerobic conditions. Lactate would then be transported across the mitochondrial membrane facilitated by monocarboxylase inhibitors where it would be converted back to pyruvate through the action of lactate dehydrogenase. This theory is supported by the facts that LDH occurs within mitochondria and that lactate is an efficient substrate for the citric acid cycle[5]. The proposed chemical steps are shown in figure 1.3. This theory does not exclude that of the ANLSH and is able to explain the accumulation of lactate during ischaemia by a build up of electrons, and hence reduced substrate, restricting the ability of lactate to be converted to pyruvate and enter the citric acid cycle. This is in contrast to conventional theory which proposes an accumulation of pyruvate driving a pathophysiological conversion of pyruvate to lactate. These theories may force us to readdress the role of lactate in cerebral metabolism. However it is generally agreed that glucose metabolism subsequently proceeds through the incorporation of intramitochondrial pyruvate into the citric acid cycle.

Figure 1.3: Schematic depiction of Schurr's hypothetical glycolytic pathway. LDH1 and LDH5 are isoforms of lactate dehydrogenase. Taken from [5].

1.3 The Citric Acid Cycle

Pyruvate enters the citric acid cycle through conversion to either acetyl coenzyme A (equation 1.3) or oxaloacetate.

$$CH_3COCOOH + CoASH + NAD^+ \Rightarrow AcetylCoA + CO_2 + NADH + H^+ \qquad Eqn\ 1.3$$

The citric acid cycle then proceeds as depicted in figure 1.4. The net reaction for one turn of the citric acid cycle is shown in equation 1.3. The rate of the citric acid cycle is tightly coupled to cellular energy requirements, primarily through regulation of the enzyme isocitrate dehydrogenase which catalyses the conversion of isocitrate to α-ketoglutarate, and this enzyme is activated by increased ADP levels and inhibited by increased NADH levels[3].

$$AcetylCoA + GDP + Pi + FAD + 3NAD^+ + 3H_2O \qquad Eqn\ 1.4$$
$$\Rightarrow CoASH + 3CO_2 + GTP + FADH_2 + 3NADH + 3H^+$$

Metabolism of glucose thus far has synthesised relatively little ATP. However, the NADH and $FADH_2$ which have been produced are potent electron donors and are able to give up high energy electrons which are fed into the electron transfer chain. The passage of these electrons along the electron transfer chain drives the generation of a protonmotive force which is then used to synthesise the majority of cellular ATP.

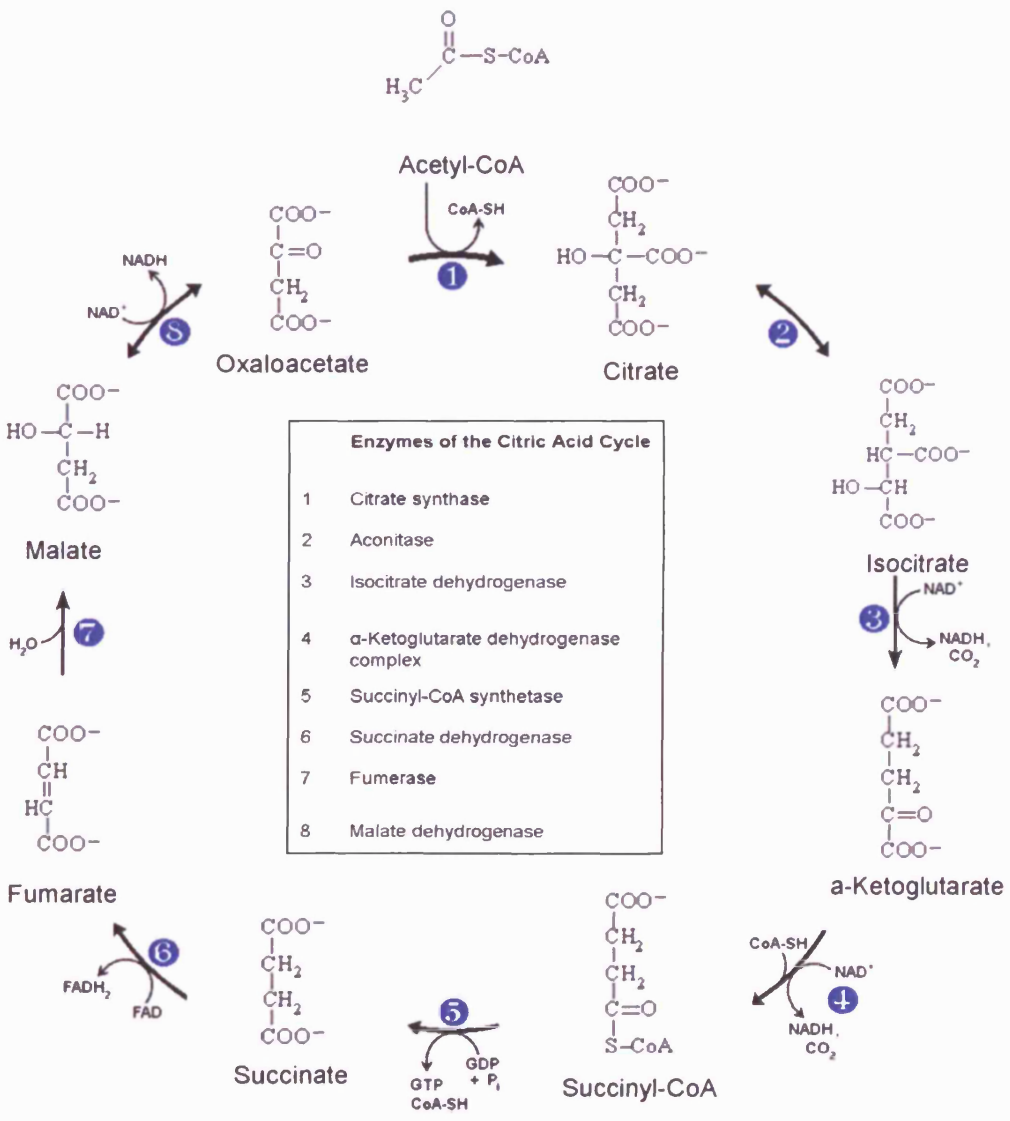

Figure 1.4: The Citric Acid Cycle.

1.4 The Electron Transfer Chain

Thus far in the metabolism of glucose, carbon atoms have been removed in the form of carbon dioxide, and a series of oxidative reactions has removed electrons and stored them in the form of NADH and $FADH_2$. The remainder of the glucose metabolic pathway transfers these electrons to oxygen. NADH and $FADH_2$ are potent electron donors, meaning that they have a low electron affinity, whereas oxygen is a potent electron acceptor. The reaction between NADH and oxygen is therefore highly energenetically favourable and occurs with a very large decrease in free energy (equation 1.5). The complete oxidation of one molecule of NADH can drive the synthesis of three molecules of ATP[2].

$$NADH + \tfrac{1}{2}O_2 + H^+ \Rightarrow NAD^+ + H_2O \qquad \textit{Eqn 1.5}$$

If this reaction were to occur directly, then a huge amount of energy would be lost as heat. The electron transfer chain allows this reaction to occur in many small steps and therefore facilitates the incremental transfer of the released energy[1]. This process requires complex control. Although oxygen is a highly reactive molecule, it has a low affinity for picking up its first electron and thus forming the superoxide radical O_2^-. Once this step is completed however it becomes highly reactive and has an extremely high affinity for a further three electrons. The electron transfer chain is able to stabilise the highly reactive oxygen free radical intermediates until they can be safely released as water.

The first description of the various components of the electron transfer chain was made by Keilin in 1925[13]. He described the existence of components present in a wide range of bacteria, yeasts and insects, which altered their absorbance of visible light as they changed between the oxidised and reduced forms. These coloured proteins were named cytochromes and three types, each with a distinctive optical absorption spectra, were discovered and designated as cytochrome a, b and c. The cytochromes are related by the presence of a haem group consisting of a porphyrin ring with a tightly bound iron atom. Since then further components of the electron transfer chain have been discovered and the nomenclature has been altered accordingly.

Modern biochemical theory depicts the electron transfer chain as consisting of 4 complexes embedded in the mitochondrial inner membrane. As electrons pass along the chain their energy state gradually reduces. Simultaneously, protons are pumped out of the mitochondrial matrix and into the intermembrane space against their concentration gradient by a mechanism known as chemiosmosis[14]. This proton gradient is the driving force for ATP synthesis which is subsequently carried out by complex V. The pathway involves more than 60 proteins, six different haem complexes, seven iron-sulphur groups and two copper atoms.

Complex I, which is also know as NADH dehydrogenase, is the largest of the electron transfer complexes and consists of more than 40 polypeptide chains[1]. NADH donates electrons to complex I, which are then passed to ubiquinone, or complex II, a small hydrophobic molecule which is freely mobile in the lipid bilayer. Electrons are then passed on to complex III, the cytochrome b-c_1 complex, which exists as a dimer, with each monomer containing three haem units and an iron-sulphur protein. Electrons then pass to cytochrome c, another small electron carrier that diffuses freely on the intermembrane side of the inner mitochondrial membrane and transports electrons to the cytochrome c oxidase (CCO) complex (complex IV). CCO functions as a dimer, with each monomer containing two haem complexes and two copper complexes. It is only at this terminal stage of glucose metabolism that the reduction of oxygen takes place with CCO accepting one electron at a time from cytochrome c and passing four at a time to oxygen. This is achieved through CCO clamping the oxygen molecule between a haem complex and a copper atom until it is reduced to water and can then be safely released. CCO will be described in greater detail in the next section.

As electrons pass along the electron transfer chain complexes I, III and IV pump protons across the mitochondrial membrane though a process which is as yet poorly understood[15]. The electrochemical gradient achieved through this process is then utilised to drive ATP synthesis. Complex V (ATP synthase) contains a hydrophilic pathway across the mitochondrial inner membrane. Protons flow through this pathway down their gradient and drive a rotating

movement which is able to synthesise more than 100 molecules of ATP per second[1]. Control of the rate of ATP synthesis is primarily achieved through the inhibitory influence of the electrochemical proton gradient which is in turn linked to the ATP:ADP ratio. Increased ATP use increases the concentration of the ATP synthase substrates ADP and Pi. This drives ATP synthesis and thereby dissipates the proton electrochemical gradient, hence promoting electron transfer along the electron transfer chain. A depiction of the mitochondrial electron transfer chain is shown in figure 1.5.

Figure 1.5: The electron transfer chain. Modified from [3].

1.5 Cytochrome C Oxidase

CCO is the terminal member of the electron transfer chain. It reduces dioxygen to water and is responsible for consuming more than 95% of the oxygen metabolised by higher organisms[16]. It is able to harness the free energy released by the reduction of dioxygen to pump protons across the mitochondrial inner membrane and generate an electrochemical gradient which can then be used to drive the synthesis of ATP.

X ray crystallography and spectroscopy studies have allowed the structure of both bacterial and bovine heart CCO to be identified, and the core subunits (subunits I-III) of these two types show remarkable similarities[16-20]. Subunit I consists of multiple membrane spanning segments and contains two *a* type haem complexes (haem *a* and haem a_3) and a copper ion (termed Cu_B). Haem a_3 and Cu_B form a binuclear centre where the binding and subsequent reduction of oxygen takes place[15,21-23]. Subunit II contains two copper ions in a mixed valence state and this copper dimer is termed the Cu_A centre. In addition to these two redox active subunits, bovine CCO contains a further 11 subunits and functions as a dimer with a molecular weight of over 400 kDa. The concentration of CCO in the rat brain has been reported as ~1 μM at birth rising to 5.5 μM by maturity[24].

The general scheme of electron transfer through CCO is well established. Electrons are donated to CCO from cytochrome c, and the initial electron acceptor is the Cu_A centre. Electrons pass from Cu_A to haem *a* and then to the haem a_3-Cu_B complex where they are eventually passed to oxygen. This process is accompanied by the transfer two protons per electron. One of these protons is involved in the reduction of oxygen and the other is pumped across the mitochondrial membrane. Many intermediate states have been proposed as mediating this process and the mechanisms of the proton pumping have not been fully characterised. However, it appears that two electrons pass to the haem a_3-Cu_B complex before oxygen binding occurs. The haem a_3-Cu_B oxygen complex then proceeds through a peroxy form and then, with the addition of a further electron, to a ferryl form before the addition of a fourth electron completes the reaction process[15,25,26]. The four main redox centres involved in electron transfer within the CCO enzyme each exhibit changes in optical absorption related to their redox state. A simplified schematic of the electron transfer is shown in figure 1.6 together with the wavelengths at which the main changes in optical absorption occur for each centre.

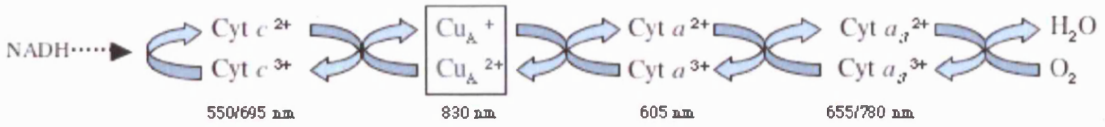

Figure 1.6: A simplified scheme of the flow of electrons through CCO and the relevant absorbing wavelengths for each centre.

The activity of CCO is regulated by a diverse set of mechanisms, nucleotides and hormones, and ten nucleotide-binding sites of CCO have been identified[16]. ATP/ADP ratio appears to be an important regulatory factor and is capable of altering H^+/e^- stoichiometry, thereby reducing the electrochemical gradient produced by electron transfer when the ATP/ADP ratio is high[27]. The proton gradient across the mitochondrial membrane inhibits electron transfer between Cu_A and haem *a* thereby reducing CCO activity when the requirement for ATP synthesis is reduced: conversely, collapsing the proton gradient has the opposite effect [28]. Increases in pH inhibit the passage of electrons to the haem a_3-Cu_B complex through an effect on the rate of protonation and therefore inhibit CCO[29]. Reduction in the rate of electron exit from the haem a_3-Cu_A complex will reduce the activity of CCO leading to further reduction of the Cu_A and haem *a* centres[30]. This can occur through the presence of inhibitors such as cyanide or NO, both of which bind to the haem a_3 centre. Importantly, this effect will also be produced when low mitochondria oxygen tension limits the rate of electron transfer from CCO to oxygen.

An increasing body of literature has demonstrated the ability of NO to inhibit CCO and this may have important implications for our understanding of the regulation of CCO activity. NO is a free radical gas which is involved in a diverse range of physiological and pathophysiological processes in the central nervous system. Specifically it is involved in cellular signalling mechanisms and the regulation of CBF. NO inhibits CCO by reversibly binding to the haem a_3-Cu_B complex in a manner which is competitive with oxygen[31-34]. NO mediated inhibition of CCO transiently increases AMP:ATP ratio, leading to activation of phosphofructokinase and GLUT-mediated glucose uptake, thus causing rapid increases in the rate of glycolysis[35-37]. Alternatively, CCO

inhibition may have the effect of redistributing oxygen away from the electron transfer chain towards non-respiratory oxygen-dependent targets when oxygen tension is low[38].

In the study of mitochondrial metabolism, CCO occupies an important role, as it is located at the terminal end of the electron transfer chain and instrumental in maintaining the driving force for ATP synthase. Mitochondrial mutations affecting CCO have been associated with several disease processes, including motor neuron disease, acquired sideroblastic anaemia, and epilepsia partialis[16] but few techniques exist with which to study CCO activity. It is possible to use histopathological techniques to assess CCO activity *in vitro*[39] but this requires removal of living tissue and is therefore of limited use in the study of the human brain. It is however possible to exploit the differences in optical absorption exhibited by the CCO redox couples to obtain information about CCO redox state. The study of this optical technique forms the major part of this thesis and is discussed in detail in chapter 3.

References

1. Alberts B, Johnson A, Lewis J, Raff M, Roberts K, Walter P. *Molecular Biology of the Cell.* 4th ed. New York: Garland Science; 2004.
2. Siesjo BK (1978) *Brain Energy Metabolism*, 1st ed. Chichester: John Wiley and Sons.
3. Zauner A, Daugherty W, Bullock M, Warner D. Brain oxygenation and energy metabolism: part I-biological function and pathophysiology. *Neurosurgery* 2002;51:289-301.
4. Alves OL, Daugherty WP, Rios M. Arterial hyperoxia in severe head injury: a useful or harmful option? *Curr Pharm Des* 2004;10:2163-2176.
5. Schurr A. Lactate: the ultimate cerebral oxidative energy substrate? *J Cereb Blood Flow Metab* 2006;26:142-152.
6. Schurr A. Lactate, glucose and energy metabolism in the ischemic brain. *Int J Mol Med* 2002;10:131-136.
7. Pedersen TH, Nielsen OB, Lamb GD, Stephenson DG. Intracellular acidosis enhances the excitability of working muscle. *Science* 2004;305:1144-1147.
8. Dringen R, Gebhardt R, Hamprecht B. Glycogen in astrocytes: possible function as lactate supply for neighboring cells. *Brain Res* 1993;623:208-214.
9. Schurr A, West CA, Rigor BM. Lactate-supported synaptic function in the rat hippocampal slice preparation. *Science* 1988;240:1326-1328.
10. Schurr A, Payne RS, Miller JJ, Rigor BM. Brain lactate is an obligatory aerobic energy substrate for functional recovery after hypoxia: further in vitro validation. *J Neurochem* 1997;69:423-426.
11. Pellerin L, Magistretti PJ. Glutamate uptake into astrocytes stimulates aerobic glycolysis: a mechanism coupling neuronal activity to glucose utilization. *Proc Natl Acad Sci U S A* 1994;91:10625-10629.
12. Dalsgaard M, Quistorff B, Danielsen ER, Selmer C, Vogelsang T, Secher NH. A reduced cerebral metabolic ratio in exercise reflects metabolism and not accumulation of lactate within the human brain. *J Physiol* 2004;554:571-578.
13. Keilin D (1966) *The History of Cell Respiration and Cytochromes* 1st ed. Cambridge: Cambridge University Press.

14. Mitchell PD. Foundations of vectorial metabolism and osmochemistry. *Biosci Rep* 2004;24:386-434.
15. Namslauer A, Brzezinski P. Structural elements involved in electron-coupled proton transfer in cytochrome c oxidase. *FEBS Lett* 2004;567:103-110.
16. Richter OM, Ludwig B. Cytochrome c oxidase--structure, function, and physiology of a redox-driven molecular machine. *Rev Physiol Biochem Pharmacol* 2003;147:47-74.
17. Tsukihara T, Aoyama H, Yamashita E, Tomizaki T, Yamaguchi H, Shinzawa-Itoh K, Nakashima R, Yaono R, Yoshikawa S. Structures of metal sites of oxidized bovine heart cytochrome c oxidase at 2.8 A. *Science* 1995;269:1069-1074.
18. Tsukihara T, Aoyama H, Yamashita E, Tomizaki T, Yamaguchi H, Shinzawa-Itoh K, Nakashima R, Yaono R, Yoshikawa S. The whole structure of the 13-subunit oxidized cytochrome c oxidase at 2.8 A. *Science* 1996;272:1136-1144.
19. Yoshikawa S, Shinzawa-Itoh K, Nakashima R, Yaono R, Yamashita E, Inoue N, Yao M, Fei MJ, Libeu CP, Mizushima T, Yamaguchi H, Tomizaki T, Tsukihara T. Redox-coupled crystal structural changes in bovine heart cytochrome c oxidase. *Science* 1998;280:1723-1729.
20. Iwata S, Ostermeier C, Ludwig B, Michel H. Structure at 2.8 A resolution of cytochrome c oxidase from Paracoccus denitrificans. *Nature* 1995;376:660-669.
21. Wikstrom M. Cytochrome c oxidase: 25 years of the elusive proton pump. *Biochim Biophys Acta* 2004;1655:241-247.
22. Yoshikawa S. A cytochrome c oxidase proton pumping mechanism that excludes the O2 reduction site. *FEBS Lett* 2003;555:8-12.
23. Ferguson-Miller S, Babcock GT. Heme/copper terminal oxidases. *Chem Rev* 1996;96:2889-2908.
24. Brown GC, Crompton M, Wray S. Cytochrome oxidase content of rat brain during development. *Biochem Biophys Acta* 1991;1057:273-275.
25. Brzezinski P. Redox-driven membrane-bound proton pumps. *Trends Biochem Sci* 2004;29:380-387.

26. Szundi I, Liao GL, Einarsdottir O. Near-infrared time-resolved optical absorption studies of the reaction of fully reduced cytochrome c oxidase with dioxygen. *Biochemistry* 2001;40:2332-2339.
27. Frank V, Kadenbach B. Regulation of the H+/e- stoichiometry of cytochrome c oxidase from bovine heart by intramitochondrial ATP/ADP ratios. *FEBS Lett* 1996;382:121-124.
28. Rich PR, West IC, Mitchell P. The location of CuA in mammalian cytochrome c oxidase. *FEBS Lett* 1988;233:25-30.
29. Thornstrom PE, Brzezinski P, Fredriksson PO, Malmstrom BG. Cytochrome c oxidase as an electron-transport-driven proton pump: pH dependence of the reduction levels of the redox centers during turnover. *Biochemistry* 1988;27:5441-5447.
30. Cooper CE, Matcher SJ, Wyatt JS, Cope M, Brown GC, Nemoto EM, Delpy DT. Near-infrared spectroscopy of the brain: relevance to cytochrome oxidase bioenergetics. *Biochem Soc Trans* 1994;22:974-980.
31. Mason MG, Nicholls P, Wilson MT, Cooper CE. Nitric oxide inhibition of respiration involves both competitive (heme) and noncompetitive (copper) binding to cytochrome c oxidase. *PNAS* 2006;103:708-713.
32. Palacios-Callender M, Quintero M, Hollis VS, Springett RJ, Moncada S. Endogenous NO regulates superoxide production at low oxygen concentrations by modifying the redox state of cytochrome c oxidase. *Proc Natl Acad Sci USA* 2004;101:7630-7635.
33. Giuffre A, Sarti P, D'Itri E, Buse G, Soulimane T, Brunori M. On the mechanism of inhibition of cytochrome c oxidase by nitric oxide. *J Biol Chem* 1996;271:33404-33408.
34. Brunori M, Giuffre A, Forte E, Mastronicola D, Barone MC, Sarti P. Control of cytochrome c oxidase activity by nitric oxide. *Biochim Biophys Acta* 2004;1655:365-371.
35. Almeida A, Moncada S, Bolanos JP. Nitric oxide switches on glycolysis through the AMP protein kinase and 6-phosphofructo-2-kinase pathway. *Nat Cell Biol* 2004;6:45-51.
36. Moncada S, Bolanos JP. Nitric oxide, cell bioenergetics and neurodegeneration. *J Neurochem* 2006;97:1676-1689.

37. Cidad P, Almeida A, Bolanos JP. Inhibition of mitochondrial respiration by nitric oxide rapidly stimulates cytoprotective GLUT3-mediated glucose uptake through 5'-AMP-activated protein kinase. *Biochem J* 2004;384:629-636.
38. Xu W, Charles IG, Moncada S. Nitric oxide: orchestrating hypoxia regulation through mitochondrial respiration and the endoplasmic reticulum stress response. *Cell Res* 2005;15:63-65.
39. Hovda DA, Yoshino A, Kawamata T, Katayama Y, Becker DP. Diffuse prolonged depression of cerebral oxidative metabolism following concussive brain injury in the rat: a cytochrome oxidase histochemistry study. *Brain Res* 1991;567:1-10.

Chapter 2
Traumatic Brain Injury

This chapter describes the epidemiology and pathophysiology of TBI. The rational of current management strategies is discussed and recent developments are presented. A key focus of modern TBI management is the minimisation of secondary cerebral insults and a wide range of monitoring modalities are used in order to detect these insults with a view to reducing their duration and impact. The available range of neurocritical care monitoring modalities is introduced and their strengths and limitations are discussed. Finally the need for novel monitoring techniques able to overcome these limitations is discussed.

2.1 Epidemiology of Traumatic Brain Injury

TBI is a major cause of morbidity and mortality. Recent data collected in a district general hospital in Southern England show TBI cases making up 3.4% of accident and emergency attendances with an overall incidence of 453 per 100 000 per year. 10.9 % of these were classified as moderate or severe TBI as defined by GCS 9-12 and 3-8 respectively[1] on admission to hospital[2], and these are associated with a mortality rate of between 22 and 46%[3-5].

Many victims of TBI survive, but the incidence of severe disability in survivors of severe TBI is between 27 and 29%[3-5]. As trauma is predominantly a disease of the young[6,7], disability after TBI results in a considerable loss of productive years and income potential, with a huge estimated annual cost to society[8]. Despite being one of the leading causes of death and disability in the western world, TBI remains incompletely understood with few evidence based treatment strategies.

2.2 Pathophysiology of Traumatic Brain Injury

The pathophysiology of TBI is often described in terms of primary and secondary injury. Primary brain injury was originally defined as physical brain injury sustained at the moment of impact, and secondary injury as injurious events which occur at any later stage. Primary injury is largely caused by

acceleration, deceleration and rotational forces to the brain[9]. Shearing forces cause disruption of tissue structure between areas of differing densities which cause immediate structural damage to neurons[10,11]. Focal injuries occur in the form of contusion injuries, gross tissue disruption and haemorrhage into the extradural, subdural, subarachnoid or intracerebral regions. These primary injuries were initially thought to be immediate and irreversible[9], however there is a growing body of evidence to suggest that a substantial component of cell death due to primary injury may occur hours after the injury[11,12]. This evolving primary injury disrupts membrane stability, and damages intra-axonal cytoskeleton function and axonal transport mechanisms. The resultant impairment of anterograde axoplasmic transport leads to local axonal swelling, and can eventually result in axonal disconnection and distal degeneration[13]. It has therefore become apparent that the primary injury will evolve over time, and that its time course will overlap with secondary, or additional, injury processes[12] (figure 2.1).

Figure 2.1: A model of primary (A) and secondary (B) injury after TBI (modified from [12]).

After TBI, the nervous system has an increased susceptibility to further damage, or secondary injury, which can include a wide range of ischaemic, ionic, neurochemical and immunological processes. Many of these injury mechanisms are common to several cerebral disease processes, such as

TBI[14], stroke[15] and subarachnoid haemorrhage[16], and have common metabolic pathways leading to failing cellular energy production, inability to maintain ionic gradients and eventual cell death. The aetiology of secondary injury is not fully understood but appears to be related in part to the presence of events which impair cellular metabolite delivery known as secondary insults. Secondary insults can be systemic, for example hypotension, hypoxaemia, anaemia, and acid-base or glucose disturbances, or intracranial, for example intracranial hypertension, cerebral oedema, seizures and regional cerebral blood flow disturbance[9,17-22].

The vast array, and interactions, of secondary brain injury mechanisms are outside the scope of this thesis, however some of the major processes are discussed below.

The detrimental effects of systemically induced secondary insults were first demonstrated by Miller, in the late 1970's and early 1980's, who demonstrated a doubling of mortality in severely head injured patients presenting to hospital with hypotension (systolic blood pressure <95 mmHg) or hypoxaemia (arterial oxygen tension<8 kPa)[23-25], and these findings have been confirmed by others[17,26]. Adequate arterial blood pressure is required to maintain CBF, Bouma *et al* demonstrated global CBF reduced below a level associated with cerebral ischaemia in animals (<18 ml/100g.min[27,28]), in the first six hours post TBI, in 13% of patients with severe head injury. Although TBI may alter the ischaemic threshold, this sub-group had poorer outcome and increased mortality when compared to those with a CBF >18 ml/100g/min[29]. These studies highlight the importance of an adequate supply of oxygen and glucose. In health, aerobic glucose metabolism is the major source of energy metabolism in the brain, as has already been noted. However, in the face of inadequate oxygen delivery, ATP production proceeds anaerobically. Anaerobic metabolism is relatively inefficient and if ATP production is inadequate to meet cellular requirements then the ionic homeostasis of the cell will fail[30], heralding intracellular changes in the concentrations of sodium, potassium and calcium, an increased concentration of lactate and corresponding drop in pH[30]. High

concentrations of lactate have been associated with poor outcome after TBI in both animal and human models[31-33].

2.2.1 Excitotoxicity

Elevated glutamate release and resultant excessive cellular depolarisation occur after cerebral ischaemia[34,35]. The neurotoxic effects of glutamate were first reported in mouse retina[36], and it was originally believed that this toxic effect was a direct consequence of an extended period of depolarisation caused by the high glutamate levels[37]. This mechanism was thus termed excitotoxicity. More recent work has suggested that glutamate has detrimental effects through two main pathways: an early phase characterised by neuronal swelling and dependent on cellular influx of extracellular sodium and chloride ions (consistent with the original concept of excitotoxicity), and a delayed phase characterised by neuronal disintegration and dependent on cellular calcium influx through both glutamate, and voltage, gated calcium channels[20,21]. NMDA[20] and AMPA[38] glutamate receptors have been implicated in these processes.

2.2.2 Calcium Influx

Calcium is involved in many facets of cell signalling and homeostasis. It is an important cellular messenger involved in the regulation of many enzymatic and synthetic pathways. However TBI is associated with dysregulation of intracellular calcium ion homeostasis and this is thought to be one of the most important underlying common pathophysiological pathways in neuronal injury[39]. The stimulus for this initial calcium influx is poorly understood but it appears to be both related to, and able to promote, the release of glutamate[40]. Uncontrolled calcium influx into the cell and release of intracellular calcium stores will activate phospholipases, disrupt mitochondrial electron transport, and release free radicals[41], while initiating a complex chain reaction leading to cytokine, and potassium release which results in depolarisation and calcium entry into neighbouring cells[14,41]. Calcium has long been implicated in cell death, and delayed neuronal degeneration after cellular ischaemia has been shown to be dependent on the presence of extracellular calcium [20]. However it has also been suggested that calcium

may have a neuroprotective role. The breakdown of neuronal cells releases phosphate and phosphatides into the extracellular space which bind calcium and thus lower extracellular calcium concentration. The calcium gradient for entry into neighbouring cells is reduced, and this process may therefore have the effect of inducing cell death in damaged cells while protecting those that are potentially viable[41].

2.2.3 Free Radical Mediated Damage

Increased levels of free radicals are found in the brains of animals post TBI and have been implicated in the pathophysiology of secondary brain injury [42-45]. Oxygen free radicals are formed during both ischaemia and reperfusion and cause damage through increased lipid peroxidation, protein oxidation and deoxy-ribonucleic acid damage[46]. An increasingly important role in cerebral homeostasis and pathophysiology has been postulated for the free radical gas NO. In the context of TBI, recent data suggest that NO may have both protective[47,48] and damaging effects[49,49]. In particular, NO has a role in the regulation of CBF after TBI[48] with low cerebral concentrations of NO found in the early post TBI period when CBF is reduced[42]. Conversely, NO has complex pathological roles. It has been implicated in the induction of macrophage apoptosis post TBI[49] and is able to react with superoxide to form the highly toxic free radical peroxynitrite[50]. The multiple interactions of these secondary injury processes are again highlighted by the discovery that NO may mediate glutamate mediated excitotoxicity, as it is generated endogenously by NMDA receptor stimulation[51], and induces mitochondrial calcium release[52].

2.2.4 Mitochondrial dysfunction

Adequately functioning mitochondria are essential to aerobic energy metabolism. It has been demonstrated in both animals[53] and humans[54] that TBI causes mitochondrial dysfunction and subsequent decreased ATP production. Severe oxidative stress and high mitochondrial calcium concentrations cause opening of the mitochondrial permeability transition pore which dissipates the mitochondrial transmembrane protonmotive force for ATP production, releases prop-apoptotic factors and contributes to free radical production[15,22,55,56]. As has been discussed above, calcium influx, NO and

glutamate are all implicated in this process. Cerebral microdialysis studies in humans after TBI show increased lactate:pyruvate ratio (LPR), demonstrating predominantly anaerobic metabolism, even when adequate regional cerebral blood flow and tissue oxygen tension is maintained indicating that cellular energy disturbances can be caused not only by a failure of metabolite delivery but also by a failure of metabolite utilisation[57]. Hovda *et al* studied a rat model of TBI using a lateral fluid percussion injury and demonstrated an injury-induced reduction in cytochrome c oxidase (CCO) activity which began on day 1 post injury and lasted for up to 10 days[58]. This finding suggests the intriguing possibility that the mitochondrial dysfunction which is observed following TBI in humans, and appears to be the common final pathway of secondary injury processes, may be related to changes in CCO activity.

A simplified schematic of pathophysiological processes involved in the evolution of TBI is shown in figure 2.2. All these pathological processes provide potential avenues for the development of pharmacological neuroprotective agents. However, despite several promising pre-clinical trials, no pharmacological neuroprotectants have shown efficacy in human trials thus far[59]. Current treatment of TBI is therefore based on physiological neuroprotection: minimising secondary insults, and thus secondary injury through optimisation of physiological parameters.

Figure 2.2: Schematic showing interaction of secondary injury processes in TBI (taken from [30]). Na^+ Sodium, K^+ Potassium, CBF Cerebral Blood Flow, $OH^\cdot$ Hydroxyl Free Radical.

2.3 Treatment of Traumatic Brain Injury

The last four decades have seen significant advances in the management of TBI. This process has been greatly aided by detailed data collection from large series of TBI patients, the introduction of cranial CT scanning in 1972 and the development in, 1974, of the Glasgow Coma Score[1], which has gained widespread acceptance as an objective measure of level of consciousness and head injury severity. Despite this, many controversies remain and although a huge amount of observational and case series data has been collected, there exists relatively little data from well conducted randomised controlled trials. Following an extensive review of the scientific literature, the American Association of Neurologic Surgeons published guidelines for the treatment of severe head injury in 1996 with subsequent revisions in 2000 and 2007. At this time they concluded that of the 14 topics analysed, only 3 were based on class I evidence and therefore deemed worthy of designation as standards of care[60]. Similar guidelines have also been published by the European Brain Injury Consortium[61].

Extensive investigation has been directed towards discovering effective drug therapies to protect the injured brain and most have attempted to disrupt the putative pathobiology of TBI. Despite several encouraging animal studies, human TBI trials assessing glutamate antagonists, steroids, free radial scavengers, calcium channel antagonists, bradykinin antagonists and growth factors have all failed to show efficacy[59]. Therefore current management strategies are directed towards providing an optimal physiological environment in order to minimise secondary insults and maximise the body's own regenerative processes.

The concept of directing management to minimise secondary cerebral insults first gained credence in the 1970s. Secondary insults are common after TBI and have been reported to occur, at some point, in as many as 91% of patients requiring treatment in the NCU[26]. Hypotension and hypoxaemia were initially identified by Miller *et al*[23-25] and then by Chesnut *et al*[17,62] as being associated with worse outcome after TBI. Jones *et al* assessed the incidence of eight potential secondary insults in 124 patients with TBI and found that the

durations of hypotension, pyrexia and hypoxaemia were significant predictors of mortality[26]. As early as 1977 it was suggested that aggressive goal directed treatment of patients with TBI was able to improve outcome, and important areas of management such as the evacuation of mass lesions, control of ICP, mechanical ventilation, and medical therapy using sedatives and osmotic agents were identified[63]. Raised ICP has been noted by several studies to be associated with increased morbidity and mortality[64-68]; however identification of the optimum threshold for the treatment of raised ICP has proved more difficult. There is some class II evidence to suggest that the threshold is in the region of 20-25 mm Hg[66,67] and strategies designed to maintain ICP below this level have been termed ICP directed therapy.

Rosner *et al* introduced the concept of CPP (defined as MAP – ICP) directed therapy in the 1990s. Rosner studied plateau waves of raised ICP in cats using a fluid-percussion model of TBI and postulated that the trigger for this event was a decrease in CPP, leading to compensatory cerebral vasodilatation. A vicious cycle is set up, consisting of raised cerebral blood volume leading to raised ICP and consequently a further decrease in CPP[69]. Rosner postulated that maintaining a CPP greater than 70 mm Hg, by manipulation of MAP, would minimise periods of raised ICP and ensure an adequate CBF with which to supply oxygen and glucose to the injured brain in the face of an altered autoregulatory threshold[70]. In health, the brain is able to maintain a constant CBF across a wide range of CPP (approximately 50-150 mm Hg) and this process is termed cerebral autoregulation (figure 2.3). However, after TBI these processes are damaged and CBF declines at CPP levels above the normal lower limits of autoregulation[71-73]. Rosner studied 158 patients who were treated using this strategy and provided class II evidence that CPP directed therapy lowered mortality and improved outcome when compared to traditional ICP directed therapy[70,74]. In contrast, Robertson *et al* randomised TBI patients to ICP or CPP directed therapy, and although they found a lower incidence of secondary insults, defined using jugular venous oximetry criteria, in the group treated using CPP directed therapy, there was no significant difference in outcome between the two groups[75]. They also discovered a five fold risk of ARDS in the CPP directed therapy group and concluded that the

vasopressor load required to maintain a CPP >70 mm Hg might induce systemic complications in some patients. Additional studies have shown that patients who develop acute lung injury after TBI have a significantly raised incidence of raised ICP and poorer outcome[76]. Analysis of physiological data from 427 patients in the Selfotel trial, carried out in 2000, showed poorer outcomes for those with a CPP persistently below 60 mm Hg[77], and in 2003, based primarily on these studies, the Brain Trauma Foundation amended its guidelines for the management of severe traumatic brain injury to suggest that CPP be maintained at a minimum of 60 mm Hg.

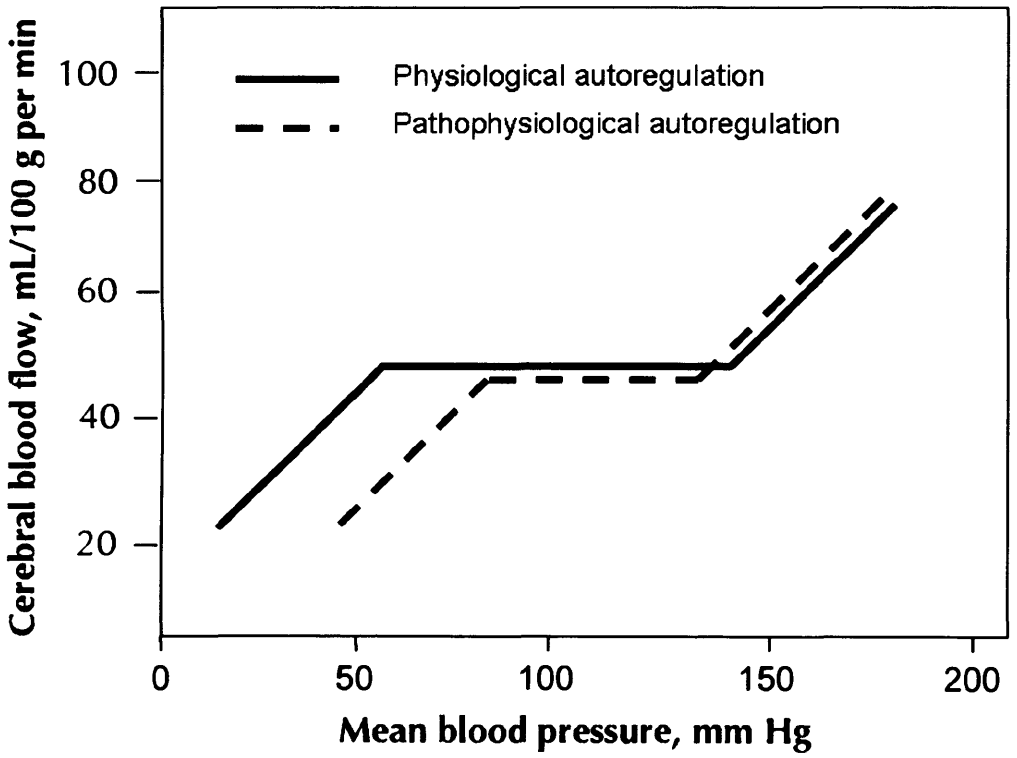

Figure 2.3: Idealised depiction of physiological and pathophysiological cerebral autoregulation.

The Lund Concept has been suggested as an alternative approach to the treatment of TBI. This focuses on avoiding brain oedema given that the blood brain barrier is impaired and is based upon prevention of raised ICP and improvement of pericontusional perfusion and oxygenation. The treatment protocol has been reviewed in depth[78], and specifically includes the

antagonisation of vasoconstriction through reduction of plasma catecholamine concentration and minimising the use of vasopressors. There is some evidence to suggest that the use of the Lund Concept might improve patient outcome after TBI when compared to historical controls[79], but to date no randomised controlled trial has been undertaken comparing the Lund Concept based treatment with CPP directed therapy.

Most consensus guidelines combine aspects of ICP and CPP directed therapy[60,61] and treatment strategies have moved from approaches simply designed to reduce ICP, toward a multifaceted approach aiming to maintain cerebral oxygen and glucose delivery. Comparison with historical controls has provided some evidence that the use of these protocolised intensive care management strategies in the care of TBI patients can reduce mortality and improve outcome[8,80,81].

There is however, a potential flaw in the use of strictly protocolised management guidelines. There exists a wide heterogeneity in TBI, both between patients, and within patients across time and space[82-84]. Minimising secondary injury to the brain after TBI requires the tailoring of metabolite supply to demand, but an 'adequate supply' may vary substantially between periods of hypermetabolism and periods of deep sedation or extensive mitochondrial dysfunction. Strictly protocolised management strategies attempt to address adequate metabolite demand for an average TBI patient but make no allowance for individual variation. The concept of individualised TBI therapy was first introduced by Miller *et al* in 1993 who noted that the empirical treatment of raised ICP was not efficacious, and suggested that treatment should be directed toward the specific cause of the raised ICP[85]. The concept that minimising cerebral ischaemia after TBI may require individual optimisation of CPP has been expounded by others[86-88].

Individualised patient management is intuitively attractive. It does, however, require clinical monitoring systems able to assess the adequacy of metabolite delivery to the brain with high temporal and spatial resolution.

2.4 Monitoring the Injured Brain

The goal of monitoring the injured brain is to facilitate the minimisation of secondary injury by detecting harmful physiological events before they cause irreversible damage. This then allows diagnosis and effective treatment of harmful pathophysiological processes and provides 'on-line' feedback to guide therapy[89].

As already noted secondary insults to the injured brain can be either systemic or cerebral in origin. Monitoring to detect these insults must also, therefore, consist of both systemic and cerebral components. Systemic variables routinely monitored on the NCU include electrocardiogram morphology, arterial blood pressure, arterial oxyhaemoglobin saturation, arterial blood analysis, central venous pressure and systemic temperature. These monitoring modalities will not be discussed further, but instead this section will concentrate on cerebral monitoring.

2.4.1 Invasive Cerebral Monitoring

2.4.1.1 Intracranial Pressure

Measurement of ICP is central to the application of both ICP and CPP directed therapy. ICP monitoring has become integral to the management of TBI in most centres and indications for its use are well established[90]. Despite this, the use of ICP monitoring is not universal[91,92] and there exists no class I evidence supporting its efficacy. Additionally some data exist to suggest that ICP directed therapy may result in increased levels of therapy intensity and prolonged mechanical ventilation compared to clinically guided therapy, without evidence for improved outcome after severe head injury[93].

Two main methods exist for the invasive measurement of ICP. The 'gold standard' technique remains a pressure transducer connected to a catheter with its tip positioned in the lateral ventricle. This method ensures that a global pressure measurement is recorded and has the additional advantages of allowing periodic external calibration and therapeutic CSF drainage. However, placement of the ventricular catheter may be difficult in cases of severely raised ICP and there is a significant risk of developing ventriculitis with its attendant

increased morbidity and mortality[94]. Transducer tipped systems can be placed in the brain parenchyma or subdural space, either through a skull bolt on the NCU or by an open technique during a neurosurgical procedure, with minimal infection and complication rates[95]. Measured pressure, however, may not be representative of true CSF pressure as interhemispheric supratentorial intracranial pressure gradients in TBI patients have been demonstrated and whilst these systems have been shown to perform well during bench testing[96], drift will still occur during long term monitoring. In addition to absolute ICP levels, information can also be gained from analysis of ICP waveform[97].

2.4.1.2 Jugular Venous Oximetry

Jugular venous oximetry is a technique which can be used to estimate the balance between global cerebral oxygen delivery and utilisation. A catheter is inserted into the dominant internal jugular vein and advanced to the jugular bulb, therefore minimising contamination from extracerebral venous return. Once catheter positioning has been checked on a lateral cervical spine radiograph, then measurement of $SjvO_2$ can be made either continuously using a spectroscopic technique, or directly by aspirating blood samples and using a co-oximeter. Reduced $SjvO_2$ indicates that cerebral oxygen delivery is inadequate to meet demand. In the context of TBI this is most often related to reduced CBF, secondary to decreased CPP or hyperventilation associated vasoconstriction. Conversely raised $SjvO_2$ indicates luxury perfusion caused by either raised CBF or reduced oxygen demand secondary to mitochondrial dysfunction or cell death. Reduction in $SjvO_2$ below 50% after TBI is associated with poor outcome[98], and $SjvO_2$ is responsive to changes in CPP[99]. However the use of jugular venous oximetry has never been shown to improve outcome after TBI. A major limitation of jugular venous oximetry is its lack of sensitivity to regional changes and PET data exist suggesting that low $SjvO_2$ values only occur after TBI when a significant volume of the brain becomes ischaemic[100]. $SjvO_2$ is a flow weighted average of cerebral venous oxygen saturation and has been shown to correlate poorly with regional tissue oxygenation in areas of focal pathology[101]. It is also possible that significant arteriovenous shunting, after TBI, might interfere with this measurement. In

addition, current monitors suffer severely from artefacts and require frequent recalibration.

2.4.1.3 Tissue Oxygen Tension

Invasive probes have been developed to monitor focal $PbrO_2$. Currently only one $PbrO_2$ monitor is commercially available for use in humans, (Licox, GMS, Kiel-Mielkendorf, Germany). This $PbrO_2$ probe utilises a closed polarographic (Clark-type) cell with electrochemical electrodes. Oxygen, which has diffused from the brain tissue across a semi-permeable membrane, is reduced by a gold polarographic cathode. This reaction produces a flow of electrical current directly proportional to the oxygen concentration and related to the brain temperature[102]. Measured $PbrO_2$ represents the balance between oxygen delivery and cellular oxygen consumption. However it requires oxygen diffusion to the probe and will therefore be affected by changes in diffusion distance from capillary to probe as well as the proportion of arterioles and venules in the region of interest, and it has been suggested that this may determine whether measured $PbrO_2$ more closely relates to CBF or oxygen extraction fraction[103]. $PbrO_2$ probes provide a highly focal measurement and whilst this offers the potential of selectively monitoring critically perfused tissue, it means that probe positioning is crucial and that global changes may be missed.

Studies in human subjects with uncompromised cerebral circulation undergoing elective cerebrovascular surgery suggest that normal $PbrO_2$ values are in the region of 4.7 to 6.7 kPa[104,105]. Studies in patients following TBI have shown that $PbrO_2$ increases with CPP and importantly that the ceiling of this effect is higher in areas of focal ischaemia[106,107]. Comparative studies have also shown correlation between $PbrO_2$ and regional CBF, and between changes in $PbrO_2$ and changes in regional venous oxygen saturation measured using PET. It has been demonstrated that reduced $PbrO_2$ is associated with poor outcome after TBI, yet the threshold for hypoxia has proved more difficult to identify and is likely to be related to both the duration and level of hypoxia. Ischaemic thresholds of between 0.7 and 2.7 kPa have been suggested[108-111]. It is clear that $PbrO_2$ can be altered using clinical intervention, and that measured levels relate to outcome. What is less clear is whether manipulation of this

variable can affect outcome. Recent evidence, however, suggests that $PbrO_2$ directed therapy can improve outcome and this possibility merits further investigation[112].

2.4.1.4 Cerebral Microdialysis

Cerebral MD is a well established laboratory tool and is being increasingly used as a bedside monitor to provide on-line analysis of brain tissue biochemistry during neurointensive care. A MD catheter consists of a fine double lumen probe, lined at its tip with a semi-permeable dialysis membrane. The probe tip is placed into biological tissue and perfused via an inlet tube with fluid isotonic to the tissue interstitium. The perfusate passes along the membrane before exiting via outlet tubing into a collecting chamber (figure 2.4).

Figure 2.4: Components of clinical MD catheter. 1, pump connector; 2, inlet tube; 3, MD catheter; 4, MD membrane; 5, outlet tube; 6, microvial holder; 7, microvial for collection of microdialysate (taken from [113].

Diffusion drives the passage of molecules across the membrane along their concentration gradient. The MD catheter therefore acts as an artificial blood capillary and the concentration of substrate in the collected fluid (microdialysate) depends in part on the balance between substrate delivery to, and uptake/excretion from, the ECF[113](figure 2.5).

Figure 2.5: Schematic representation of relationship between blood capillary and MD catheter in brain tissue (taken from [113].

Placement of the MD catheter in 'at risk' tissue, such as the area surrounding a mass lesion after traumatic brain injury allows biochemical changes to be measured in the area of brain most vulnerable to secondary damage (figure 2.6). Guidance has been issued on catheter placement for monitoring patients after TBI and positioning should be checked by subsequent computed tomography scan[114].

Commercial assays are available to measure dialysate concentrations of glucose, lactate, pyruvate, glycerol and glutatate, and tentative normal values for these variables have been described (table 2.1)[115,116].

Figure 2.6: Changes in LPR in 'at-risk' (A) and normal appearing (B) brain during a period of low and normal CPP. The normal range for LPR is shown by the shaded area. Note the increase in LPR in the 'at-risk' tissue during a period of cerebral hypoperfusion with normal values measured by the catheter in normally appearing brain (taken from [113].

Table 2.1: Suggested normal concentrations of commonly measured biochemical markers in microdialysate samples from the uninjured human brain, collected at a perfusate flow rate of 0.3 μL min^{-1} (taken from [113].

The pathophysiological changes associated with commonly monitored cerebral MD biomarkers have been reviewed recently [113,117] and are summarised in table 2.2.

The measurement of MD lactate and pyruvate concentrations provides information on the extent of anaerobic glycolysis, and the extracellular LPR reflects the intracellular redox state - a marker of mitochondrial function[118,119]. LPR is a more robust and reliable biomarker of tissue ischaemia than lactate concentration alone[120] and, because lactate and pyruvate have very similar molecular weights, the LPR is independent of catheter recovery *in vivo*[121]. LPR is therefore the most widely monitored MD variable after TBI.

In the human brain, severe hypoxia/ischaemia is typically associated with marked increases in the LPR[122] which correlates with PET measured oxygen extraction fraction[123]. An increase in LPR above established thresholds (20-25) is associated with poor outcome in TBI[32,33], and has traditionally been assumed to indicate tissue ischaemia. However, it has proved difficult to establish the tissue hypoxic threshold for a raised LPR[57] and it is increasingly apparent that anaerobic glycolysis may occur due to failure of effective utilisation of delivered oxygen because of mitochondrial failure as well as because of hypoxia/ischaemia[124].

The use of cerebral MD may be able to assist in clinical decision making, such as management of cerebral perfusion pressure[88], guidance of hyperventilation[125] and the appropriateness of extensive surgical procedures[126].

Table 2.2: Biochemical markers of secondary brain injury (taken from [113].

2.4.2 Non-invasive Cerebral Monitoring

2.4.2.1 Cerebral Blood Flow Velocity

Transcranial Doppler ultrasonography (TCD) is a non-invasive technique which uses ultrasound waves to derive cerebral blood flow velocity from the Doppler shift caused by red blood cells moving through the field of view. TCD is not able to provide absolute measurements of CBF, but if the angle of insonation and the diameter of the insonated vessel remain constant then changes in TCD measured cerebral blood flow velocity correlate with changes in CBF. Several studies have shown minimal changes in the diameter of basal cerebral arteries during various physiological challenges[127,128]. The TCD signal is directed through areas of thin cranium and can then insonate several vessels arising from the circle of Willis. The transtemporal route is most commonly employed

although measurements can also be made through the suboccipital or transorbital routes. TCD has been used to test autoregulatory reserve by monitoring changes in cerebral blood flow velocity in response to changes in MAP and this technique may have a role in providing an individual-specific CPP target[129]. Typical TCD instrumentation for continuous monitoring is shown in figure 2.7.

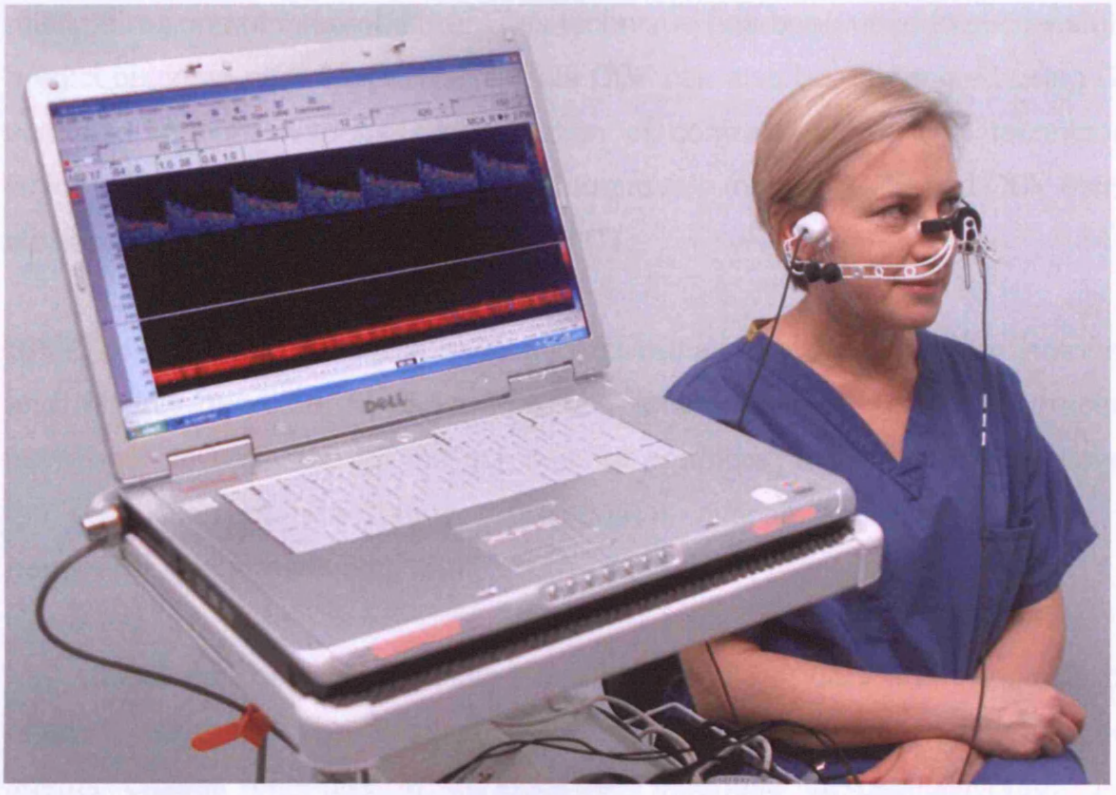

Figure 2.7: TCD instrumentation with probes fixed in place for continuous monitoring.

2.4.2.2 Imaging Techniques

Cerebral imaging techniques such CT, SPECT, MRI, MRS, and PET can provide detailed haemodynamic and metabolic information over multiple regions of interest. Many of these techniques are powerful research tools, yet they are all limited by two disadvantages.

Firstly they are only able to provide snapshot images of the brain and therefore cannot be used to track the course of brain injury over time and are therefore restricted in their ability to guide neuroprotective treatments strategies.

Secondly they require the transfer of critically ill patients to specialised imaging facilities: a process which can be detrimental to the patient's condition, especially in the context of raised ICP, and may preclude investigation of the sickest amongst them, who may be most at need of the investigation.

Xenon enhanced CT is a technique which uses CT scanning during inhalation of 30% xenon gas in oxygen to measure regional cerebral blood flow across multiple regions of interest. [130]. This technique has been used to successfully predict outcome after TBI[131]. Absolute CBF can also be determined using CT scanning and intravenous administration of contrast agent. This technique, which is known as CT perfusion is able to provide maps of CBF and CBV using similar methodology to Xenon enhanced CT.

SPECT is a technique which uses gamma radiation emitting nuclear isotopes and multiple detectors to generate tomographic images[132]. Several tracers have been investigated for the purposes of producing maps of CBF. However the production of quantitative information is difficult and image quality is generally of poor resolution[130].

MRI studies can be used to obtain information on CBF, CBV and the presence of acute ischaemia. The introduction of gadolinium based intravascular contrast agents causes changes in intravascular magnetic susceptibility[130] and perfusion-weighted MRI techniques can be used to derive information regarding CBF and CBV. However the generation of absolute values has proved difficult and most studies therefore present relative CBF and CBV[132]. MRS uses similar technology to MRI and is able to assess the metabolic state of the brain, non-invasively and without using exogenous tracers. It detects magnetic resonance signals from individual tissue solutes rather than just water and lipids as in the case in standard MRI[133]. Signals relating to either hydrogen or phosphorous nuclei are most commonly obtained and can provide information relating to adenosine triphosphate, lactate and phosphocreatine concentrations. Data can either be obtained for a single region of interest, or, given longer acquisition times, metabolite maps can be produced. Many studies have been

published using MRS to investigate TBI in animal models and human studies are now forthcoming[133].

PET remains the gold standard technique for the imaging of cerebral blood flow and metabolite concentrations in the injured brain. It is, however, hampered by the requirement for radioactive tracers and it is not widely available. PET uses photon detectors to detect electromagnetic radiation produced from the collision of electrons and positrons and is thus able to monitor the accumulation of positron-emitting radioisotopes within the brain. The tracer 15-oxygen is used to measure CBF, CBV, $CMRO_2$ and oxygen extraction fraction, while 18-fluorodeoxyglucose is used to measure cerebral glucose metabolism[132]. PET studies in humans have demonstrated the wide inter-patient heterogeneity present after TBI[83] and have tried to define ischaemic thresholds after head injury[134]. Due to the practicalities of its use, and its availability, PET is primarily a research tool and is unlikely to become part of routine clinical care.

2.5 Summary

Invasive cerebral monitoring techniques are able to provide continuous information at the bedside, but can only provide information on a single and hyperfocal area of the brain and carry an attendant risk of complications. Imaging techniques are the gold standard for providing structural, haemodynamic and metabolic information with high spatial resolution over multiple sites. However they have greatly reduced temporal resolution and require the transfer of critically ill patients.

There is a need for a non-invasive bedside monitoring technique which is able to provide realtime quantitative haemodynamic and metabolic information at multiple sites with high temporal and spatial resolution. Several techniques which meet some or all of these criteria are being investigated such as electrocorticography[135], fluorescence spectroscopy[136] and photoacoustic spectroscopy[137].

NIRS involves the measurement of changes in the attenuation of near infrared light due to absorption and scatter by tissue. This technique has the potential to

fulfil all of the criteria detailed above, with the exception of the high spatial resolution, and thus is an attractive option as a system for monitoring the injured brain. NIRS will be described in detail in chapter 3.

References

1. Teasdale G, Jennett B. Assessment of coma and impaired consciousness. A practical scale. *Lancet* 1974;2:81-84.
2. Yates PJ, Williams WH, Harris A, Round A, Jenkins R. An epidemiological study of head injuries in a UK population attending an emergency department. *J Neurol Neurosurg Psychiatry* 2006;77:699-701.
3. Murray GD, Teasdale GM, Braakman R, Cohadon F, Dearden M, Iannotti F, Karimi A, Lapierre F, Maas A, Ohman J, Persson L, Servadei F, Stocchetti N, Trojanowski T, Unterberg A. The European Brain Injury Consortium survey of head injuries. *Acta Neurochir (Wien)* 1999;141:223-236.
4. Marshall LF, Gautille T, Klauber MR, Eisenberg HM, Jane JA, Luerssen TG, Marmarou A, Foulkes MA. The outcome of severe closed head injury. *J Neurosurg* 1991;75:28-36.
5. Murray LS, Teasdale GM, Murray GD, Miller DJ, Pickard JD, Shaw MD. Head injuries in four British neurosurgical centres. *Br J Neurosurg* 1999;13:564-569.
6. Hoyert DL, Heron MP, Murphy SL, Kung HC. Deaths: final data for 2003. *Natl Vital Stat Rep* 2006;54:1-120.
7. Anderson RN, Smith BL. Deaths: leading causes for 2002. *Natl Vital Stat Rep* 2005;53:1-89.
8. Fakhry SM, Trask AL, Waller MA, Watts DD. Management of brain-injured patients by an evidence-based medicine protocol improves outcomes and decreases hospital charges. *J Trauma* 2004;56:492-499.
9. Mulvey JM, Dorsch NWC, Mudaliar Y, Lang EW. Multimodality monitoring in severe traumatic brain injury: the role of brain tissue oxygenation monitoring. *Neurocrit Care* 2004;1:402.
10. Maxwell WL, Watt C, Graham DI, Gennarelli TA. Ultrastructural evidence of axonal shearing as a result of lateral acceleration of the head in non-human primates. *Acta Neuropathol (Berl)* 1993;86:136-144.
11. Povlishock JT, Christman CW. The pathobiology of traumatically induced axonal injury in animals and humans: a review of current thoughts. *J Neurotrauma* 1995;12:555-564.

12. Reilly PL. Brain injury: the pathophysiology of the first hours.'Talk and Die revisited'. *J Clin Neurosci* 2001;8:398-403.
13. Erb DE, Povlishock JT. Axonal damage in severe traumatic brain injury: an experimental study in cat. *Acta Neuropathol (Berl)* 1998;76:347-358.
14. Gaetz M. The neurophysiology of brain injury. *Clin Neurophysiol* 2004;115:4-18.
15. Neumar RW. Molecular mechanisms of ischemic neuronal injury. *Ann Emerg Med* 2000;36:483-506.
16. Ostrowski RP, Colohan AR, Zhang JH. Molecular mechanisms of early brain injury after subarachnoid hemorrhage. *Neurol Res* 2006;28:399-414.
17. Chesnut RM. Secondary brain insults after head injury: clinical perspectives. *New Horiz* 1995;3:366-375.
18. Unterberg AW, Stover JF, Kress B, Kiening KL. Edema and brain trauma. *Neuroscience* 2004;129:1019-1027.
19. Schmidt OI, Heyde CE, Ertel W, Stahel PF. Closed head injury - an inflammatory disease? *Brain Res Brain Res Rev* 2005;48:388-399.
20. Goldberg MP, Choi DW. Combined oxygen and glucose deprivation in cortical cell culture: calcium-dependent and calcium-independent mechanisms of neuronal injury. *J Neurosci* 1993;13:3510-3524.
21. Choi DW. Ionic dependence of glutamate neurotoxicity. *J Neurosci* 1987;7:369-379.
22. Crompton M. The mitochondrial permeability transition pore and its role in cell death. *Biochem J* 1999;341:233-249.
23. Miller JD, Becker DP. Secondary insults to the injured brain. *J Royal Coll Surg (Edinburgh)* 1982;27:298.
24. Miller JD, Sweet RC, Narayan R, Becker DP. Early insults to the injured brain. *JAMA* 1978;240:439442-442.
25. Miller JD, Butterworth JF, Gudeman SK, Faulkner JE, Choi SC, Selhorst JB, Harbison JW, Lutz HA, Young HF, Becker DP. Further experience in the management of severe head injury. *J Neurosurg* 1981;54:289-299.
26. Jones PA, Andrews PJD, Midgley S, Anderson SI, Piper IR, Tocher JL, Housley AM, Corrie JA, Slattery J, Dearden NM, Miller JD. Measuring the burden of secondary insults in head-injured patients during intensive care. *J Neurosurg Anesth* 1994;6:4-14.

27. Astrup J, Siesjo Bk, Symon L. Thresholds in cerebral ischemia - the ischemic penumbra. *Stroke* 1981;12:723-725.
28. Jones TH, Morawetz RB, Crowell RM, Marcoux FW, FitzGibbon SJ, DeGirolami U, Ojemann RG. Thresholds of focal cerebral ischemia in awake monkeys. *J Neurosurg* 1981;54:773-782.
29. Bouma GJ, Muizelaar P, Choi SC, Newlon PG, Young HF. Cerebral circulation and metabolism after severe traumatic brain injury: the elusive role of ischaemia. *J Neurosurg* 1991;75:685-693.
30. Zauner A, Daugherty W, Bullock M, Warner D. Brain oxygenation and energy metabolism: part I-biological function and pathophysiology. *Neurosurgery* 2002;51:289-302.
31. Zauner A, Clausen T, Alves OL, Rice A, Levasseur J, Young HF, Bullock R. Cerebral metabolism after fluid-percussion injury and hypoxia in a feline model. *J Neurosurg* 2002;97:643-649.
32. Zauner A, Doppenberg E, Woodward J, Choi S, Young H, Bullock R. Continuous monitoring of cerebral substrate delivery and clearance: initial experience in 24 patients with severe acute brain injuries. *Neurosurgery* 1997;41:1082-1093.
33. Hutchinson P, Al-Rawi P, O'Connell M, Gupta A, Maskell L, Hutchinson D, Pickard J, Kirkpatrick P. On-line monitoring of substrate delivery and brain metabolism in head injury. *Acta Neurochir Suppl* 2000;76:431-435.
34. Benveniste H, Drejer J, Schousboe A, Diemer NH. Elevation of the extracellular concentrations of glutamate and aspartate in rat hippocampus during transient cerebral ischaemia monitored by intracellular microdialysis. *J Neurochem* 1984;43:1369-74.
35. Katayama Y, Becker DP, Tamura T, Hovda DA. Massive increases in extracellular potassium and the indiscriminate release of glutamate following concussive brain injury. *J Neurosurg* 1990;73:889-900.
36. Lucas DR, Newhouse JP. The toxic effect of sodium L-glutamate on the inner layers of the retina. *Arch Opthalmol* 1957;58:193-201.
37. Olney JW, Ho OL, Rhee V. Cytotoxic effects of acidic and sulphur containing amino acids on the infant mouse central nervous system. *Exp Brain Res* 1971;14:61-76.

38. Goforth PB, Ellis EF, Satin LS. Enhancement of AMPA-mediated current after traumatic injury in cortical neurons. *J Neurosci* 1999;19:7367-7374.
39. Tymianski M, Tator C. Normal and abnormal calcium homeostasis in neurons: a basis for the pathophysiology of traumatic and ischemic central nervous system injury. *Neurosurgery online* 1996;38:1176-1195.
40. Choi DW. Glutamate neurotoxicity and diseases of the nervous system. *Neuron* 1988;1:623-634.
41. Young W. Role of calcium in central nervous system injuries. *J Neurotrauma* 1992;9:9-25.
42. Cherian L, Goodman JC, Robertson CS. Brain nitric oxide changes after controlled cortical impact injury in rats. *J Neurophysiol* 2000;83:2171-2178.
43. Povlishock J, Kontos HA. The role of oxygen radicals in the pathobiology of traumatic brain injury. *Hum Cell* 1992;5:345-353.
44. Tavazzi B, Signoretti S, Lazzarino G, Amorini AM, Delfini R, Cimatti M, Marmarou A, Vagnozzi R. Cerebral oxidative stress and depression of energy metabolism correlate with severity of diffuse brain injury in rats. *Neurosurgery* 2005;56:582-589.
45. Cazevieille C, Muller A, Meynier F, Bonne C. Superoxide and nitric oxide cooperation in hypoxia/reoxygenation-induced neuron injury. *Free Radic Biol Med* 1993;14:389-395.
46. Siesjo Bk. Basic mechanisms of traumatic brain damage. *Annals of emergency medicine* 1993;22:959-969.
47. Sinz EH, Kochanek PM, Dixon CE, Clark RSB, Carcillo JA, Schiding JK, Chen M, Wisniewski SR, Carlos TM, Williams D, DeKosky ST, Watkins SC, Marion DW, Billiar TR. Inducible nitric oxide synthase is an endogenous neuroprotectant after traumatic brain injury in rats and mice. *J Clin Invest* 1999;104:647-656.
48. Hlatky R, Goodman JC, Valadka AB, Robertson CS. Role of nitric oxide in cerebral blood flow abnormalities after traumatic brain injury. *J Cereb Blood Flow Metab* 2003;23:582-588.
49. Lu J, Moochhala S, Shirhan M, Ng KC, Tan MH, Teo AL, Ling EA. Nitric oxide induces macrophage apoptosis following traumatic brain injury in rats. *Neurosci Lett* 2003;339:147-150.

50. Blough NV, Zafiriou OC. Reactions of superoxide with nitric oxide to from peroxynitrite in alkaline aqueous solution. *Inorg Chem* 1985;24:3502-3504.
51. Marks JD, Boriboun C, Wang J. Mitochondrial nitric oxide mediates decreased vulnerability of hippocampal neurons from immature animals to NMDA. *J Neurosci* 2005;25:6561-6575.
52. Moncada S, Bolanos JP. Nitric oxide, cell bioenergetics and neurodegeneration. *J Neurochem* 2006;97:1676-1689.
53. Xiong Y, Gu Q, Peterson PL, Muizelaar JP, Lee CP. Mitochondrial dysfunction and calcium perturbation induced by traumatic brain injury. *J Neurotrauma* 1997;14:23-34.
54. Verweij BH, Muizelaar JP, Vinas FC, Peterson PL, Xiong Y, Lee CP. Impaired cerebral mitochondrial function after traumatic brain injury in humans. *J Neurosurg* 2000;93:815-820.
55. Sullivan PG, Rabchevsky AG, Waldmeier PC, Springer JE. Mitochondrial permeability transition in CNS trauma: cause or effect of neuronal cell death? *J Neurosci Res* 2005;79:231-239.
56. Blomgren K, Zhu C, Hallin U, Hagberg H. Mitochondria and ischemic reperfusion damage in the adult and in the developing brain. *Biochem Biophys Res Commun* 2003;304:551-559.
57. Johnston AJ, Steiner LA, Coles JP, Chatfield DA, Fryer TD, Smielewski P, Hutchinson PJ, O'Connell MT, Al-Rawi PG, Aigbirihio FI, Clark JC, Pickard JD, Gupta AK, Menon DK. Effect of cerebral perfusion pressure augmentation on regional oxygenation and metabolism after head injury. *Crit Care Med* 2005;33:189-195.
58. Hovda DA, Yoshino A, Kawamata T, Katayama Y, Becker DP. Diffuse prolonged depression of cerebral oxidative metabolism following concussive brain injury in the rat: a cytochrome oxidase histochemistry study. *Brain Res* 1991;567:1-10.
59. Narayan RK, Michel ME, Ansell B, Baethmann A, Biegon A, Bracken MB, Bullock MR, Choi SC, Clifton GL, Contant CF, Coplin WM, Dietrich WD, Ghajar J, Grady SM, Grossman RG, Hall ED, Heetderks W, Hovda DA, Jallo J, Katz RL, Knoller N, Kochanek PM, Maas AI, Majde J, Marion DW, Marmarou A, Marshall LF, McIntosh TK, Miller E, Mohberg N, Muizelaar JP, Pitts LH. Clinical trials in head injury. *J Neurotrauma* 2002;19:503-557.

60. American Association of Neurological Surgeons JSoNaCC. Guidelines for the management of severe head injury. Brain Trauma Foundation. *J Neurotrauma* 1996;13:641-734.
61. Maas AI, Dearden M, Teasdale GM, Braakman R, Cohadon F, Iannotti F, Karimi A, Lapierre F, Murray G, Ohman J, Persson L, Servadei F, Stocchetti N, Unterberg A. EBIC-guidelines for management of severe head injury in adults. European Brain Injury Consortium. *Acta Neurochir (Wien)* 1997;139:286-294.
62. Chesnut RM, Marshall LF, Klauber MR, Blunt BA, Baldwin N, Eisenberg HM, Jane JA, Marmarou A, Foulkes MA. The role of secondary brain injury in determing outcome from severe head injury. *J Trauma* 1993;34:216-222.
63. Becker DP, Miller JD, Ward JD, Greenberg RP, Young HF, Sakalas R. The outcome from severe head injury with early diagnosis and intensive management. *J Neurosurg* 1977;47:491-502.
64. Miller JD, Becker DP, Ward JD, Sullivan HG, Adams WE, Rosner MJ. Significance of intracranial hypertension in severe head injury. *J Neurosurg* 1977;47:503-516.
65. Narayan RK, Kishore PR, Becker DP, Ward JD, Enas GG, Greenberg RP, Domingues Da SA, Lipper MH, Choi SC, Mayhall CG, Lutz HA, III, Young HF. Intracranial pressure: to monitor or not to monitor? A review of our experience with severe head injury. *J Neurosurg* 1982;56:650-659.
66. Marmarou A, Anderson RL, Ward JD, Choi SC, Young HF, Eisenberg HM, Foulkes MA, Marshall LF, Jane JA. Impact of ICP instability and hypotension on outcome in patients with severe head trauma. *J Neurosurg* 1991;75:59-66.
67. Eisenberg HM, Frankowski RF, Contant CF, Marshall LF, Walker MD. High-dose barbiturate control of elevated intracranial pressure in patients with severe head injury. *J Neurosurg* 1988;69:15-23.
68. Marshall LF, Smith RW, Shapiro HM. The outcome with aggressive treatment in severe head injuries. Part I: the significance of intracranial pressure monitoring. *J Neurosurg* 1979;50:21-25.

69. Rosner MJ, Becker DP. Origin and evolution of plateau waves. Experimental observations and a theoretical model. *J Neurosurg* 1984;60:312-324.
70. Rosner MJ, Daughton S. Cerebral perfusion pressure management in head injury. *J Trauma* 1990;30:933-940.
71. Engelborghs K, Haseldonckx M, Van Reempts J, Van Rossem K, Wouters L, Borgers M, Verlooy J. Impaired autoregulation of cerebral blood flow in an experimental model of traumatic brain injury. *J Neurotrauma* 2000;17:667-677.
72. Ter Minassian A, Dubé L, Guilleux AM, Wehrmann N, Ursino M, Beydon L. Changes in intracranial pressure and cerebral autoregulation in patients with severe traumatic brain injury. *Crit Care Med* 2002;30:1616-1622.
73. Lewelt W, Jenkins LW, Miller JD. Autoregulation of cerebral blood flow after experimental fluid percussion injury of the brain. *J Neurosurg* 1980;53:500-511.
74. Rosner MJ, Rosner SD, Johnson AH. Cerebral perfusion pressure: management protocol and clinical results. *J Neurosurg* 1995;83:949-962.
75. Robertson CS, Valadka AB, Hannay HJ, Contant CF, Gopinath SP, Cormio M, Uzura M, Grossman RG. Prevention of secondary ischemic insults after severe head injury. *Crit Care Med* 1999;27:2086-2095.
76. Bratton SL, Davis RL. Acute lung injury in isolated traumatic brain injury. *Neurosurgery* 1997;40:707-712.
77. Juul N, Morris GF, Marshall SB, Marshall LF. Intracranial hypertension and cerebral perfusion pressure: influence on neurological deterioration and outcome in severe head injury. The Executive Committee of the International Selfotel Trial. *J Neurosurg* 2000;92:1-6.
78. Grande PO. The "Lund Concept" for the treatment of severe head trauma - physiological principles and and clinical application. *Intensive Care Med* 2006;32:1475-1484.
79. Eker C, Asgeirsson B, Grande PO, Schalen W, Nordstrom CH. Improved outcome after severe head injury with a new therapy based on principles for brain volume regulation and preserved microcirculation. *Crit Care Med* 1998;26:1881-1886.

80. Clayton TJ, Nelson RJ, Manara AR. Reduction in mortality from severe head injury following introduction of a protocol for intensive care management. *Br J Anaesth* 2004;93:761-767.
81. Patel HC, Menon DK, Tebbs S, Hawker R, Hutchinson PJ, Kirkpatrick PJ. Specialist neurocritical care and outcome from head injury. *Intensive Care Med* 2002;28:547-553.
82. Coles JP, Fryer TD, Bradley PG, Nortje J, Smielewski P, Rice K, Clark JC, Pickard JD, Menon DK. Intersubject variability and reproducibility of 15O PET studies. *J Cereb Blood Flow Metab* 2006;26:48-57.
83. Coles JP. Regional ischemia after head injury. *Curr Opin Crit Care* 2004;10:120-125.
84. Vespa P, McArthur DL, Alger J, O'Phelan K, Hattori N, Wu C, Glenn T, Bergsneider M, Martin NA, Hovda DA. Regional heterogeneity of post-traumatic brain metabolism as studied by microdialysis, magnetic resonance spectroscopy and positron emission tomography. *Brain Pathol* 2004;14:210-214.
85. Miller JD, Piper IR, Dearden NM. Management of intracranial hypertension in head injury: matching treatment with cause. *Acta Neurochir Suppl (Wien)* 1993;57:152-159.
86. Robertson CS. Management of cerebral perfusion pressure after traumatic brain injury. *Anesthesiology* 2001;95:1513-1517.
87. Vespa P. What is the optimal threshold for cerebral perfusion pressure following traumatic brain injury? *Neurosurg Focus* 2003;15:E4.
88. Nordstrom C, Reinstrup P, Xu W, Gardenfors A, Ungerstedt U. Assessment of lower limit for cerebral perfusion pressure in severe head injuries by bedside monitoring of regional energy metabolism. *Anesthesiology* 2003;98:809-14.
89. Gupta AK (2001) Application of multimodal monitoring. In: *Notes in Neuroanaesthesia and Critical Care* (Gupta AK, Summors A, eds), London: Greenwich Medical Media, pp 260-262
90. Smith M. Monitoring intracranial pressure in traumatic brain injury. *Anesth Analg* 2008;106:240-248.

91. Bulger EM, Nathens AB, Rivara FP, Moore M, MacKenzie EJ, Jurkovich GJ. Management of severe head injury: institutional variations in care and effect on outcome. *Crit Care Med* 2002;30:1870-1876.
92. Hesdorffer DC, Ghajar J, Iacono L. Predictors of compliance with the evidence-based guidelines for traumatic brain injury care: a survey of United States trauma centers. *J Trauma* 2002;52:1202-1209.
93. Cremer O, van Dijk G, van Wenson E, Brekelmans G, Moons K, Leenen L, Kalkman C. Effect of intracranial pressure monitoring and targeted intensive care on functional outcome after severe head injury. *Crit Care Med* 2005;33:2207-2213.
94. Lozier AP, Sciacca RR, Romagnoli MF, Connolly ES Jr. Ventriculostomy-related infections: a critical review of the literature. *Neurosurgery* 2002;51:170-181.
95. Martinez-Manas RM, Santamarta D, de Campos JM, Ferrer E. Camino intracranial pressure monitor: prospective study of accuracy and complications. *J Neurol Neurosurg Psychiatry* 2000;69:82-86.
96. Czosnyka M, Czosnyka Z, Pickard JD. Laboratory testing of three intracranial pressure microtransducers: technical report. *Neurosurgery* 1996;38:219-224.
97. Czosnyka M, Guazzo E, Whitehouse M, Smielewski P, Czosnyka Z, Kirkpatrick P, Piechnik S, Pickard JD. Significance of intracranial pressure waveform analysis after head injury. *Acta Neurochir (Wien)* 1996;138:531-541.
98. Robertson CS, Gopinath SP, Goodman JC, Contant CF, Valadka AB, Narayan RK. SjvO2 monitoring in head-injured patients. *J Neurotrauma* 1995;12:891-896.
99. Murr R, Schurer L. Correlation of jugular venous oxygen saturation to spontaneous fluctuations of cerebral perfusion pressure in patients with severe head injury. *Neurol Res* 1995;17:329-333.
100. Coles J, Fryer T, Smielewski P, Chatfield D, Steiner L, Johnston A, Downey S, Williams G, Aigbirhio F, Hutchinson P, Rice K, Carpenter T, Clark J, Pickard J, Menon D. Incidence and mechanisms of cerebral ischemia in early clinical head injury. *J Cereb Blood Flow Metab* 2004;24:202-211.

101. Gupta AK, Hutchinson PJ, al-Rawi P, Gupta S, Swart M, Kirkpatrick PJ, Menon DK, Datta AK. Measuring brain tissue oxygenation compared with jugular venous oxygen saturation for monitoring cerebral oxygenation after traumatic brain injury. *Anesth Analg* 1999;88:549-553.
102. Nortje J, Gupta AK. The role of tissue oxygen monitoring in patients with acute brain injury. *Br J Anaesth* 2006;97:95-106.
103. Scheufler KM, Rohrborn HJ, Zentner J. Does tissue oxygen-tension reliably reflect cerebral oxygen delivery and consumption. *Anesth Analg* 2002;95:1042-1048.
104. Meixensberger J, Dings J, Kuhnigk H, Roosen K. Studies of tissue pO2 in normal and pathological human brain cortex. *Acta Neurochir Suppl (Wien)* 1993;59:58-63.
105. Hoffman WE, Charbel FT, Edelman G. Brain tissue oxygen, carbon dioxide, and pH in neurosurgical patients at risk for ischemia. *Anesth Analg* 1996;82:582-586.
106. Kiening KL, Hartl R, Unterberg AW, Schneider GH, Bardt T, Lanksch WR. Brain tissue pO2-monitoring in comatose patients: implications for therapy. *Neurol Res* 1997;19:233-240.
107. Stocchetti N, Chieregato A, De Marchi M, Croci M, Benti R, Grimoldi N. High cerebral perfusion pressure improves low values of local brain tissue O2 tension (PtiO2) in focal lesions. *Acta Neurochir Suppl* 1998;71:162-165.
108. Kiening KL, Unterberg AW, Bardt TF, Schneider GH, Lanksch WR. Monitoring of cerebral oxygenation in patients with severe head injuries: brain tissue PO2 versus jugular vein oxygen saturation. *J Neurosurg* 1996;85:751-757.
109. Valadka AB, Gopinath SP, Contant CF, Uzura M, Robertson CS. Relationship of brain tissue PO2 to outcome after severe head injury. *Crit Care Med* 1998;26:1576-1581.
110. van den Brink WA, van Santbrink H, Steyerberg EW, Avezaat CJ, Suazo JA, Hogesteeger C, Jansen WJ, Kloos LM, Vermeulen J, Maas AI. Brain oxygen tension in severe head injury. *Neurosurgery* 2000;46:868-876.

111. van Santbrink H, Maas AI, Avezaat CJ. Continuous monitoring of partial pressure of brain tissue oxygen in patients with severe head injury. *Neurosurgery* 1996;38:21-31.
112. Stiefel MF, Spiotta A, Gracias VH, Garuffe AM, Guillamondegui O, Maloney-Wilensky E, Bloom S, Grady MS, LeRoux PD. Reduced mortality rate in patients with severe traumatic brain injury treated with brain tissue oxygen monitoring. *J Neurosurg* 2005;103:805-811.
113. Tisdall MM, Smith M. Cerebral microdialysis: research technique or clinical tool. *Br J Anaesth* 2006;97:18-25.
114. Bellander BM, Cantais E, Enblad P, Hutchinson P, Nordstrom CH, Robertson C, Sahuquillo J, Smith M, Stocchetti N, Ungerstedt U, Unterberg A, Olsen NV. Consensus meeting on microdialysis in neurointensive care. *Intensive Care Med* 2004;30:2166-2169.
115. Reinstrup P, Stahl N, Mellergard P, Uski T, Ungerstedt U, Nordstrom CH. Intracerebral microdialysis in clinical practice: baseline values for chemical markers during wakefulness, anesthesia, and neurosurgery. *Neurosurgery* 2000;47:701-709.
116. Schulz M, Wang L, Tange M, Bjerre P. Cerebral microdialysis monitoring: determination of normal and ischemic cerebral metabolism in patients with aneurysmal subarachnoid hemorrhage. *J Neurosurg* 2000;93:233-8.
117. Hillered L, Vespa PM, Hovda DA. Translational neurochemical research in acute human brain injury: the current status and potential future for cerebral microdialysis. *J Neurotrauma* 2005;22:3-41.
118. Persson L, Hillered L. Chemical monitoring of neurosurgical intensive care patients using intracerebral microdialysis. *J Neurosurg* 1992;76:72-80.
119. Siesjo BK. Cerebral circulation and metabolism. *J Neurosurg* 1984;60:883-908.
120. Enblad P, Valtysson J, Andersson J, Lilja A, Valind S, Antoni G, Langstrom B, Hillered L, Persson L. Simultaneous intracerebral microdialysis and positron emission tomography in the detection of ischemia in patients with subarachnoid hemorrhage. *J Cereb Blood Flow Metab* 1996;16:637-644.
121. Persson L, Hillered L. Intracerebral microdialysis. *J Neurosurg* 1996;85:984-85.

122. Stahl N, Mellergard P, Hallstrom A, Ungerstedt U, Nordstrom CH. Intracerebral microdialysis and bedside biochemical analysis in patients with fatal traumatic brain lesions. *Acta Anaesthesiol Scand* 2001;45:977-985.
123. Hutchinson PJ, Gupta AK, Frywe T.F., Al-Rawi PG, Chatfield DA, Coles JP, O'Connell MT, Kett-White R, Minhas P.S., Aigbirhio F.I., Clark J.C., Kirkpatrick PJ, Menon DK, Pickard JD. Correlation between cerebral blood flow, substrate delivery, and metabolism in head injury: a combined microdialysis and triple oxygen positron emission tomography study. *J Cereb Blood Flow Metab* 2002;22:735-745.
124. Vespa P, Bergsneider M, Hattori N, Wu HM, Huang SC, Martin NA, Glenn TC, McArthur DL, Hovda DA. Metabolic crisis without brain ischemia is common after traumatic brain injury: a combined microdialysis and positron emission tomography study. *J Cereb Blood Flow Metab* 2005;25:763-774.
125. Marion DW, Puccio A, Wisniewski SR, Kochanek P, Dixon CE, Bullian L, Carlier P. Effect of hyperventilation on extracellular concentrations of glutamate, lactate, pyruvate, and local cerebral blood flow in patients with severe traumatic brain injury. *Crit Care Med* 2002;30:2619-2625.
126. Boret H, Fesselet J, Meaudre E, Gaillard P, Cantais E. Cerebral microdialysis and Ptio2 for neuro-monitoring before decompressive craniectomy. *Acta Anaesthesiologica Scand* 2006;50:252-254.
127. Valdueza JM, Balzer JO, Villringer A, Vogl TJ, Kutter R, Einhaupl KM. Changes in blood flow velocity and diameter of the middle cerebral artery during hyperventilation: assessment with MR and transcranial Doppler sonography. *Am J Neuroradiol* 1997;18:1929-1934.
128. Giller CA, Bowman G, Dyer H, Mootz L, Krippner W. Cerebral arterial diameters during changes in blood pressure and carbon dioxide during craniotomy. *Neurosurgery* 1993;32:737-741.
129. Czosnyka M, Smielewski P, Czosnyka Z, Piechnik S, Steiner LA, Schmidt E, Gooskens I, Soehle M, Lang EW, Matta BF, Pickard JD. Continuous assessment of cerebral autoregulation: clinical and laboratory experience. *Acta Neurochir Suppl* 2003;86:581-585.
130. Latchaw RE, Yonas H, Hunter GJ, Yuh WT, Ueda T, Sorensen AG, Sunshine JL, Biller J, Wechsler L, Higashida R, Hademenos G. Guidelines

and recommendations for perfusion imaging in cerebral ischemia: A scientific statement for healthcare professionals by the writing group on perfusion imaging, from the Council on Cardiovascular Radiology of the American Heart Association. *Stroke* 2003;34:1084-1104.

131. Inoue Y, Shiozaki T, Tasaki O, Hayakata T, Ikegawa H, Yoshiya K, Fujinaka T, Tanaka H, Shimazu T, Sugimoto H. Changes in cerebral blood flow from the acute to the chronic phase of severe head injury. *J Neurotrauma* 2005;22:1411-1418.
132. Coles JP. Imaging of cerebral blood flow and metabolism. *Curr Opin Anaesthesiol* 2006;19:473-480.
133. Brooks WM, Friedman SD, Gasparovic C. Magnetic resonance spectroscopy in traumatic brain injury. *J Head Trauma Rehabil* 2001;16:149-164.
134. Cunningham AS, Salvador R, Coles JP, Chatfield DA, Bradley PG, Johnston AJ, Steiner LA, Fryer TD, Aigbirhio FI, Smielewski P, Williams GB, Carpenter TA, Gillard JH, Pickard JD, Menon DK. Physiological thresholds for irreversible tissue damage in contusional regions following traumatic brain injury. *Brain* 2005;128:1931-1942.
135. Fabricius M, Fuhr S, Bhatia R, Boutelle M, Hashemi P, Strong AJ, Lauritzen M. Cortical spreading depression and peri-infarct depolarization in acutely injured human cerebral cortex. *Brain* 2006;129:778-790.
136. Mik E, Stap J, Sinaasappel M, Beek J, Aten J, van Leeuwen T, Ince C. Mitochondrial PO2 measured by delayed fluorescence of endogenous protoporphyrin IX. *Nature Methods* 2006;3:939-945.
137. Laufer J, Delpy D, Elwell C, Beard P. Quantitative spatially resolved measurement of tissue chromophore concentrations using photoacoustic spectroscopy: application to the measurement of blood oxygenation and haemoglobin concentration. *Phys Med Biol* 2007;52:141-168.

Chapter 3
Near Infrared Spectroscopy

In this chapter the theoretical bases of near infrared spectroscopy and the various NIRS techniques used in this thesis are discussed. Particular mention is made of the main chromophores and optical properties of biological tissue. Continuous wave spectroscopy is introduced first and then followed by a description of spatially resolved (SRS) and frequency domain spectroscopy (FDS), and techniques for measuring optical pathlength.

3.1 Principles of Light Transport in Tissue

The simplest form of spectroscopy described in this thesis is known as continuous wave spectroscopy and is based on observing the attenuation of light of fixed incident intensity, by tissue at a single constant distance *d* from the incident light. The interpretation of the attenuation data is based upon a series of observations which together from the basis of the modified Beer-Lambert Law (MBLL).

Bouguer observed in 1729 that successive layers of a homogenous material of equal thickness δd absorb the same fraction, $\partial I/I$ of light of initial intensity I which is incident upon them. This relationship, which is known as the Lambert-Bouguer law, can be stated mathematically as:

$$\frac{\partial I}{I} = -\mu_a \cdot \delta d \qquad \textit{Eqn 3.1}$$

μ_a is a constant defined as absorption coefficient (cm^{-1}).

Integration of equation 3.1 gives:

$$I = I_0 e^{-\mu_a \cdot d} \qquad \textit{Eqn 3.2}$$

I = the transmitted intensity of light of initial intensity I_0 after it has passed a distance d through a homogenous absorber with absorption coefficient μ_a.

This can also be expressed in base 10 as:

$$I = I_0 10^{-k \cdot d} \qquad \textit{Eqn 3.3}$$

k = the extinction coefficient (cm^{-1}).

Therefore

$$A = \log_{10}\left(\frac{I_0}{I}\right) = k \cdot d \qquad \textit{Eqn 3.4}$$

A = attenuation and has units of optical density (OD) when defined in log base 10.

In 1852 Beer determined a relationship between absorption coefficient and absorber concentration.[1]. He found that that for an absorber dissolved in a non-absorbing solution, the attenuation is directly proportional to the concentration of the solution, or

$$\mu_a = \alpha \cdot c \qquad \textit{Eqn 3.5}$$

c=concentration of solute (molar) and α=specific absorption coefficient ($molar^{-1}\ cm^{-1}$).

This is known as the Beer law. Combining equations 3.2 and 3.5 gives the Beer-Lambert law:

$$I = I_0 e^{-\alpha c d} \qquad \textit{Eqn 3.6}$$

A further important principle is that, for a solution containing a mixture of absorbing compounds, the extinction coefficients are additive and the total attenuation is given by the sum of the attenuations attributable to each of the absorbers. Therefore for a mixture of n absorbers dissolved in a non-absorbing solution:

$$A = (k_1 + k_2 + \ldots + k_n)d \qquad \textit{Eqn 3.7}$$

These terms can all be defined in both natural logs and log base 10 but consistency of the log base used is essential.

The Beer-Lambert law assumes that all light incident on the interrogated material is either absorbed or transmitted. It assumes therefore no reflection at tissue interfaces and no light scattering. The situation in biological tissue is more complex and does not satisfy these assumptions. In biological tissue there exist multiple boundaries between different media. Refractive index mismatches

occur at these boundaries and these will deflect photons from their initial path. This photon deflection away from a single detector gives rise to attenuation and is known as light scatter (figure 3.1). If we assume no absorption then by analogy with absorption:

$$I = I_0 e^{-\mu_s d} \qquad \textit{Eqn 3.8}$$

μ_s = the scattering coefficient (cm^{-1}).

The contribution of various tissue components to total scatter is determined by both their relative scattering efficiency and the number of scattering particles. Types of scatter interactions can be classified by the diameter of the scattering particles with respect to wavelength. Scattering caused by intracellular structures such as organelles and mitochondria with diameter less than λ/π is described by the theory of Rayleigh scattering. This describes scatter occurring when an incoming photon excites an atom into a transiently elevated state. This produces an oscillating electric dipole moment. The induced oscillating electric dipole moment then re-radiates a photon at the same frequency as the incoming photon but in a random direction travelling radially away from the centre of the interaction: this is an example of isotropic scatter. Rayleigh Ganz Debye theory describes scattering events caused by structures with diameter greater than λ/π. In this situation the large particle is considered as a collection of smaller Rayleigh scatterers with additional refraction and reflection effects taking place at boundaries. Constructive and destructive interference effects between the refracted and reflected components produce an angular dependence of the scattered intensity and thus anisotropic scatter. Biological tissue contains a large number of small Rayleigh scatterers, each with a relatively low scattering efficiency due to the low refractive mismatches with surrounding media, and a smaller number of Rayleigh Ganz Debye scatterers with a higher relative scattering efficiency.

The anisotropy (direction of scatter) is commonly characterised by the mean cosine of the scattering angle which is defined as the anisotropy factor *g*. When scattering is isotropic, g=0 and for tissue, which is predominantly forward scattering, g=0.7-0.97. In tissue multiple scattering occurs and light rapidly loses directionality. The situation can be simplified by considering a case of isotropic

scatter when the scatter coefficient has been reduced by a factor (1-*g*). This modified scattering coefficient is called the transport scattering coefficient μ_{st} and:

$$\mu_{st} = \mu_s(1-g) \qquad \textit{Eqn 3.9}$$

Light scattering has two important implications. Firstly light that is scattered may not reach the detector and so measured light attenuation will be caused by both scattering and absorption. Secondly, as photons undergo multiple scattering interactions they will travel further than the direct distance between source and detector and the chance of further scatter or absorption will relate to this optical pathlength rather than the direct distance (figure 3.1).

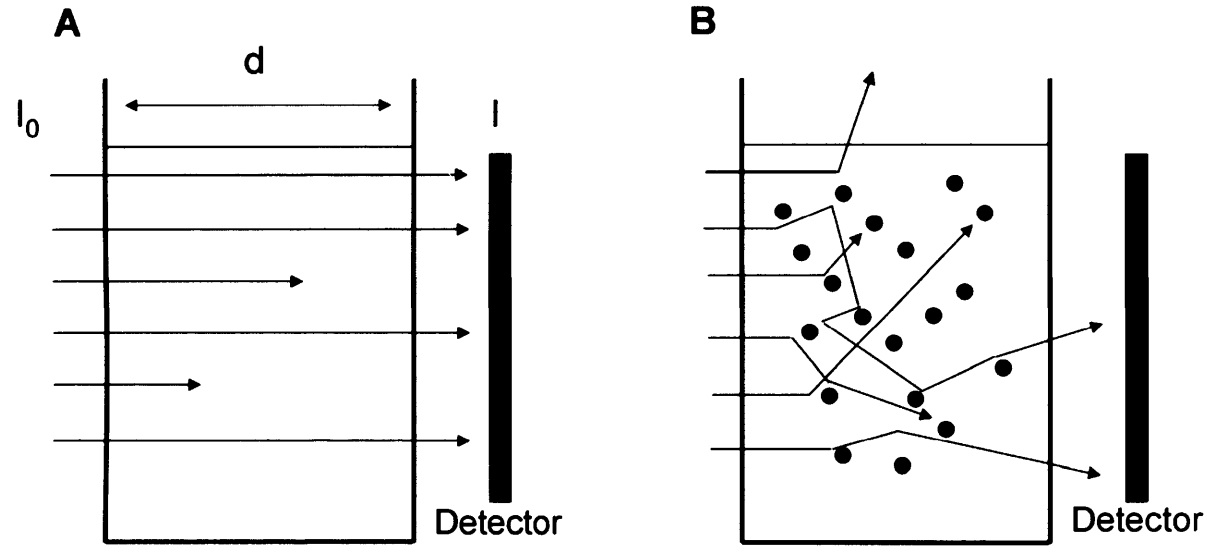

Figure 3.1: Schematic of light transport under (A) absorbing, non-scattering conditions and (B) scattering and absorbing conditions. In B the pathlength travelled is increased and a proportion of photons are scattered in such a way as to miss the detector.

The MBLL takes account of light attenuation due to scattering and the increase in optical pathlength[2]. In log base 10 it is stated as:

$$A = \log_{10}\left(\frac{I_0}{I}\right) = \varepsilon \cdot c \cdot d \cdot DPF + G \qquad \textit{Eqn 3.10}$$

G = light attenuation due to scattering, ε = the specific extinction coefficient and DPF=the differential pathlength factor, a multiplier which accounts for the increased optical pathlength due to scattering.

The majority of near infrared light absorption and scatter in biological tissue is caused by constituents whose concentration we can assume to be fixed. We can therefore make the assumption that, although attenuation due to light scatter is wavelength dependent, its magnitude at a given wavelength is fixed. This assumption allows the use of the MBLL to relate changes in light attenuation to changes in chromophore concentration which can be stated:

$$\Delta A = \Delta c \cdot \varepsilon \cdot d \cdot DPF \qquad \textit{Eqn 3.11}$$

DPF is highly dependent on the degree of light scattering, but is also dependent on μ_a and this makes intuitive sense as in the limit $\mu_a >> \mu_s$ we would revert to the Beer-Lambert Law implying that $\ln(I_0/I)$ is a non-linear function of μ_a. Diffusion theory can be used to generate theoretical relationships between $\ln(I_0/I)$ and μ_a at different values of μ_s and the local slope of the of the curve will then be the optical pathlength. When $\mu_s=0$ the relationship between $\ln(I_0/I)$ and μ_a is a straight line, corresponding to the Beer-Lambert Law, and has gradient equal to the geometric pathlength and but as μ_s increases the relationship becomes progressively non-linear (figure 3.2) and the DPF is therefore a function of both μ_a and μ_s. In general however we are measuring relatively small changes in attenuation superimposed on a large background attenuation and so the optical pathlength over the range of measurement is assumed to be constant and equation 3.11 can be employed[3]. It is possible to measure the differential pathlength factor DPF by a variety of methods and this topic will be discussed separately. Experimentally measured values of DPF for brain and muscle of children, adults and animals have been published[2,4-6].

With these assumptions and given the knowledge of ε, the source detector distance d and the differential pathlength factor DPF we are able to convert measured change in attenuation into change in chromophore concentration. At this stage it is useful to discuss the chromophores present in biological tissue.

Figure 3.2: Theoretical form of relationship between $\ln(I_0/I)$ and μ_a calculated for an infinite slab of thickness 1cm. The linear relationship corresponds to zero scattering and has slope equal to the geometric pathlength d, whereas the non-linear curves correspond to non-zero scattering and have local gradient equal to the optical pathlength d.DPF (modified from [6]).

3.2 Optical Chromophores in Biological Tissue

The main chromophores present in biological tissue are water, lipids, melanin, haemoglobin and cytochrome c oxidase.

3.2.1 Water

Water accounts for 60-90% of total body mass but its concentration varies greatly between tissue types[7]. Due to its high concentration, water is one of the main absorbers in tissue. Its extinction spectrum is shown in figure 3.3 and demonstrates that photon absorption due to water becomes extremely high above about 1700 nm. In this range photons will travel a very short distance

before being absorbed and this will limit the volume of tissue that can be interrogated.

Figure 3.3: The extinction spectra of pure water (taken from [8]).

3.2.2 Lipids

Lipids are present in the subcutaneous tissue and are the principle component of the myelin sheaths of nerves. The extinction spectrum of lipid is relatively flat with some broad peaks in the region of 650-1000 nm, but these peaks have much lower magnitude than those of water and thus have a much smaller effect on the light attenuation across cranial tissue.

3.2.3 Melanin

Melanin is present in the epidermis and is arranged in a structure which produces effective light scattering. Melanin is a significant attenuator of light especially in the ultraviolet region (200-400 nm). It serves to protect the body mainly by scattering incident photons and thus reducing the photon density.

The concentrations of each of these chromophores in tissue will not change rapidly. Over the time course of the studies described in this thesis, one can assume that their concentrations will remain stable and they can therefore be termed fixed absorbers. The chromophores of interest are those whose concentrations would be expected to change in relationship to changes in tissue physiology.

3.2.4 Haemoglobin

Haemoglobin binds to oxygen in a reversible manner to form oxy-haemoglobin and this binding of oxygen induces a conformational change in the haemoglobin molecule. HbO_2 and HHb both exhibit high absorption at wavelengths less than ~600 nm (figure 3.4). There exists a so-called 'window of transparency' between the large absorption peaks of the haemoglobin and water at wavelengths between 600-100 nm. This region is known as the near infrared (NIR) and due to the relatively low tissue absorption at these wavelengths, light incident on the skin surface can travel a sufficient distance to allow interrogation of structures beneath the tissue surface[9]. HbO_2 and HHb both have distinctive spectra within this wavelength range (figure 3.5).

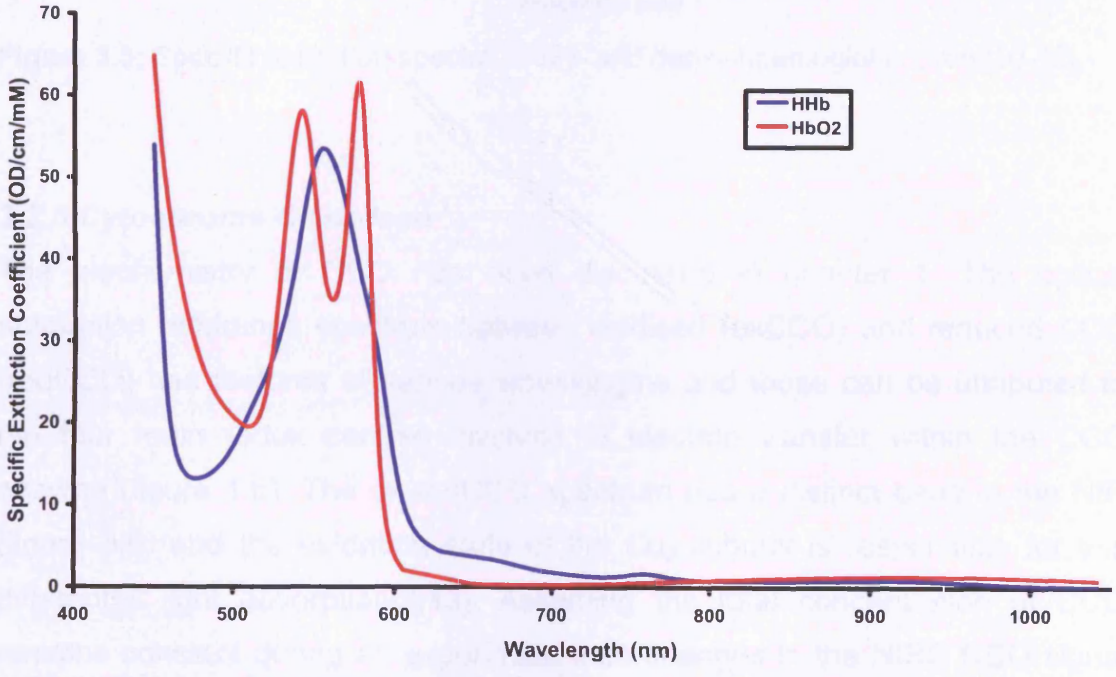

Figure 3.4: Specific extinction spectra of oxy- and deoxy-haemoglobin (from [10-12]).

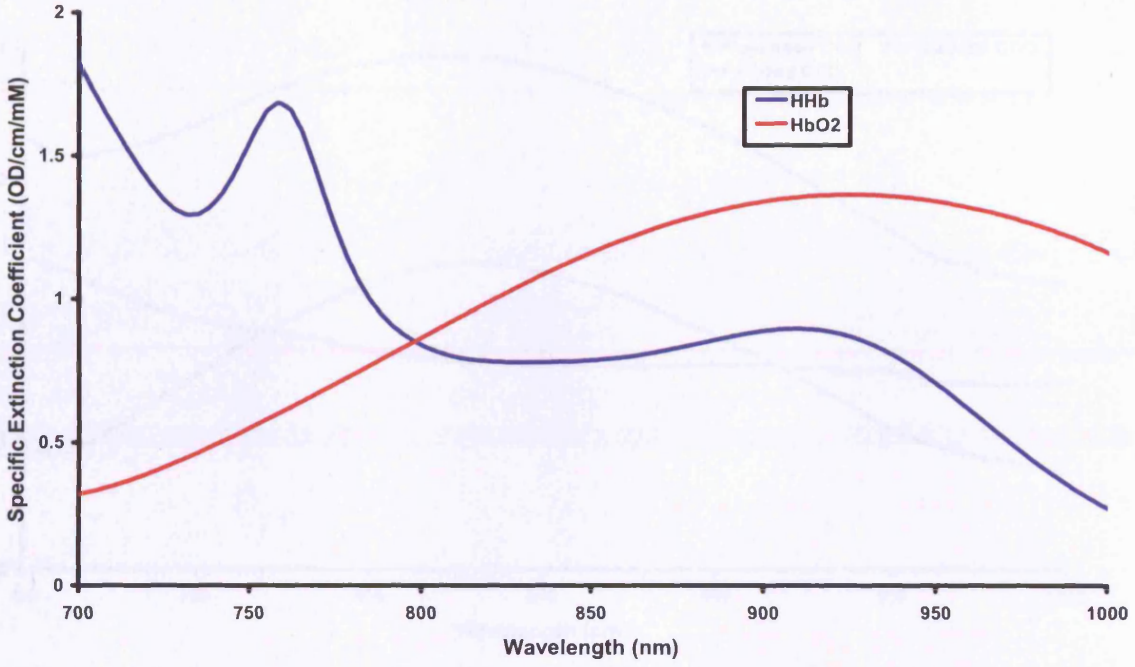

Figure 3.5: Specific extinction spectra of oxy- and deoxy-haemoglobin (from[10-12].

3.2.5 Cytochrome C Oxidase

The biochemistry of CCO has been discussed in chapter 1. The optical absorption difference spectrum between oxidised (oxCCO) and reduced CCO (redCCO) has features at various wavelengths and these can be attributed to the four main redox centres involved in electron transfer within the CCO enzyme (figure 1.6). The ox-redCCO spectrum has a distinct band in the NIR (figure 3.6) and the oxidation state of the Cu_a subunit is responsible for this differential light absorption[9,13]. Assuming the total concentration of CCO remains constant during an experiment then changes in the NIRS CCO signal represent changes in the CCO redox state. This signal has the potential to provide a non-invasive marker of changes in mitochondrial oxygen delivery and utilisation.

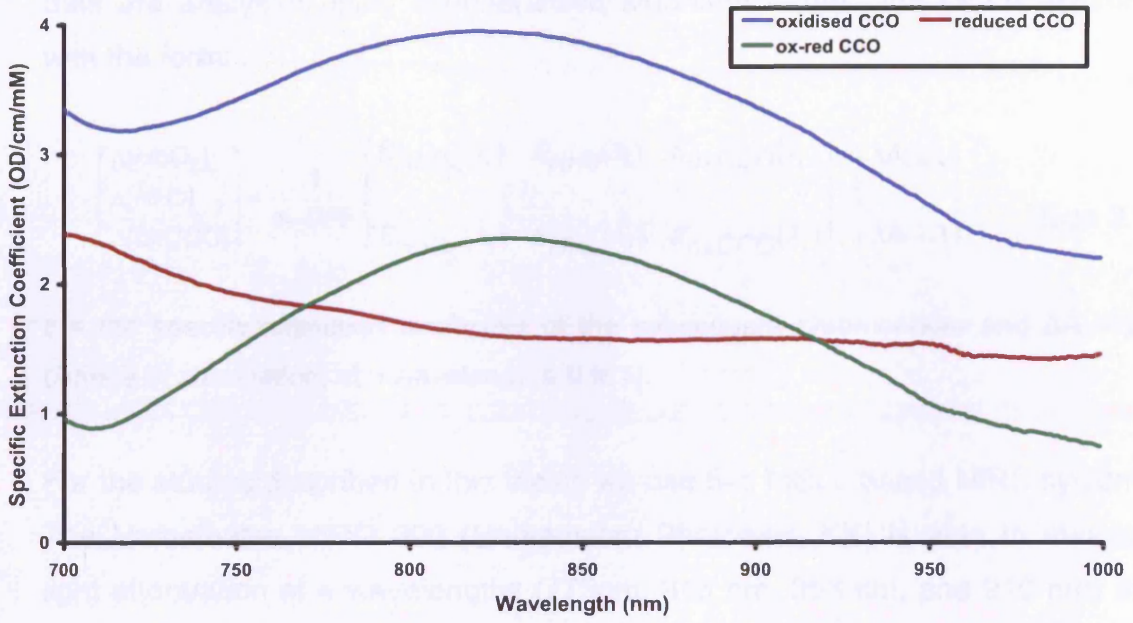

Figure 3.6: Specific extinction spectra of oxidised and reduced CCO and the oxidised - reduced difference spectra (ox-red CCO) (data from Dr. J Moody, Plymouth University).

Using knowledge of the spectra of these chromophores, Jöbsis published the first description of *in vivo* NIRS in 1977[9]. When using MBLL to measure $\Delta[HbO_2]$, Δ[HHb] and Δ[oxCCO] there are clearly three unknowns. Solving for these requires at least three simultaneous equations and these can be provided by measuring light attentuation at a minimum of 3 wavelengths.

However, although the specific extinction coefficients of the ox-redCCO difference spectrum in the near infrared region are similar in magnitude to those of HbO_2 and HHb[14], the concentration of CCO in the brain is approximately one order of magnitude less than these other two chromophores[15]. This complicates its detection and raises the possibility that NIRS measured changes in Δ[oxCCO] might be subject to artefacts resulting from measurement algorithm errors[16,17]. Modelling studies have demonstrated that these errors can be reduced by measuring light attenuation at multiple wavelengths[10].

This technique is called broadband spectroscopy (BBS) and in this thesis BBS data are analysed using a generalised algorithm termed the UCL*n* algorithm with the form:

$$\begin{pmatrix}\Delta[HbO_2]\\ \Delta[HHb]\\ \Delta[oxCCO]\end{pmatrix}=\frac{1}{d\cdot DPF}\begin{pmatrix}\varepsilon_{HbO_2}(\lambda_i) & \varepsilon_{HHb}(\lambda_i) & \varepsilon_{oxCCO}(\lambda_i)\\ \vdots & \vdots & \vdots\\ \varepsilon_{HbO_2}(\lambda_j) & \varepsilon_{HHb}(\lambda_j) & \varepsilon_{oxCCO}(\lambda_j)\end{pmatrix}^{-1}\begin{pmatrix}\Delta A(\lambda_i)\\ \vdots\\ \Delta A(\lambda_j)\end{pmatrix} \qquad \textit{Eqn 3.12}$$

ε = the specific extinction coefficient of the subsequent chromophore and ΔA = the change in attenuation, at n wavelengths λi to λj.

For the studies described in this thesis we use two MBLL based NIRS systems. The Hamamatsu NIRO 300 (Hamamatsu Photonics, KK) is able to measure light attenuation at 4 wavelengths (775nm, 813 nm, 853 nm, and 910 nm) and uses the UCL_4 algorithm which has the same form as equation 3.10 with n=4. Additionally in order to overcome some of the difficulties of making measurements of Δ[oxCCO] we use a BBS system which measures attenuation at 120 wavelengths between 780 and 900 nm and uses a least square fitting procedure to determine the changes in chromophore concentrations. This system is described in detail in chapter 5.

3.3 Spatially Resolved Spectroscopy

The use of the MBBL allows calculation of absolute changes in chromophore concentration, but can only therefore measure change from an arbitrary baseline and cannot derive absolute concentrations. SRS is a technique which allows calculation of absolute tissue oxyhaemoglobin saturation. The spatially resolved spectroscopy system used for the studies described in this thesis is the Hamamatsu NIRO 300 and the measured tissue oxyhaemoglobin saturation is known as tissue oxygenation index (TOI).

$$TOI=\frac{[HbO_2]}{[HbO_2]+[HHb]}\times 100 \qquad \textit{Eqn 3.13}$$

In order to calculate absolute concentrations of chromophores we need to further investigate the issue of light scattering.

Photon transport through tissue can be described by the diffusion approximation to the transport equation [18]. Assuming a semi-infinite homogenous half-space geometry:

$$R(\rho,\tau)=(4\pi Dv)^{\frac{-3}{2}}\cdot\frac{1}{\mu_{st}}\cdot\tau^{\frac{-5}{2}}\cdot\exp(-\mu_a\cdot v\cdot\tau)\cdot\exp\left(-\frac{\rho^2+\mu_{st}^{-2}}{4Dv\tau}\right) \qquad \textit{Eqn 3.14}$$

R= reflected light intensity at a distance ρ and time *t* from an impulse input. μ_a and μ_{st} = the absorption and transport scattering coefficients respectively, D = the diffusion coefficient ($D=1/3(\mu_a+\mu_{st})$ and *v* = the velocity of light in the medium.

In the case of continuous wave light input, the intensity *I* at distance ρ from the input can be expressed as the integral of $R(\rho,t)$ over time and so the attenuation is defined as:

$$A(\rho)=-\log_{10}\int_0^\infty R(\rho,\tau)dt \qquad \textit{Eqn 3.15}$$

Differentiation of equation 3.15 with respect to ρ gives:

$$\frac{\partial A}{\partial\rho}=\frac{1}{\ln 10}\cdot\left(\sqrt{3\mu_a\cdot\mu_{st}}+\frac{2}{\rho}\right)^2 \qquad \textit{Eqn 3.16}$$

The SRS technique measures attenuation at several wavelengths using multiple closely spaced detectors. This allows calculation of $\partial A/\partial\rho$ which can then be used to derive a wavelength specific value of $\mu_a\cdot\mu_{st}$. μ_{st} is almost constant across wavelength in the NIR but more formally it is found that based on a homogenous model:

$$\mu_{st(\lambda)}=k(1-h\lambda) \qquad \textit{Eqn 3.17}$$

h = the normalised slope of μ_{st} against λ which is approximately constant across tissue types and subjects with a value of 6.3×10^{-4} mm^{-1} nm[19] and k is a constant.

Knowledge of $\partial A/\partial\rho$ and equations 3.16 and 3.17 then allows the calculation of scaled wavelength specific absorption coefficients $k\cdot\mu_a$. The NIRO 300 measures $\partial A/\partial\rho$ using 3 closely separated photodiodes at 3 wavelengths (775, 813 and 850 nm) (figure 3.7) and uses a least square error method to calculate scaled absolute concentrations of HbO_2 and HHb.

In matrix form this is shown as:

$$\begin{pmatrix} k[HbO_2] \\ k[HHb] \end{pmatrix} = \begin{pmatrix} \varepsilon_{HbO_2}(\lambda_1) & \varepsilon_{HHb}(\lambda_1) \\ \varepsilon_{HbO_2}(\lambda_1) & \varepsilon_{HHb}(\lambda_2) \\ \varepsilon_{HbO_2}(\lambda_3) & \varepsilon_{HHb}(\lambda_3) \end{pmatrix}^{-1} \begin{pmatrix} k \cdot \mu_a(\lambda_1) \\ k \cdot \mu_a(\lambda_2) \\ k \cdot \mu_a(\lambda_3) \end{pmatrix} \qquad \textit{Eqn 3.18}$$

λ_1, λ_2, λ_3 represent the 3 wavelengths.

If we assume that k is constant then the calculation of TOI is possible:

$$TOI = \frac{k[HbO_2]}{k[HbO_2] + k[HHb]} \times 100 \qquad \textit{Eqn 3.19}$$

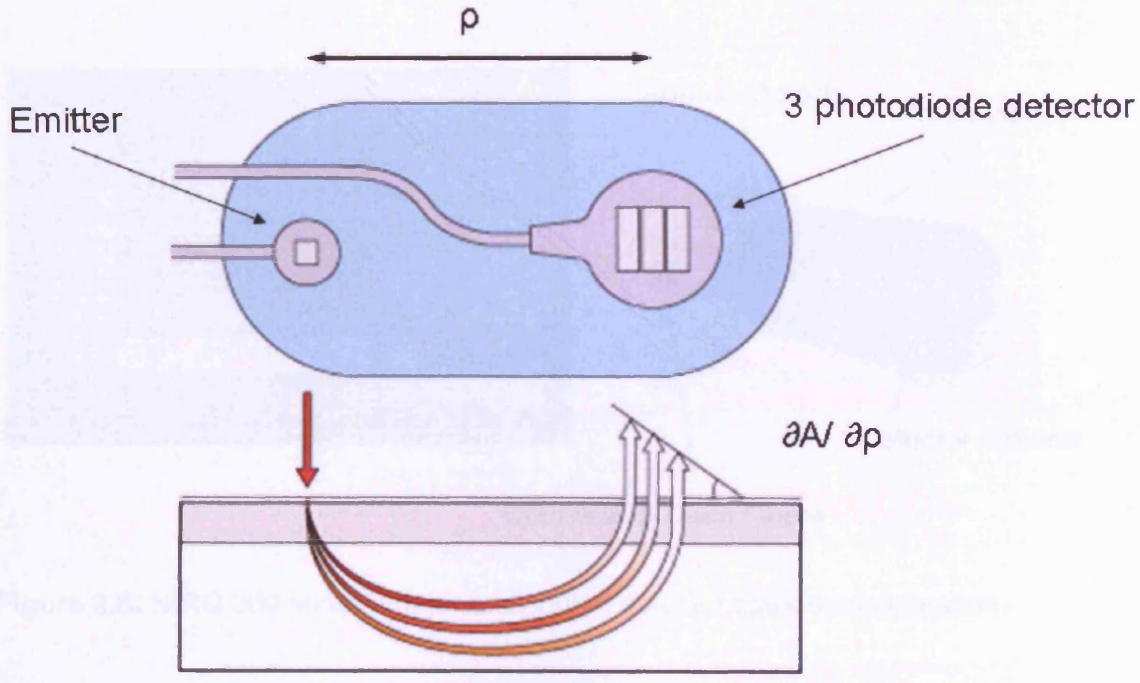

Figure 3.7: The NIRO 300 optode with a schematic of spatially resolved spectroscopy.

The NIRO 300 is a 2 channel NIRS system which allows simultaneous measurement at two sites and has a maximum acquisition rate of 6 Hz. In addition to its SRS capability it uses change in light attenuation measured at four wavelengths (775, 813, 850 and 910 nm) by the central photodiode to calculate $\Delta[HbO_2]$, $\Delta[HHb]$ and Δ[oxCCO] using the MBLL. The NIRO 300 spectrometer is shown in figure 3.8.

When applying non-invasive NIRS to the adult head, our goal is to make measurements of chromophore concentrations in the brain. Using the interoptode spacings described in this thesis (35-50mm), near infrared light will pass through the cerebral cortex and thus light attenuation will be affected by changes in cerebral chromophore concentrations[20]. However, some light will pass through only the skin and scalp before reaching the detector and will also contribute to the measured signal. The extra- and intracranial contributions to the measured signal may vary between individuals and disease states, but studies investigating cranial SRS measurements during selective clamping of the internal and external carotid circulation suggest that SRS is less prone to extracerebral contamination and has increased sensitivity and specificity to intracerebral layers than NIRS using the MBBL[21].

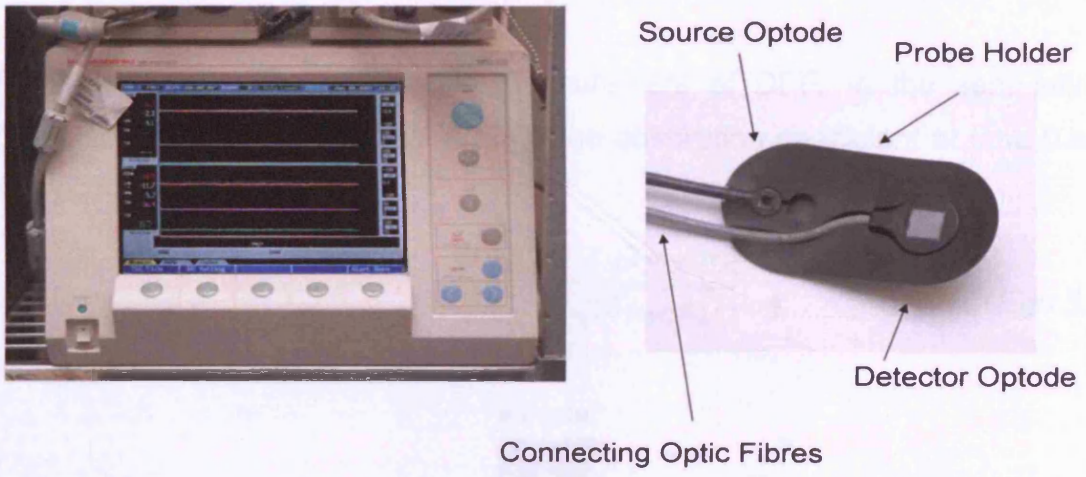

Figure 3.8: NIRO 300 spectrometer and source detector optode configuration.

3.4 Frequency Domain Spectroscopy

In order to calculate absolute concentrations of chromophore concentrations it is necessary to calculate values for μ_{st}. One technique through which this can be achieved is frequency domain spectroscopy (FDS). This entails using a light source with the intensity modulated at high frequency. The frequency domain NIRS system we are currently using produces light at 4 wavelengths (690, 750, 790, 850 nm) intensity modulated at 110 MHz allowing detection of the average value (dc), amplitude (ac) and phase (Φ) of the detected light at two source detector separations (figure 3.9) (ISS, Inc., Champaign, IL). Following the work

of Fantini *et al* [22,23] if r is the detector source separation, S_{ac} is the slope of ln (r^2ac) as a function of r and S_Φ is the slope of Φ as a function of r, then it has been shown for a semi-infinite medium, that the diffusion approximation yields:

$$\mu_a = \frac{\omega}{2v}\left(\frac{S_\phi}{S_{ac}} - \frac{S_{ac}}{S_\phi}\right) \qquad \textit{Eqn 3.20}$$

$$\mu_{st} = \frac{{S_{ac}}^2 - {S_\phi}^2}{3\mu_a} - \mu_a \qquad \textit{Eqn 3.21}$$

where ω = the angular modulation frequency of the light source and v = the speed of light in the tissue.

The conditions under which these equations are valid ($\mu_a << \mu_{st}$, $\omega/2\pi << v\mu_{st}$) are well satisfied by most biological tissues in the NIR for modulation frequencies up to 1 GHz.

FDS also allows the continuous measurement of DPF. In the semi-infinite geometry it can be shown that if μ_{a0} is the absorption coefficient at time 0 and $\Delta\mu_a/\mu_{a0}<<1$ then:

$$DPF = \frac{\sqrt{3\mu_{st}}}{2\sqrt{\mu_{a0}}} \cdot \frac{r\sqrt{3\mu_{a0}\mu_{st}}}{r\sqrt{(3\mu_{a0}\mu_{st})}+1} \qquad \textit{Eqn 3.22}$$

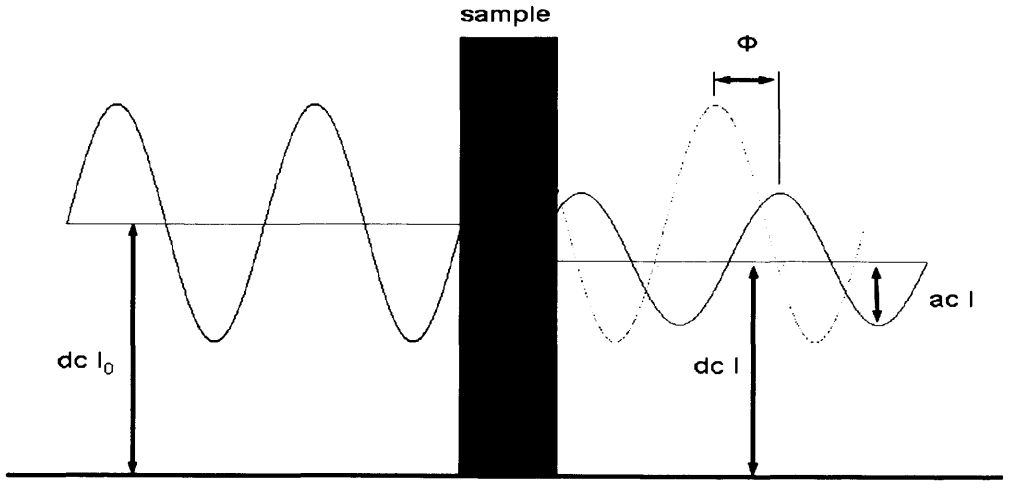

Figure 3.9: FDS demonstrating changes in dc intensity (dc I), ac intensity (ac I) and phase (Φ) when intensity modulated light passes across tissue.

3.5 Calculation of Optical Pathlength

The main NIRS techniques which exist for the calculation of optical pathlength are FDS, time resolved spectroscopy (TRS) and 2nd differential spectroscopy. The FDS technique has proved to be easily applicable to clinical situations and has been used to measure DPF in both neonates and adult volunteers[4,5]. The results suggest an effect of age on DPF with the relationship:

$$DPF_{780} = 5.13 + 0.07 \cdot Y^{0.81} \qquad \textit{Eqn 3.23}$$

DPF_{780} = DPF at 780 nm and Y is the age of the subject in years.

3.5.1 TRS

Using TRS, a tunable laser is used to send an ultrashort picosecond laser pulse across the tissue sample. A streak camera then detects the transmitted light pulse and thus measures the time of flight of the light across the tissue (figure 3.10). If t is the mean time taken for the light to cross the tissue then the DPF can be calculated from:

$$DPF = \frac{c \cdot t}{d \cdot n} \qquad \textit{Eqn 3.24}$$

c= the speed of light in a vacuum, d is the refractive index of tissue and d is the interoptode spacing.

The equipment required for this technique requires a laser capable of delivering pico second light pulses and tends to be confined to optical laboratories, but measurements have been made on both animals and humans[2,24-26].

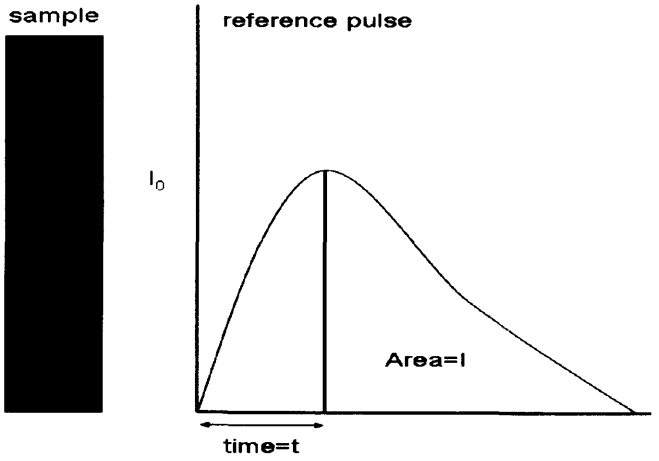

Figure 3.10: Time domain spectroscopy.

3.5.2 2nd Differential Spectroscopy

We have already noted that the water absorption spectrum has several weak features in the NIR (figure 3.3). The water content of tissue is known with reasonable accuracy[7], and therefore if we could calculate the apparent water concentration from the amplitude of the spectral features and divide it by the known water concentration we would obtain an estimate of the optical pathlength[6]. Mathematically from equations 3.7 and 3.8:

$$d \cdot DPF = \frac{A_{H_2O}}{\varepsilon_{H_2O} \cdot c_{H_2O}} \qquad \textit{Eqn 3.25}$$

A_{H2O} = the attenuation attributable to water, ε_{H2O} and c_{H2O} = the specific extinction coefficient and assumed concentration of water respectively.

When illuminating tissue this calculation is not trivial: measurement of the amplitude of the water feature is complicated by the presence of an arbitrary dc baseline, relating to scattering losses and the absolute photometry of the system, and the wavelength dependence of these scattering losses. However, the wavelength dependence of scatter is approximately linear in the NIR. Thus if we take a second differential of the attenuation spectrum with respect to wavelength, and perform a least squares fit with the corresponding second differential spectra of relevant tissue chromophores including water, we can determine the amplitude of the tissue water feature relative to the amplitude of the pure water reference irrespective of any dc or linear background [6,11].

In order for this technique to be of use the second differential NIR absorption spectrum of water must be sufficiently featured so as to constrain the fitting procedure and suitable features exist at 710-760 nm and 820 nm (figure 3.11). This technique has been validated *in vitro*[6] and has been used *in vivo* to measure DPF in animals and humans[11,27-30].

Figure 3.11: Second differential spectra of 20 μM HHb, 40 μM HbO_2 (which are an approximation to their *in vivo* concentrations) and 100% H_2O (taken from [6]).

References

1. Beer A. Bestimmung der absorption des rothen lichts in farbigen flüssigkeiten. *Ann Phys Chem* 1852;162:78.
2. Delpy DT, Cope M, van der Zee P, Arridge S, Wray S, Wyatt J. Estimation of optical pathlength through tissue from direct time of flight measurement. *Phys Med Biol* 1988;33:1433-1442.
3. Delpy DT, Cope M. Quantification in tissue near-infrared spectroscopy. *Phil Trans R Soc Lond* 1997;352:649-659.
4. Duncan A, Meek JH, Clemence M, Elwell CE, Fallon P, Tyszczuk L, Cope M, Delpy DT. Measurement of cranial optical path length as a function of age using phase resolved near infrared spectroscopy. *Pediatr Res* 1996;39:889-894.
5. Duncan A, Meek JH, Clemence M, Elwell CE, Tyszczuk L, Cope M, Delpy D. Optical pathlength measurements on adult head, calf and forearm and the head of the newborn infant using phase resolved optical spectroscopy. *Phys Med Biol* 1995;295-304.
6. Matcher SJ, Cope M, Delpy DT. Use of the water absorption spectrum to quantify tissue chromophore concentration changes in near-infrared spectroscopy. *Phys Med Biol* 1994;39:177-196.
7. Woodard HQ, White DR. The composition of body tissues. *B J Radiol* 1986;59:1209-1219.
8. Elwell C (1995) *A practical users guide to near infrared spectroscopy*, London: Hamamatsu Photonics.
9. Jöbsis FF. Noninvasive, infrared monitoring of cerebral and myocardial oxygen sufficiency and circulatory parameters. *Science* 1977;198:1264-1267.
10. Matcher SJ, Elwell CE, Cooper CE, Cope M, Delpy DT. Performance comparison of several published tissue near-infrared spectroscopy algorithms. *Anal Biochem* 1995;227:54-68.
11. Matcher SJ, Cooper CE. Absolute quantification of deoxyhaemoglobin concentration in tissue near infrared spectroscopy. *Phys Med Biol* 1994;39:1295-1312.
12. Zijlstra W, Buursma A, van Assendelft O (2000) *Visible and near infrared absorption spectra of human and animal haemoglobin.* Utrecht: VSP.

13. Ferrari M, Hanley DF, Wilson DA, Traystman RJ. Redox changes in cat brain cytochrome-c oxidase after blood-fluorocarbon exchange. *Am J Physiol* 1990;258:1706-1713.
14. Cooper CE, Matcher SJ, Wyatt JS, Cope M, Brown GC, Nemoto EM, Delpy DT. Near-infrared spectroscopy of the brain: relevance to cytochrome oxidase bioenergetics. *Biochem Soc Trans* 1994;22:974-980.
15. Brown GC, Crompton M, Wray S. Cytochrome oxidase content of rat brain during development. *Biochem Biophys Acta* 1991;1057:273-275.
16. Sakamoto T, Jonas RA, Stock UA, Hatsuoka S, Cope M, Springett RJ, Nollert G. Utility and limitations of near-infrared spectroscopy during cardiopulmonary bypass in a piglet model. *Pediatr Res* 2001;49:770-776.
17. Skov L, Greisen G. Apparent cerebral cytochrome aa3 reduction during cardiopulmonary bypass in hypoxaemic children with congenital heart disease. A critical analysis of in vivo near-infrared spectrophotometric data. *Physiol Meas* 1994;15:447-457.
18. Arridge S, Cope M, Delpy D. The theoretical basis for the determination of optical pathlengths in tissue: temporal and frequency analysis. *Phys Med Biol* 1992;37:1531-1560.
19. Suzuki S, Takasaki S, Ozaki T, Kobayashi Y. A tissue oxygenation monitor using NIR spatially resolved spectroscopy. *SPIE Proc* 1999;3597:582-592.
20. Okada E, Delpy DT. Near-infrared light propagation in an adult head model. II. Effect of superficial tissue thickness on the sensitivity of the near-infrared spectroscopy signal. *Appl Opt* 2003;42:2915-2922.
21. Al-Rawi PG, Smielewski P, Kirkpatrick PJ. Evaluation of a near-infrared spectrometer (NIRO 300) for the detection of intracranial oxygenation changes in the adult head. *Stroke* 2001;32:2492-2500.
22. Fantini S, Hueber D, Franceschini MA, Gratton E, Rosenfeld W, Stubblefield PG, Maulik D, Stankovic MR. Non-invasive optical monitoring of the newborn piglet brain using continuous-wave and frequency-domain spectroscopy. *Phys Med Biol* 1999;44:1543-1563.
23. Fantini S, Franceschini MA, Fiskin J, Barbieri B, Gratton E. Quantitative determination of the absorption spectra of chromophores in scattering

media: a light-emitting-diode based technique. *Appl Opt* 1994;33:5204-5213.

24. Wyatt JS, Cope M, Delpy DT, van der Zee P, Arridge S, Edwards AD, Reynolds EO. Measurement of optical path length for cerebral near-infrared spectroscopy in newborn infants. *Dev Neurosci* 1990;12:140-144.
25. Essenpreis M, Elwell CE, Cope M, van der Zee P, Arridge SR, Delpy DT. Spectral dependence of temporal point spread functions in human tissues. *Appl Optics* 1993;32:418-425.
26. Essenpreis M, Cope M, Elwell CE, Arridge SR, van der Zee P, Delpy DT. Wavelength dependence of the differential pathlength factor and the log slope in time-resolved tissue spectroscopy. *Adv Exp Med Biol* 1993;333:9-20.
27. Heekeren HR, Kohl M, Obrig H, Wenzel R, von Pannwitz W, Matcher SJ, Dirnagl U, Cooper CE, Villringer A. Noninvasive assessment of changes in cytochrome-c oxidase oxidation in human subjects during visual stimulation. *J Cereb Blood Flow Metab* 1999;19:592-603.
28. Cooper CE, Elwell CE, Meek JH, Matcher SJ, Wyatt JS, Cope M, Delpy DT. The noninvasive measurement of absolute cerebral deoxyhemoglobin concentration and mean optical path length in the neonatal brain by second derivative near infrared spectroscopy. *Pediatr Res* 1996;39:32-38.
29. Cooper CE, Cope M, Springett R, Amess PN, Penrice J, Tyszczuk L, Punwani S, Ordidge R, Wyatt J, Delpy DT. Use of mitochondrial inhibitors to demonstrate that cytochrome oxidase near-infrared spectroscopy can measure mitochondrial dysfunction noninvasively in the brain. *J Cereb Blood Flow Metab* 1999;19:27-38.
30. Tisdall M, Tachtsidis I, Leung T, Ewell C, Smith M. Near infrared spectroscopic quantification of changes in the concentration of oxidized cytochrome oxidase in the healthy human brain during hypoxemia. *J Biomed Opt* 2007;12:024002.

Chapter 4

Response of cerebral tissue oxygenation index to changes in inspired concentrations of oxygen and end tidal carbon dioxide tension in healthy adult volunteers

This chapter describes an experimental study using NIRS to measure changes in TOI and CBV in the brains of healthy adult volunteers during alterations in the composition of inspired gases. Specifically a two channel NIRO 300 spectrometer is used to measure TOI, $\Delta[HbO_2]$ and $\Delta[HHb]$ using SRS and the MBLL. The physiological challenges consist of isocapnoeic hypoxia and hyperoxia, and normoxic hypocapnoea and hypercapnoea. Responses to these four challenges are described individually and the results are then combined in order to relate changes in TOI to changes in SaO_2, $EtCO_2$, CBV, CBF, HR and MBP.

4.1 Introduction

TOI provides a measure of tissue oxyhaemoglobin saturation and has been discussed in chapter 3. Measurement of TOI using the NIRO 300 has been studied using tissue phantoms filled with intralipid, water and human blood during studies where the oxygenation is varied using yeast and oxygen bubbling and has been found to correlate well with co-oximeter analysis of the phantom contents[1]. NIRO 300 measurement of TOI also correlates well with TRS measurement of tissue oxygen saturation in the human arm during arterial and venous occlusion[1]. The development of TOI has been motivated, in part, by the desire to provide clinicians with an easily accessible measure of the balance of tissue oxygen delivery and utilisation and hence the adequacy of tissue oxygen delivery. Cerebral TOI has been evaluated during selective internal and external carotid artery clamping and shows high sensitivity and specificity to intracranial changes[2]. Cerebral TOI appears less affected by changes in the extracranial vasculature than NIRS measurements made using the MBLL. However the interpretation of clinical TOI data remains complex. TOI measurement has been compared to jugular venous oximetry in both adults[3,4] and children[5] and has shown considerable variation in terms of baseline

values and the rate and magnitude of recorded changes. A recent study by Rasmussen *et al* estimated capillary oxyhaemoglobin saturation as a mean of arterial and jugular bulb oxyhaemoglobin saturation and compared this derived value with TOI changes in FiO_2 and $FiCO_2$. They demonstrated a correlation between the two measures, but the comparison between TOI and the modelled capillary saturation showed wide variation[6] and this variation may limit the use of absolute TOI values to define ischaemic thresholds or guide targeted therapy in the clinical environment.

There may be several reasons for these findings. Comparisons between TOI and jugular venous oximetry are hindered by technical issues relating to the regions interrogated: jugular oximetry provides a flow weighted global measure of the adequacy of cerebral oxygen delivery and is therefore insensitive to regional heterogeneity, whereas NIRS is a regional technique. There are also methodological issues specific to NIRS: cranial NIRS interrogates a multi-compartmental system of arteries, arterioles, capillaries, venules and veins and each compartment has different volumes and oxyhaemoglobin saturations: conversely the theory behind SRS is based on a the interrogated medium being flat and homogenous. The typical cerebral arterial:venous volume ratio is 1:3[7] (25% arterial and 75% venous) yet this will depend on individual anatomy, local physiology and/or the presence of disease[8]. It is intuitively obvious that baseline arterial:venous volume ratio (AVR) will affect baseline TOI and furthermore that changes in AVR will cause changes in TOI.
By derivation from equation 3.13 it can be shown theoretically that:

$$TOI = SaO_2 - \left(\frac{V_V}{V_a + V_V}\right) \cdot \left(\frac{CMRO_2}{k.CBF.[Hb]}\right) \times 100 \qquad \textit{Eqn 4.1}$$

SaO_2 = arterial oxyhaemoglobin saturation, V_v and V_a = venous and arterial blood volume respectively, $CMRO_2$ = cerebral metabolic rate for oxygen, k = oxygen carrying ability of haemoglobin, CBF = cerebral blood flow and [Hb] = blood haemoglobin concentration.

This equation helpfully demonstrates the factors which might affect cerebral TOI measurements. Most of these factors will affect either cerebral oxygen delivery or utilisation and one would therefore expect TOI to be sensitive to the balance between these two and hence reflect the adequacy of cerebral oxygen delivery. AVR however will have no direct effect (if one ignores the indirect effects on vascular resistance and hence CBF) on either oxygen delivery or utilisation and yet from equation 4.1 one would expect it to affect TOI. Changes in AVR might therefore induce changes which precipitate erroneous interpretation of TOI data. Baseline variability in absolute TOI might be addressed by using change in TOI as a measure of change in the adequacy of oxygen delivery, but this might also be confounded by changes in AVR.

CBF responses to changes in $PaCO_2$ and PaO_2 are well documented and are mediated by changes in the calibre of arterioles[9] (figure 4.1). Ito *et al* used PET to investigate CBV changes in the various cerebral vascular compartments during hypo- and hypercapnoea[10]. They observed increases in arterial CBV during hypercapnoea and decreases during hypocapnoea yet found no associated changes in capillary or venous volume and concluded that changes in CBV during hypo and hypercapnoea are caused only by changes in arterial blood volume. Changes in $PaCO_2$ and, by extension, PaO_2 will therefore induce changes in cerebral AVR and we can use these paradigms to investigate the importance of changes in AVR on TOI.

Figure 4.1: Cerebral blood flow response to changes arterial carbon dioxide and oxygen tension (taken from [9]).

In this study we use alterations in FiO_2 and $EtCO_2$ (a surrogate of $PaCO_2$) to induce changes in cerebral oxygen delivery, CBF and CBV and investigate the resulting TOI response. We use TCD to measure mean blood flow velocity in the basal middle cerebral artery (VMCA) and use this as a surrogate measure of CBF. This technique relies on there being no change in the diameter of the insonated vessel and no change in the insonation angle. MRI studies suggest that basal middle cerebral arterial diameter does not change during the types of challenge described in this study[11] and the use of a head fixation system ensures a stable insonation angle. Experimental studies have shown that changes in VMCA correlate reliably with ^{133}Xenon measured changes in CBF[12]. Additionally we calculate changes in CBV from the MBLL NIRS data in order to assess its effect on TOI.

4.2 Methods

This study was approved by the Joint Research Ethics Committee of the National Hospital for Neurology and Neurosurgery and the Institute of Neurology. We studied 15 healthy subjects (5 female and 10 male) with median age 31 years (range 27-39).

4.2.1 Instrumentation

The source-detector optode pair for each channel of the NIRO 300 was placed in a black plastic holder with a source-detector separation of 5cm. One channel was fixed to the right hand side of the forehead and the other to the left hand side of the forehead in the midpupillary line with the channel laterality allocated randomly. Within each pair the source fibres were positioned medially and the detector optodes laterally in order to minimise the transmission of light from the channel 1 source to the channel 2 detector and vice versa. A bandage and a light absorbing cloth were placed over the optode holders to eliminate stray light and prevent optode movement. SRS and MBBL data was collected at 6 Hz.

A modified oximeter probe (Novametrix Medical Systems Inc., Wallingford, CT, USA) measured beat-to-beat SaO_2, and a Portapres finger cuff (Biomedical Instrumentation, TNO Institute of Applied Physics, Belgium) measured MBP and HR non-invasively. VMCA was collected at 50 Hz using a 2 MHz transcranial

Doppler ultrasonography (Pioneer TC2020, Nicolet, UK) fixed in place over the right temporal region. A modified anesthetic machine delivered gas to the subject via a Mapelson E breathing system connected to a mouthpiece with the expiratory limb having length 50 cm (figure 4.2). FiO_2 and $EtCO_2$ were measured using an inline gas analyser (Hewlett Packard, UK) and a CO_2SMO optical sensor (Novametrix Medical Systems Inc.) respectively. The monitoring configuration is shown in figure 4.3.

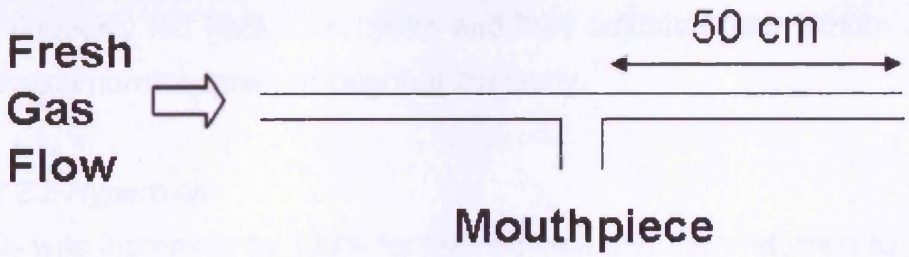

Figure 4.2: Mapelson E breathing system.

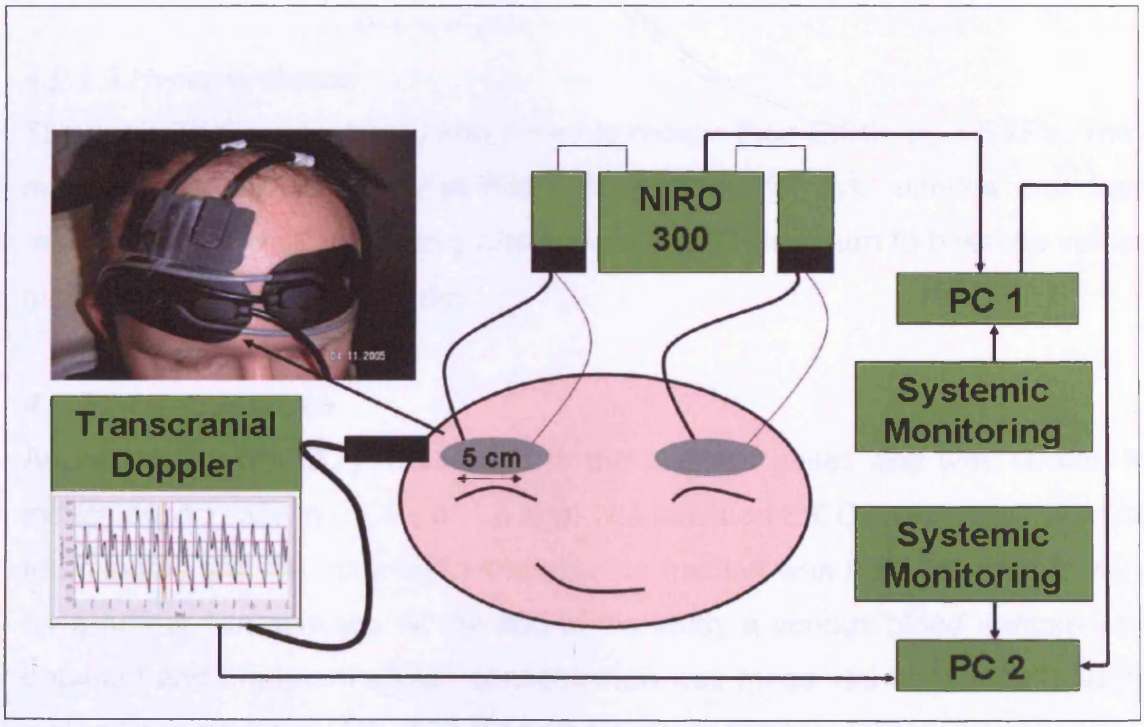

Figure 4.3: Monitoring configuration showing positioning of two channel NIRO 300 NIRS system and TCD.

4.2.2 Study Protocol

The study was divided into four sections with a rest period between each. Each challenge period was preceded by five minutes data collection at normoxia and normocapnea.

4.2.2.1 Hypoxaemia

Nitrogen was added to the inspired gases, to induce a gradual fall in SaO_2 to 80%, and immediately after this was achieved, the FiO_2 was returned to normoxia for five minutes. This cycle was repeated three times. $EtCO_2$ was continuously fed back to subjects and they adjusted their minute ventilation to maintain normocapnea throughout the study.

4.2.2.2 Hyperoxia

FiO_2 was increased to 100% for five minutes and then returned to normoxia for five minutes. Similar to the hypoxaemia phase of the study, the cycle was repeated three times and the subjects adjusted their minute ventilation to maintain normocapnea throughout the study.

4.2.2.3 Hyperventilation

The subjects hyperventilated and aimed to reduce their $EtCO_2$ by 1.5 kPa. They maintained a stable $EtCO_2$ at this reduced level for five minutes and then returned to a normal ventilatory rate allowing $EtCO_2$ to return to baseline values over approximately five minutes.

4.2.2.4 Hypercapnoea

Approximately 6% CO_2 was added to the inspired gases and was titrated to induce an increase in $EtCO_2$ of 1.5 kPa. The elevated $EtCO_2$ was maintained for ten minutes and the inspired carbon dioxide fraction was then returned to zero for a further five minutes. At the end of the study a venous blood sample was obtained and the haemoglobin concentration was measured immediately using a blood gas analyser (ABL 700, Radiometer Copenhagen, Denmark).

4.2.3 Data Analysis

Absolute $\Delta[HbO_2]$ and $\Delta[HHb]$ for each channel were calculated from changes in light attenuation using the UCL_4 algorithm assuming a DPF of 6.26[13]. Change in total hemoglobin concentration ($\Delta[HbT]$) was defined as $\Delta[HbO_2]+\Delta[HHb]$. VMCA was calculated from the CBF velocity envelope using a trapezoidal integration function (MatLab, Mathworks Inc., USA).

The start and end of each period of hypoxaemia, hyperoxia or CO_2 manipulation was identified from the SaO_2 data, the FiO_2 data or the $EtCO_2$ data respectively. To enable comparison between subjects and across paradigms, within each individual period of alteration of FiO_2 or $EtCO_2$ (the challenge period) eight time points were selected so that the period between adjacent points represented an eighth of the total time course of the challenge period. This produced nine time points with point 1 representing the point just prior to the start, and point 9 the end of the challenge period. The same technique was applied separately to the recovery period, producing points 9 (just prior to start of recovery) to 17 (end of recovery period). At each time point, the mean of the preceding ten seconds of data was calculated (figure 4.4). For the hypoxaemia and hyperoxia challenges, data from the three experimental cycles were averaged to give a single course for each subject and, for each of the paradigms, a mean of the two NIRS channels was calculated. Group median changes from baseline at each time point were produced.

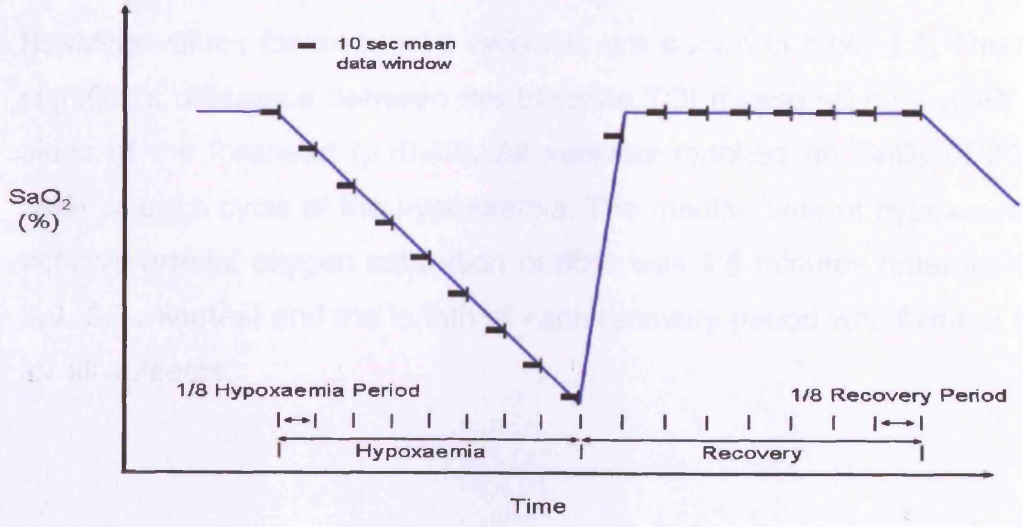

Figure 4.4: Schematic of data analysis for hypoxaemia paradigms using SaO_2 data to define data windows for summary analysis.

Changes in CBV were calculated using the formula:

$$\Delta CBV = \frac{\Delta[HbT] \cdot MW_{Hb} \times 100}{[Hb] \cdot CSLVH \cdot \rho_{Brain}} \qquad \textit{Eqn 4.2}$$

ΔCBV = change in cerebral blood volume (ml/100g of brain), Δ[HbT] =change in total haemoglobin concentration (mol/l), MW_{Hb} = molecular weight of haemoglobin (64 500 g/mole), [Hb] = the large vessel haemoglobin concentration (g/l), CSLVH = the cerebral small vessel to large systemic vessel haematocrit[14] and ρ = the brain density (1.05 g/ml)[15].

Statistical analysis was carried out using SAS software (v9.1, SAS Institute, USA). Percentage changes from baseline for VMCA, and absolute changes from baseline for other measured variables were compared using non-parametric analysis of variance (ANOVA) with *post hoc* pairwise comparisons[16] and p values less than 0.05 were considered significant.

Multiple regression analysis was carried out using ΔTOI as the dependent variable and changes in other systemic variables as regression variables. Regression variables which were not significant were then removed and the regression analysis repeated.

4.3 Results

4.3.1 Hypoxaemia

Baseline values for measured variables are shown in table 4.1. There was no significant difference between the baseline TOI measured on the left and right sides of the forehead (p=0.49). All subjects reached an SaO_2 of 80% at the nadir of each cycle of the hypoxaemia. The median time of hypoxia required to achieve arterial oxygen saturation of 80% was 4.5 minutes (interquartile range 3.9 -5.9 minutes) and the length of each recovery period was fixed at 5 minutes for all subjects.

	Median	*IQR*
FiO_2 (%)	21.0	21.0 to 21.0
SaO_2 (%)	99.2	98.2 to 99.2
$EtCO_2$ (kPa)	5.4	5.2 to 5.7
HR (min^{-1})	62.5	60.0 to 71.5
MBP (mmHg)	77.6	70.3 to 88.8
VMCA (cms^{-1})	43.2	37.9 to 51.1
Hb (g/l)	147	137.5 to 149.5
TOI R (%)	68.3	65.2 to 71.9
TOI L (%)	67.4	65.9 to 69.2
TOI R- TOI L (%)	0.5	-2.2 to 2.3

Table 4.1: Median and interquartile range for baseline values of measured variables prior to the start of hypoxaemia (n=15). TOI R is TOI measured over the right side of the forehead, TOI L is TOI measured over the left side of the forehead and TOI R-TOI L is the difference in TOI between the two sides.

Data from the hypoxaemic protocol for a single subject is shown in figure 4.5 in order to demonstrate the experimental time course. Group data showing median and interquartile range for measured variable values is shown in figure 4.6.

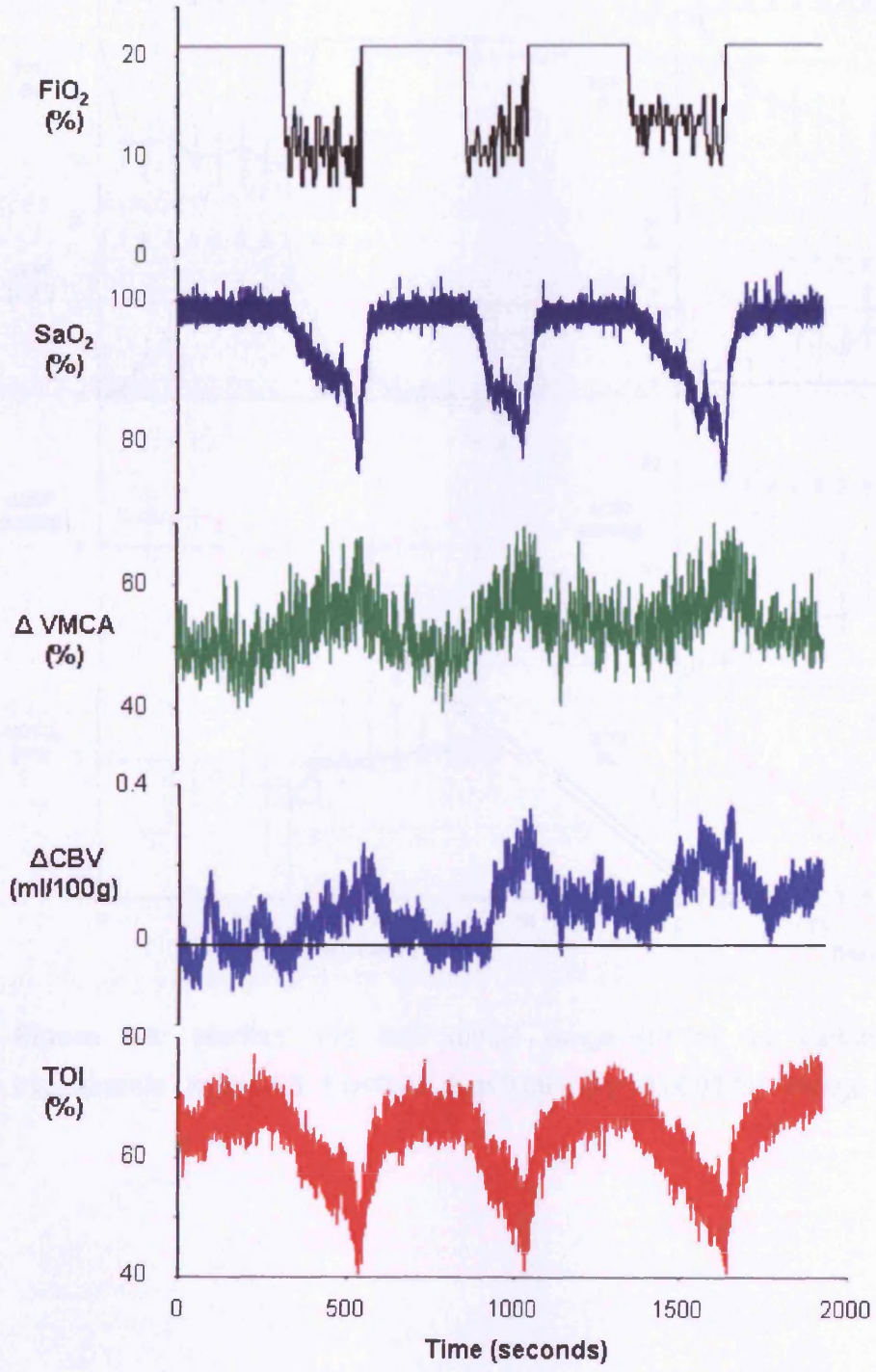

Figure 4.5: Data for individual subject during three cycles of hypoxaemia.

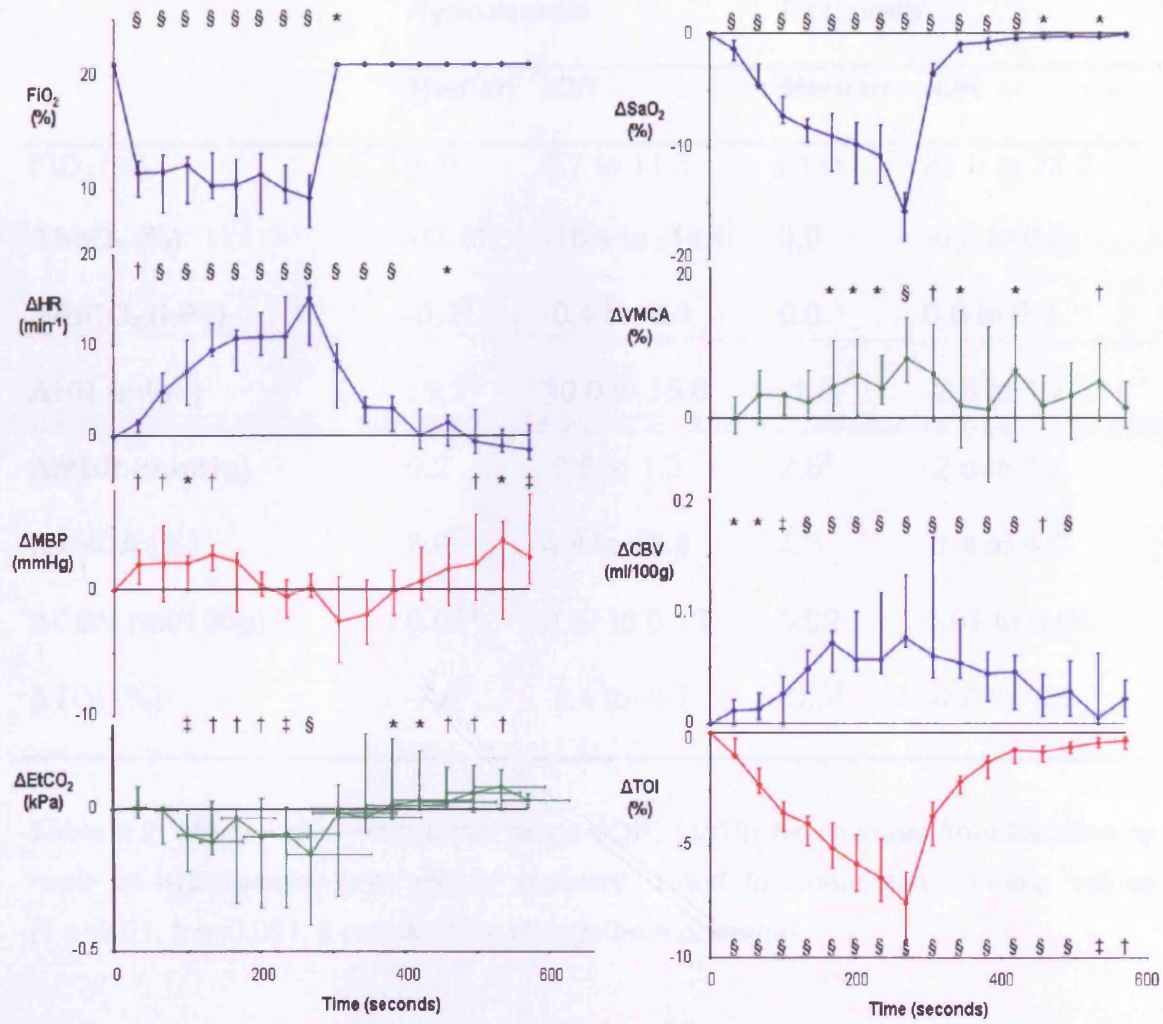

Figure 4.6: Median and interquartile range (n=15) for variable values during hypoxaemia (✶ $p<0.05$, † $p<0.01$, ‡ $p<0.001$, § $p<0.0001$ for change from baseline).

	Hypoxaemia		*Recovery*	
	Median	***IQR***	***Median***	***IQR***
FiO_2 (%)	9.3§	6.7 to 11.3	21.0	21.0 to 21.0
ΔSaO_2 (%)	-15.8§	-18.4 to -14.1	0.0	-0.3 to 0.0
$\Delta EtCO_2$ (kPa)	-0.2§	-0.4 to -0.1	0.0	0.0 to 0.1
ΔHR (min^{-1})	15.2§	10.0 to 16.6	-1.5	-2.6 to 1.2
ΔMBP (mmHg)	0.2	-0.5 to 1.3	2.6‡	-2.6 to 1.2
ΔvMCA (%)	7.9§	4.8 to 13.4	1.3	-1.4 to 4.8
ΔCBV (ml/100g)	0.08§	0.07 to 0.13	0.02	0.01 to 0.04
ΔTOI (%)	-7.6§	-9.4 to -6.2	-0.3†	-0.7 to -0.2

Table 4.2: Median and interquartile range (IQR) (n=15) for changes from baseline to nadir of hypoxaemia, and end of recovery period for measured variable values († $p<0.01$, ‡ $p<0.001$, § $p<0.0001$ for change from baseline).

4.3.2 Hyperoxia

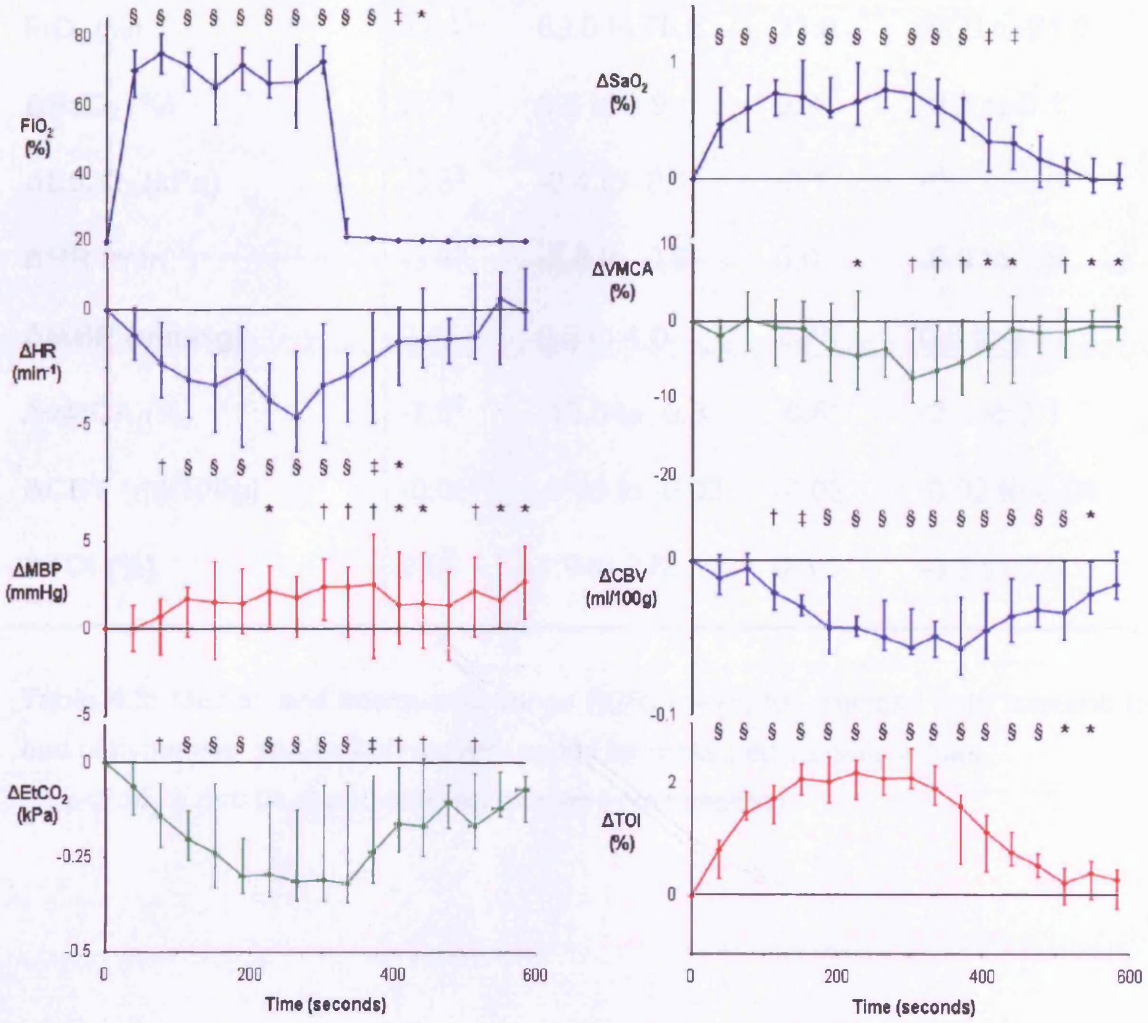

Figure 4.7: Median and interquartile range (n=15) for variable values during hyperoxia (* p<0.05, † p<0.01, ‡ p<0.001, § p<0.0001 for change from baseline).

	Hyperoxia		*Recovery*	
	Median	***IQR***	***Median***	***IQR***
FiO_2 (%)	72.4§	69.0 to 76.8	21.0	21.0 to 21.0
ΔSaO_2 (%)	0.7§	0.5 to 0.9	0.0	-0.1 to 0.1
$\Delta EtCO_2$ (kPa)	-0.3§	-0.4 to -0.1	-0.1	-0.2 to 0.0
ΔHR (min^{-1})	-3.3§	-5.8 to -0.6	0.0	-0.9 to 1.8
ΔMBP (mmHg)	2.4†	0.5 to 4.0	2.7*	0.6 to 4.7
ΔvMCA (%)	-7.3†	-10.5 to -0.8	-0.6*	-2.3 to 2.1
ΔCBV (ml/100g)	-0.06§	-0.06 to -0.03	-0.02	-0.02 to 0.04
ΔTOI (%)	2.0§	1.9 to 2.6	0.3	-0.2 to 0.5

Table 4.3: Median and interquartile range (IQR) (n=15) for changes from baseline to end of hyperoxia, and end of recovery period for measured variable values (* $p<0.05$, † $p<0.01$, § $p<0.0001$ for change from baseline).

4.3.3 Hyperventilation

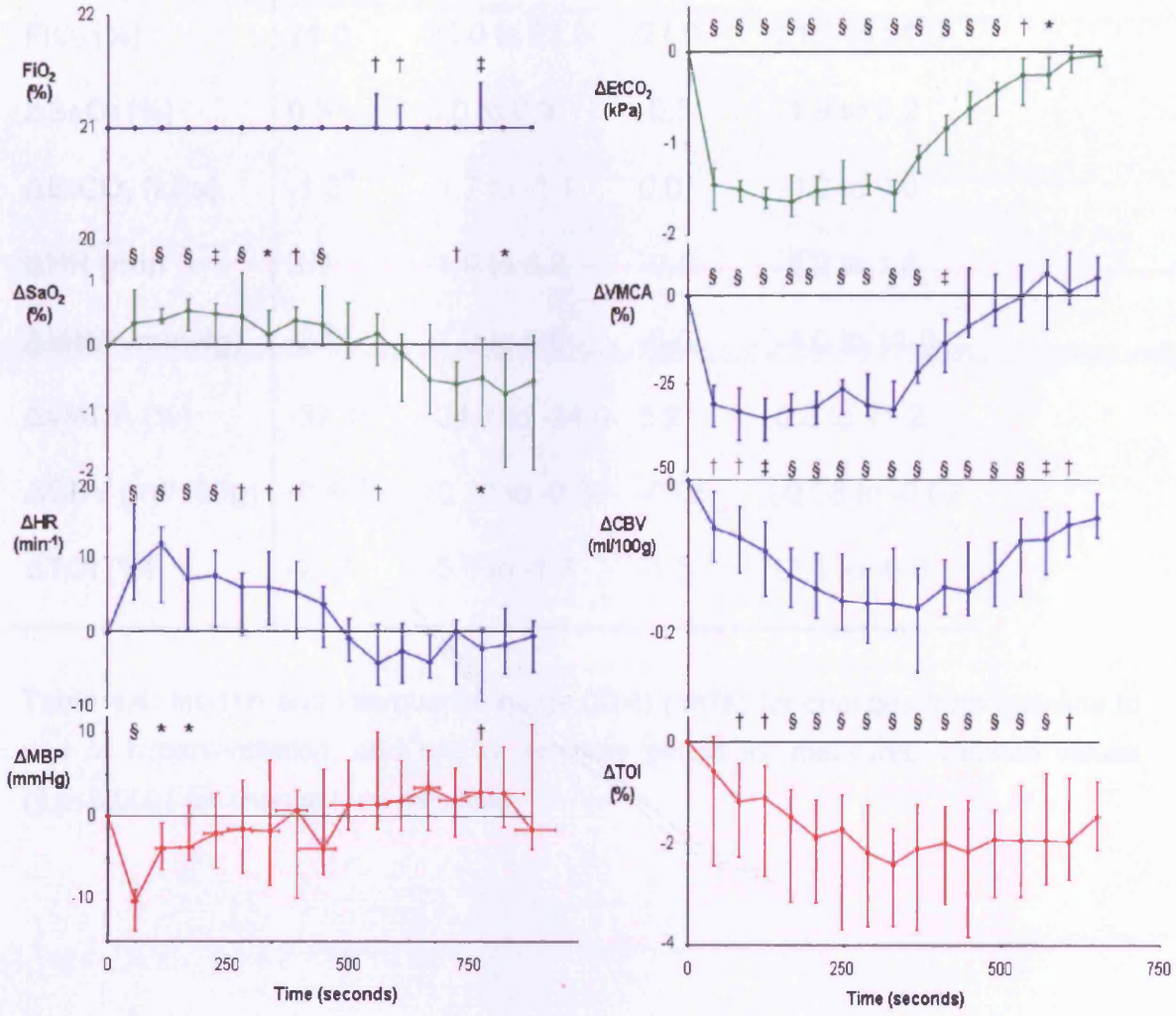

Figure 4.8: Median and interquartile range (n=15) for variable values during hyperventilation (✶ $p<0.05$, † $p<0.01$, ‡ $p<0.001$, § $p<0.0001$ for change from baseline).

	Hyperventilation		*Recovery*	
	Median	***IQR***	***Median***	***IQR***
FiO_2 (%)	21.0	21.0 to 21.0	21.0	21.0 to 21.0
ΔSaO_2 (%)	0.3§	0.0 to 0.9	-0.5	-1.9 to 0.2
$\Delta EtCO_2$ (kPa)	-1.5§	-1.7 to -1.4	0.0	-0.2 to 0.0
ΔHR (min^{-1})	3.9	-1.9 to 6.2	-0.4	-5.2 to 1.6
ΔMBP (mmHg)	-3.9	-7.0 to 5.6	-5.6	-4.0 to 11.0
ΔvMCA (%)	-32.1§	-34.1 to -24.0	5.2	0.3 to 11.2
ΔCBV (ml/100g)	-0.16§	-0.20 to -0.09	-0.05	-0.08 to -0.02
ΔTOI (%)	-2.4§	-3.6 to -1.7	-1.5	-2.1 to -0.8

Table 4.4: Median and interquartile range (IQR) (n=15) for changes from baseline to end of hyperventilation, and end of recovery period for measured variable values (§ $p<0.0001$ for change from baseline).

4.3.4 Hypercapnoea

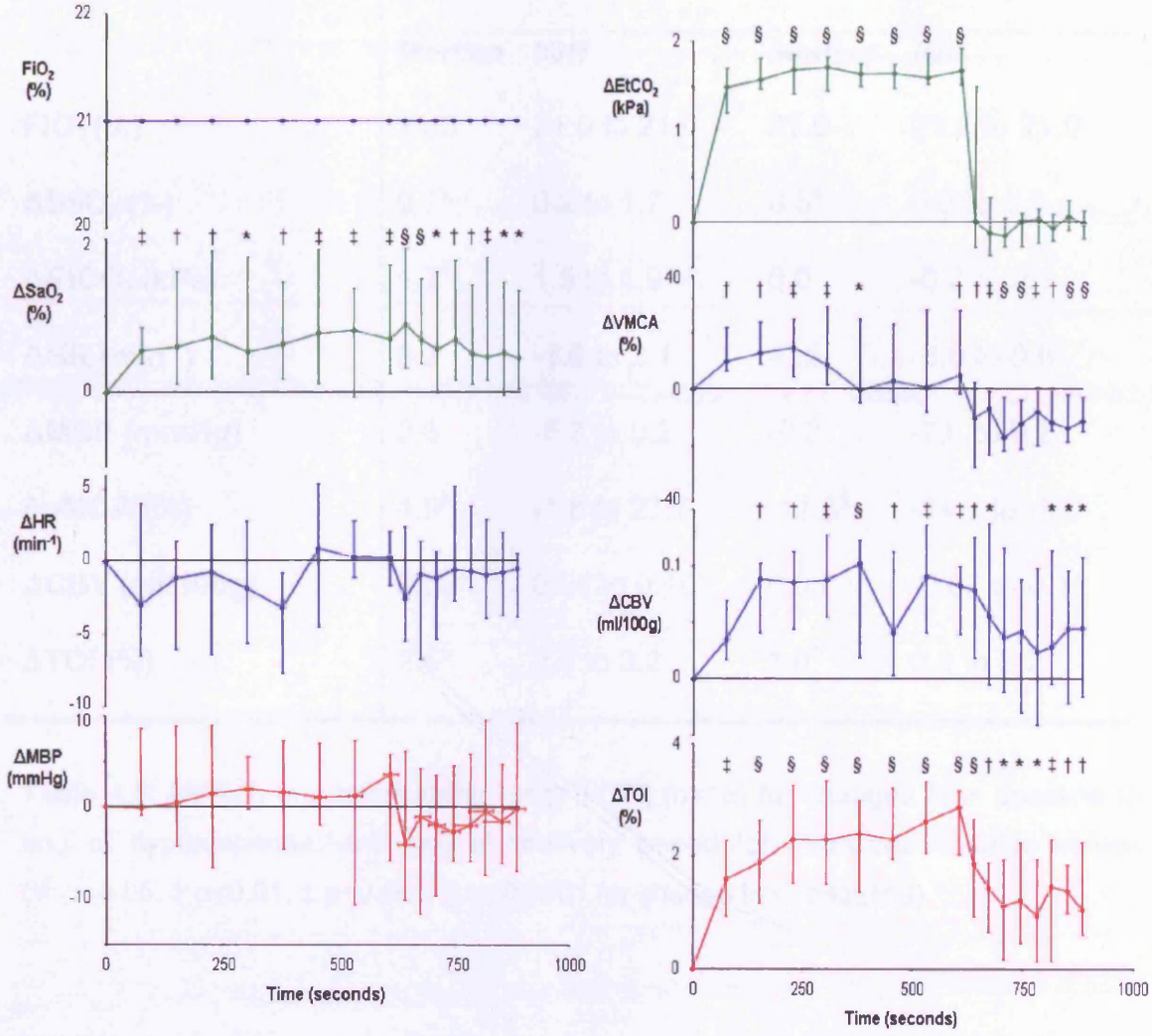

Figure 4.9: Median and interquartile range (n=15) for variable values during hypercapnoea (✶ $p<0.05$, † $p<0.01$, ‡ $p<0.001$, § $p<0.0001$ for change from baseline).

	Hypercapnoea		*Recovery*	
	Median	***IQR***	***Median***	***IQR***
FiO_2 (%)	21.0	21.0 to 21.0	21.0	21.0 to 21.0
ΔSaO_2 (%)	0.7‡	0.2 to 1.7	0.5*	0.0 to 1.3
$\Delta EtCO_2$ (kPa)	1.7§	1.5 to 1.9	0.0	-0.2 to 0.1
ΔHR (min^{-1})	0.3	-1.6 to 2.1	-0.5	-3.8 to 0.6
ΔMBP (mmHg)	3.6	-5.9 to 9.2	-0.2	-7.0 to 9.2
ΔvMCA (%)	4.9*	-1.8 to 27.7	-11.5§	-14.9 to -3.0
ΔCBV (ml/100g)	0.09‡	0.04 to 0.10	0.05*	-0.02 to 0.11
ΔTOI (%)	2.6§	2.0 to 3.2	1.0†	0.6 to 2.2

Table 4.5: Median and interquartile range (IQR) (n=15) for changes from baseline to end of hypercapnoea, and end of recovery period for measured variable values (* $p<0.05$, † $p<0.01$, ‡ $p<0.001$, § $p<0.0001$ for change from baseline).

4.3.5 Combined Analysis

Multiple regression was initially carried out using ΔTOI as the independent variable and the other systemic variables as the regression variables.

The significant variables were ΔSaO_2 ($p<0.0001$), $\Delta EtCO_2$ ($p<0.0001$), ΔCBV ($p=0.0003$) and ΔMBP ($p=0.03$), whereas ΔVMCA ($p=0.7$) and ΔHR ($p=0.2$) were not significant factors.

The regression analysis was repeated using only the significant regression variables to determine the regression beta values.

The regression analysis revealed:

$$\Delta TOI = 0.53 \times \Delta SaO_2 + 1.13 \times \Delta EtCO_2 + 2.35 \times \Delta CBV + 0.01 \times \Delta MBP \qquad \textit{Eqn 4.3}$$

with overall adjusted *r* value 0.82 ($p<0.0001$).

The standardised beta coefficients, p values and variance inflation factors for each variable are shown in table 4.6.

Variable	*ΔSaO_2*	*$\Delta EtCO_2$*	*ΔCBV*	*ΔMBP*
standard β	0.71	0.37	0.09	0.04
p value	<0.0001	<0.0001	0.0005	0.03
VIF	1.1	1.7	1.9	1.1

Table 4.6: Standardised regression estimates (standard β), p values and variance inflation factors (VIF) for multiple regression analysis variables shown in equation 4.3.

4.4 Discussion

In this study four paradigms were used in order to measure the response of TOI to changes in cerebral oxygen delivery. Hypoxaemia and hyperoxia were used to alter arterial oxygen content and changes in arterial CO_2 tension were used to alter cerebral blood flow. TOI increased significantly in response to hyperoxia and hypercapnoea and significantly decreased in response to hypoxaemia and hyperventilation. PET studies suggest that changes in CBV occurring during experimental protocols of this type only occur in the arterial compartment[10] and will therefore alter the AVR. Analysis of the combined datasets revealed that changes in TOI are significantly affected by changes in SaO_2, $EtCO_2$, CBV and MBP. However analysis of the standardised beta estimates of the multiple regression analysis indicated that changes in SaO_2 and $EtCO_2$ are far stronger predictors of ΔTOI whereas the other two variables are only weak predictors. We can therefore conclude that the confounding affect of CBV changes on ΔTOI is minimal and that ΔTOI has the potential to provide a clinically useful marker of changes in the balance of cerebral oxygen delivery and utilisation.

Table 4.1 shows a large variation in baseline TOI values across this group of healthy volunteers: the IQR for baseline TOI recorded over the right frontal lobe was 6.7%. The magnitude of this interindividual variation will limit the clinical

usefulness of absolute TOI: the IQR of the absolute right sided TOI is similar in magnitude to the median ΔTOI of 7.6% recorded during hypoxaemia to SaO_2 of 80% and only half the ΔTOI value of 13% which has recently been suggested as a threshold for cerebral ischaemia[17].

As one would expect there was no significant difference in TOI between the right and left sided measurements, with a median difference of 0.5%, and similarly the median values for left and right sided baseline TOI were similar (67.4 vs. 68.3) yet the interquartile range of 4.5% demonstrates the degree of intra-individual variation. This is particularly important when assessing the use of SRS as a clinical monitor with the aim of being able to make clinical inferences about a single individual and again suggests that this variation may limit the use of absolute TOI as a clinical monitoring tool. Several investigators have compared cerebral oxygenation measured using SRS, with jugular venous oximetry in children and adults in healthy and pathological states. The predominant finding is one of strong individual correlations but less marked group correlations between the two measures[4,18-21]. This may be explained to some extent by the baseline variation. Each section of the results will now be discussed individually.

4.4.1 Hypoxaemia

This protocol was successful in desaturating all subjects to an SaO_2 of 80%. There was a significant increase in heart rate and minimal change in MBP during the study in agreement with previous investigations[22]. An $EtCO_2$ feedback loop was used to minimise changes in $EtCO_2$. Despite this, a small but significant median reduction in $EtCO_2$ of 0.2 kPa was found at the nadir of hypoxemia due to the hypoxaemic stimulus to hyperventilate. The multiple regression analysis suggests that this magnitude of $\Delta EtCO_2$ would induce a ΔTOI of ~ 0.2%.

The threshold for hypoxaemic vasodilatation in healthy volunteers has been investigated using NIRS and TCD and has been reported to be in the region of an SaO_2 of 90%[22]. We also show an increase in VMCA and CBV during

hypoxaemia and this was associated with a median decrease in TOI of 7.6%. Al-Rawi *et al* attempted to define the ΔTOI associated with cerebral ischaemia by studying patients undergoing carotid artery clamping during surgery. They used EEG to define the presence of ischaemia and no patients with a ΔTOI<13% met their ischaemic criteria. The paradigm used here is therefore unlikely to be causing EEG changes in our study cohort.

4.3.2 Hyperoxia

During the hyperoxic phase of the study, the FiO_2 at the anaesthetic machine was increased to 100% with a FGF of 8l/min. This FGF is less than the peak inspiratory flow of a healthy subject and with the Mapelson E system employed there will be a degree of mixing between the FGF and room air entrained via the expiratory limb. The FiO_2 presented in these results is measured at the mouth and due to this gaseous mixing the median FiO_2 attained during hyperoxia was 72.4%.

A significant reduction in HR was observed and similar findings have been found in the conscious dog[23]. A significant decrease in $EtCO_2$ of 0.3 kPa was observed and this occurred despite subjects attempting to maintain isocapnoea. This is most likely to be related to the Haldane effect which describes how increasing oxyhaemoglobin saturation decreases the affinity of haemoglobin for carbon dioxide[24,25]. This would reduce carbon dioxide uptake from tissue and might therefore translate to a reduction in $PaCO_2$ and hence $EtCO_2$. It has also been suggested that Haldane effect mediated carbon dioxide retention in the respiratory centres of the brain might induce a hyperventilatory response[26].

We demonstrate a reduction in VMCA and CBV in response to hyperoxia. This may be in part due to the reduction in arterial carbon dioxide tension however arterial-spin-labelled MRI investigations suggest that normobaric hyperoxia has a direct vasoconstrictive effect as well as an indirect effect mediated via the reduced $PaCO_2$[26].

Despite this reduction in CBV and VMCA which might tend to reduce TOI, we show an increase in TOI which is of a greater magnitude (median 2.0%) than the increase in SaO_2 (median 0.7%). This implies that the increase in dissolved blood oxygen is contributing to the increase in TOI. An important corollary of this finding is that, assuming a constant cerebral metabolic rate for oxygen, our data suggest that the combined effect of the increased arterial oxygen content and reduced cerebral blood flow is an overall increase in cerebral oxygen delivery.

4.3.3 Hyperventilation

During the hyperventilation phase of the study a median reduction in $EtCO_2$ of 1.5 kPa was achieved with an interquartile range of 0.3 kPa indicating that the experimental challenge was well controlled. Hyperventilation was associated with an increase in SaO_2 and HR reflecting the increased physical work involved. The reduction in $PaCO_2$ caused a reduction in CBV, presumably related to arteriolar vasoconstriction, and a reduction in VMCA was also observed. These findings are in agreement with many studies investigating cerebrovascular responses to changes in arterial CO_2 tension[27-29].

It is interesting to note that the CBV and VMCA responses have different timescales. VMCA returns to baseline during the recovery period whereas the CBV returns towards but does not reach baseline by the end of the study. This suggests that the autoregulatory processes which attempt to maintain a stable CBF entail further mechanisms beyond changes in arteriolar calibre. TOI reduced during hyperventilation despite the small increase in SaO_2 suggesting that the effect of the arteriolar vasoconstriction and hence reduction in arterial volume and CBF is the predominant driver of TOI during this paradigm.

4.3.4 Hypercapnoea

During the hypercapnoea phase of the study a median increase in $EtCO_2$ of 1.7 kPa was recorded. This was associated with an increase in SaO_2 which is likely to be caused by hyperventilation induced by the increase in $PaCO_2$. During the early part of the hypercapnoeic phase there was an increase in VMCA, however this returned towards baseline before the end of the hypercapnoeic period,

again demonstrating that further autoregulatory mechanism are occurring. CBV increased during hypercapnoea and returned towards but did not reach baseline values during the recovery period. TOI increased during hypercapnoea and the time course of the response suggests that this effect is related more closely to the increase in CBV rather than the increase in VMCA. Similar to the CBV response TOI returned towards but did not reach baseline values by the end of the recovery period. A similar increase in $PbrO_2$ in response to hypercapnoea which outlasts the CO_2 changes has been demonstrated in a rat model[30].

4.3.5 Combined Analysis

The multiple regression analysis revealed the factors which significantly affect ΔTOI. From equation 4.3 and assuming constant $CMRO_2$ and intravascular haemoglobin concentration, one would expect ΔTOI to be affected by changes in SaO_2, CBF and CBV. We find that changes in SaO_2 and CBV are significant factors, yet change in VMCA is not. The dominant factor likely to cause change in VMCA is change $EtCO_2$ and the multiple regression results describe the significance of various factors while controlling for the effects of all the other regression variables. These results indicate that changes in $EtCO_2$ can account for the changes in VMCA and this leads to changes in VMCA not being a significant factor in the prediction of ΔTOI. This is confirmed by running the regression analysis with changes in $EtCO_2$ omitted, in which case changes in VMCA becomes a significant factor (analysis not shown). Change in MBP is also a significant regression variable but changes in HR is not. The y intercept produced by our regression analysis was not significantly different from zero and so can be ignored.

The standardised beta values demonstrate the relative importance of each of the significant regression variables. Change in SaO_2 is the most important factor with a standardised beta value of 0.71 and change in $EtCO_2$ is the second most important factor. The remaining two factors, change in CBV and change in MBP have standardised beta values an order of magnitude lower and therefore, although they are significant factors they have relatively little effect on

the magnitude of ΔTOI. The variable inflation factors (VIF) demonstrate the degree of colinearity between the regression variables and a value of >10 is usually considered unacceptable. In this analysis all the VIF are <2.

For ΔTOI to be clinically useful it should represent changes in the balance of cerebral oxygen delivery and utilisation. Change in arterial CBV has no direct effect on cerebral oxygen delivery or utilisation and yet it has a small but significant effect on ΔTOI. It is possible to use the results from our multiple regression analysis to derive a modification to TOI (TOIm) which is insensitive to changes in cerebral blood volume by simply subtracting a factor of ΔCBV scaled by the regression constant. Based on the data presented here this would result in equation 4.4.

$$\Delta TOIm = \Delta TOI - 2.35 \times \Delta CBV \qquad \textit{Eqn 4.4}$$

This modification merits further evaluation in clinical studies to assess if it has greater sensitivity and specificity to changes in the adequacy of cerebral oxygen delivery than ΔTOI. Clearly however our data from healthy volunteers may not reflect the cerebrovascular responses in disease states and clinical studies are required.

Multiple linear regression is one of many ways in which it is possible to model the relationship between TOI and the variables recorded during this study. Whilst the overall adjusted *r* value 0.82 ($p<0.0001$) suggests that the linear model fits the data with reasonable accuracy, there may be other models which provide better fits. One potential source of error relates to the measurement of TOI. The multiple linear regression model assumes no error in the TOI measurement and this assumption may not be valid. Regression techniques exist which are able to account for errors in the dependent variable. These techniques, which are known as errors-in-variables, or major axis, regression, are based on minimising the orthogonal distance between the data points and the regression line. This can be contrasted with standard linear regression which minimises the distance along the y axis between the data points and the

regression line. Employing these techniques in the context of multiple independent variables is complex and will not be discussed further.

This study could be improved by direct measurement of PaO_2 and $PaCO_2$, however this would entail the placement of invasive arterial catheters into healthy volunteers with its attendant risks. We have therefore used SaO_2 as a measure of arterial oxygen content, which therefore does not account for arterial oxygen carriage in solution and $EtCO_2$ as a surrogate for $PaCO_2$. The quantity of dissolved oxygen is likely to be negligible under conditions of normoxia and hypoxia, but it may become significant during the hyperoxic phase of the study and this might lead to errors in our regression results. Conversely change in $EtCO_2$ is an accurate surrogate of change in $PaCO_2$ and is therefore unlikely to affect our results[31].

4.5 Conclusion

Absolute TOI shows considerable variability in healthy volunteers and this may limit its clinical usefulness as an absolute measure of the adequacy of oxygen delivery. ΔTOI also has theoretical limitations as one would expect it to be sensitive to arterial CBV changes which do not directly affect cerebral oxygenation or utilisation. We confirm the influence of changes in CBV on ΔTOI in healthy volunteers, yet multiple regression analysis suggests that the effects of ΔCBV and ΔMBP are small and that the predominant factors affecting ΔTOI are changes in SaO_2 and $\Delta EtCO_2$. One would also expect ΔTOI to be sensitive to changes in $CMRO_2$ but this study protocol does not allow for altering $CMRO_2$ and it is hard to envisage a protocol able to achieve this in healthy volunteers. ΔTOI may therefore be clinically useful as a monitor of trends in the balance between cerebral oxygen delivery and utilisation. Clinical studies are required in order to establish the magnitude of ΔTOI associated with inadequate cerebral oxygen delivery. Studies are required in patients groups at risk of cerebral ischaemia such as those suffering from TBI, subarachnoid haemorrhage or undergoing complex cardiac surgery. In particular useful comparisons could be made between ΔTOI and invasive cerebral monitors such as cerebral

microdialysis and brain tissue oxygen tension in the context of TBI. The comparison between ΔTOI and EEG changes also shows particular promise. Ultimately large well controlled studies will be required to determine whether the use of TOI trend monitoring in patient groups at high risk of cerebral ischaemic events can lead to improved clinical outcomes.

References

1. Suzuki S, Takasaki S, Ozaki T, Kobayashi Y. A tissue oxygenation monitor using NIR spatially resolved spectroscopy. *SPIE Proc* 1999;3597:582-592.
2. Al-Rawi PG, Smielewski P, Kirkpatrick PJ. Evaluation of a near-infrared spectrometer (NIRO 300) for the detection of intracranial oxygenation changes in the adult head. *Stroke* 2001;32:2492-2500.
3. McLeod AD, Igielman F, Elwell C, Cope M, Smith M. Measuring cerebral oxygenation during normobaric hyperoxia: a comparison of tissue microprobes, near-infrared spectroscopy, and jugular venous oximetry in head injury. *Anesth Analg* 2003;97:851-856.
4. Ali MS, Harmer M, Vaughan RS, Dunne JA, Latto IP. Spatially resolved spectroscopy (NIRO-300) does not agree with jugular bulb oxygen saturation in patients undergoing warm bypass surgery. *Can J Anaesth* 2001;48:497-501.
5. Nagdyman N, Fleck T, Schubert S, Ewert P, Peters B, Lange PE, Abdul-Khaliq H. Comparison between cerebral tissue oxygenation index measured by near-infrared spectroscopy and venous jugular bulb saturation in children. *Intensive Care Med* 2005;31:846-850.
6. Rasmussen P, Dawson E, Nybo L, van Lieshout J, Secher N, Gjedde A. Capillary-oxygenation-level-dependent near-infrared spectrometry in frontal lobe of humans. *J Cereb Blood Flow Metab* 2007;27:1082-1093.
7. An H, Lin W. Cerebral venous and arterial volumes can be estimated separately in humans using magnetic resonance imaging. *Mag Res Med* 2002;48:583-588.
8. Watzman HM, Kurth CD, Montenegro LM, Rome J, Steven JM, Nicolson SC. Arterial and venous contributions to near-infrared cerebral oximetry. *Anesthesiology* 2000;93:947-953.
9. Harper A (1990) Physiological control of the cerebral circulation. In: *Cerebral blood flow and metabolism* (Harper A, Jennett S, eds), Manchester and New York: Manchester University Press, pp 4-25.
10. Ito H, Ibaraki M, Kanno I, Fukuda H, Miura S. Changes in the arterial fraction of human cerebral blood volume during hypercapnia and hyocapnia measured by positron emission tomography. *J Cereb Blood Flow Metab* 2005;25:852-857.

11. Valdueza JM, Balzer JO, Villringer A, Vogl TJ, Kutter R, Einhaupl KM. Changes in blood flow velocity and diameter of the middle cerebral artery during hyperventilation: assessment with MR and transcranial Doppler sonography. *Am J Neuroradiol* 1997;18:1929-1934.
12. Jorgensen L. Transcranial Doppler ultrasound for cerebral perfusion. *Acta Physiol Scand Suppl* 1995;625:1-44.
13. Duncan A, Meek JH, Clemence M, Elwell CE, Tyszczuk L, Cope M, Delpy D. Optical pathlength measurements on adult head, calf and forearm and the head of the newborn infant using phase resolved optical spectroscopy. *Phys Med Biol* 1995:95-304.
14. Lammertsma A, Brooks D, Beaney R, Turton D, Kensett M, Heather J, Marshall J, Jones T. In vivo measurement of regional cerebral haematocrit using positron emission tomography. *J Cereb Blood Flow Metab* 1984;4:317-322.
15. Rostrup E, Law I, Pott F, Ide K, Knudsen GM. Cerebral hemodynamics measured with simultaneous PET and near-infrared spectroscopy in humans. *Brain Res* 2002;954:183-193.
16. Siegel S, Castellan NJ (1988) *Nonparametric Statistics for the Behavioural Sciences*, Singapore: McGraw-Hill.
17. Al-Rawi P, Kirkpatrick P. Tissue oxygen index: thresholds for cerebral ischemia using near-infrared spectroscopy. *Stroke* 2006;37:2720-2725.
18. Henson LC, Calalang C, Temp JA, Ward DS. Accuracy of a cerebral oximeter in healthy volunteers under conditions of isocapnic hypoxia. *Anesthesiology* 1998;88:58-65.
19. Daubeney PE, Pilkington SN, Janke E, Charlton GA, Smith DC, Webber SA. Cerebral oxygenation measured by near-infrared spectroscopy: comparison with jugular bulb oximetry. *Ann Thorac Surg* 1996;61:930-934.
20. Lewis SB, Myburgh JA, Thornton EL, Reilly PL. Cerebral oxygenation monitoring by near-infrared spectroscopy is not clinically useful in patients with severe closed-head injury: a comparison with jugular venous bulb oximetry. *Crit Care Med* 1996;24:1334-1338.
21. Ter Minassian A, Poirier N, Pierrot M, Menei P, Granry JC, Ursino M, Beydon L. Correlation between cerebral oxygen saturation measured by

near-infrared spectroscopy and jugular oxygen saturation in patients with severe closed head injury. *Anesthesiology* 1999;91:985-990.

22. Gupta AK, Menon DK, Czosnyka M, Smielewski P, Jones JG. Thresholds for hypoxic vasodilatation in volunteers. *Anesth Analg* 1997;85:817-820.
23. Lodato R. Decreased O2 consumption and cardiac output during normobaric hyperoxia in conscious dogs. *J Appl Physiol* 1989;67:1551-1559.
24. Dash RK, Bassingthwaighte JB. Blood HbO2 and HbCO2 dissociation curves at varied O2, CO2, pH, 2,3-DPG and temperature levels. *Ann Biomed Eng* 2004;32:1676-1693.
25. Jensen F. Red blood cell pH, the Bohr effect, and other oxygenation-linked phenomena in blood O2 and CO2 transport. *Acta Physiol Scand* 2004;182:215-227.
26. Floyd TF, Clark JM, Gelfand R, Detre JA, Ratcliffe S, Guvakov D, Lambertson CJ, Eckenhoff RG. Independent cerebral vasoconstrictive effects of hyperoxia and accompanying arterial hypocapnia at 1 ATA. *J Appl Physiol* 2003;95:2453-2461.
27. Greenberg J, Alavi A, Reivich M, Kuhl D, Uzzell B. Local cerebral blood volume response to carbon dioxide in man. *Circ Res* 1978;43:324-331.
28. Rosenberg A, Jones MJ, Traystman R, Simmons M, Molteni R. Response of cerebral blood flow to changes in PCO2 in fetal, newborn, and adult sheep. *Am J Physiol* 1982;242:H862-H866.
29. Ashwal S, Dale P, Longo L. Regional cerebral blood flow: studies in the fetal lamb during hypoxia, hypercapnia, acidosis, and hypotension. *Pediatr Res* 1984;18:1309-1316.
30. Hare G, Kavanagh B, Mazer C, Hum K, Kim S, Coackley C, Barr A, Baker AJ. Hypercapnia increases cerebral tissue oxygen tension in anesthetized rats. *Can J Anaesth* 2007;50:1061-1068.
31. Whitesell R, Asiddao C, Gollman D, Jablonski J. Relationship between arterial and peak expired carbon dioxide pressure during anesthesia and factors influencing the difference. *Anesth Analg* 1981;60:508-512.

Chapter 5

Changes in cerebral mitochondrial redox state during alterations in inspired oxygen fraction and end tidal carbon dioxide tension in healthy adult volunteers.

This chapter describes an experimental study using BBS to measure changes in CCO redox state, and HbO_2 and HHb concentrations in the brains of healthy adult volunteers during alterations in the composition of inspired gases. The physiological challenges are identical to those used in the studies in chapter 4. Additionally, a moderate graded hyperventilation study is used to investigate change in oxidised cytochrome c oxidase concentration in response to small changes in end tidal CO_2 tension such as those which occur coincidentally during our hypoxaemia protocol. The stability of the BBS system is investigated by conducting a five hour phantom study and measuring changes in attenuation over this time period.

5.1 Introduction

CCO is the terminal electron acceptor of the mitochondrial electron transfer chain and catalyses over 95% of oxygen metabolism, thereby driving ATP synthesis[1]. CCO redox state reflects the balance between electron donation from cytochrome c, and oxygen reduction to water. Although many factors can influence CCO redox state[2], the most significant is the availability of molecular oxygen[3].

In chapter 3 the spectroscopic features of the difference spectrum between oxidised and reduced CCO were discussed and the distinct feature at ~830 nm which allows measurement Δ[oxCCO] using NIRS was noted [4,5]. Assuming the total concentration of CCO remains constant during an experiment then changes in the NIRS CCO signal represent changes in the CCO redox state.

The CCO signal therefore has the potential to provide a non-invasive marker of changes in mitochondrial oxygen delivery and utilisation, and might allow detection of ischaemic thresholds and guidance of subsequent clinical

interventions. The potential to make non-invasive measurements of mitochondrial metabolism has proved an exciting prospect to biochemists, clinicians and physicists alike. NIRS modelling studies suggest that detection of the CCO signal is improved by using BBS, thus increasing the number of wavelengths at which NIR light intensity is measured and using a least squares regression technique to convert changes in NIR light attenuation to changes in chromophore concentrations[6].

NIRS measured Δ[oxCCO] has been validated, in animals, as a marker of cellular energy status against magnetic resonance spectroscopy measured reduction in phosphocreatine and nucleoside triphosphate levels[7,8] suggesting that Δ[oxCCO] measurement may be able to provide clinically useful information at the bedside. Cerebral Δ[oxCCO] has been measured in humans in clinical situations associated with reduced cerebral oxygen delivery, namely cardiac surgery[9] and obstructive sleep apnea[10], but these studies are hard to standardise. Controversy remains regarding the relationship between Δ[oxCCO] and oxygen delivery and specifically the reduction in cerebral oxygen delivery required to produce Δ[oxCCO].

This study aims to quantify BBS measured cerebral Δ[oxCCO] during changes in arterial oxyhaemoglobin saturation and cerebral haemodynamics induced by changes in FiO_2 and $EtCO_2$ in healthy human volunteers and examine its relationship to cerebral oxygen delivery and NIRS haemoglobin measurements.

5.2 Methods

This study was approved by the Joint Research Ethics Committee of the National Hospital for Neurology and Neurosurgery and the Institute of Neurology. We studied 8 healthy volunteers (7 male, 1 female, median age 31.5 years, range 30-36). A second cohort of twelve subjects underwent an identical hypercapnoea protocol as part of a separate study but with identical instrumentation. For analysis of the hypercapnoea protocol these data sets were combined to give a final subject number of 20 (14 male, 4 female, median age 31 years, range 24-36).

A further 9 subjects underwent the moderate graded hyperventilation study (5 male, 4 female, median age 29 years, range 27-31).

5.2.1 Instrumentation

The BBS utilises light from a stabilised tungsten halogen light source which is filtered with 610nm long-pass and heat absorbing filters, and transmitted to the tissue sample via a 3.3mm diameter glass optic fibre bundle. Light incident on the detector optode is then focused via an identical fibre bundle onto the 400 μm entrance slit of a 0.27m spectrograph (270M, Instruments SA, France) with a 300g/mm grating. NIR spectra between 650 and 980 nm are collected at 1Hz on a cooled charge coupled device detector (Wright Instruments, UK) giving a spectral resolution of ~5nm.

Prior to the commencement of each study a reference spectrum was recorded onto the spectrometer by measuring absolute light intensity across a hollow box lined with light absorbing material. BBS optodes were then placed 3.5 cm apart in a black plastic holder, and fixed to the right side of the subject's forehead in the midpupilary line. A modified pulse oximeter probe (Novametrix Medical Systems Inc., USA) measured SaO_2, and a Portapres finger cuff (Biomedical Instrumentation, TNO Institute of Applied Physics, Belgium) measured MBP and HR non-invasively. Blood flow velocity in the basal right middle cerebral artery was collected at 50 Hz using 2 MHz transcranial Doppler ultrasonography (Pioneer TC2020, Nicolet, UK) fixed in place over the right temporal region. A modified anesthetic machine delivered gas to the subject via a Mapelson E breathing system connected to a mouthpiece with the expiratory limb having length 50 cm. FiO_2 and $EtCO_2$ were measured using an inline gas analyser (Hewlett Packard, UK) and a CO_2SMO optical sensor (Novametrix Medical Systems Inc.) respectively.

5.2.2 BBS Stability Protocol

The BBS optodes were placed on an epoxy phantom with optical properties similar to biological tissue, fixed firmly with an adhesive bandage and then covered with a light absorbing cloth. Intensity data were collected onto the BBS for a period of three hours. A study length of three hours was chosen because,

although the studies in this chapter had a maximum duration of approximately 40 minutes, the studies described in chapter 7 lasted approximately three hours.

5.2.3 Human Subject Study Protocols

Study protocols were identical to those described in section 4.2.2 and consisted of phases of hypoxaemia, hyperoxia, hyperventilation and hypercapnoea. When analysing the hypoxaemia and hyperoxia study data it became apparent that small changes in $EtCO_2$ were occurring despite our efforts to avoid them. In order to address this, an additional moderate graded hyperventilation study with a reduced set of measured variables consisting of FiO_2, SaO_2, $EtCO_2$ and BBS was carried out. The aim of this study was to determine the effect of the small changes in $EtCO_2$ we observed during the hypoxaemia and hyperoxia studies. This moderate hyperventilation study commenced with five minutes baseline monitoring at normoxia and normocapnoea. Subjects then hyperventilated and aimed to reduce their $EtCO_2$ by 0.1 kPa every minute for five minutes resulting in a final $EtCO_2$ 0.5 kPa below baseline. They then returned to a normal ventilatory rate allowing $EtCO_2$ to return to baseline values over approximately five minutes.

5.2.4 Data Analysis

In order to assess the stability of the BBS system, five minute means of intensity data between 780 and 900 nm were calculated at the beginning and end of the three hour phantom test. Change in attenuation over the three hour period of study was then calculated using equation 3.4.

For the human subject study protocols, absolute Δ[oxCCO], $\Delta[HbO_2]$ and Δ[HHb] were calculated from changes in light attenuation with a multiple regression technique termed the UCL*n* algorithm using 120 wavelengths between 780 and 900 nm[6]. This wavelength range has been suggested as optimal for measuring Δ[oxCCO] as it minimises absorption induced changes in light scattering during deoxygenation which might occur if the HHb absorbance peak between 740 and 780 nm were included in the spectral fit[11].

Chromophore spectra used were those available on the UCL Medical Physics website[12] with correction factors for the wavelength dependence of the optical pathlength applied to the chromophore absorption coefficients[13].

Individual baseline optical pathlength (PL) was calculated using second differential analysis of the 740 nm water feature[14] of the initial 60 seconds of spectral data. NIR light attenuation due to the illuminated tissue was calculated using equation 3.4 with the reference spectrum assumed to be I_0. The attenuation spectrum attained has an arbitrary dc baseline, but the second differential pathlength measurement is insensitive to this offset. For the pathlength calculation, the tissue water concentration was calculated as an average of skin, bone and cerebral grey matter water content[15] giving a value of 60.7%.

Change in total hemoglobin concentration (Δ[HbT]) was defined as $\Delta[HbO_2]+\Delta[HHb]$ and change in haemoglobin difference concentration (Δ[Hbdiff]) as $\Delta[HbO_2]-\Delta[HHb]$[16]. VMCA was calculated from the cerebral blood flow velocity envelope using a trapezoidal integration function (MatLab, Mathworks Inc., USA). Data analysis was identical to that described in section 4.2.3 and figure 4.4.

Cerebral oxygen delivery (cDO_2) in ml O_2/100g tissue/min is defined as:

$$cDO_2 = CBF(1.39 \times Hb \times SaO_2 + 0.003 \times PaO_2) \qquad \textit{Eqn 5.1}$$

CBF=cerebral blood flow (ml/100g tissue/min), 1.39 = the oxygen carrying capacity of haemoglobin (ml/g Hb), Hb=arterial haemoglobin saturation (g/dL), 0.003=solubility of oxygen in blood (ml/mmHg PaO_2/dL) and PaO_2=arterial partial pressure of oxygen (mm Hg).

Assuming that TCD insonation angle and basal middle cerebral artery diameter remain unchanged during a study, then mean VMCA correlates with cerebral blood flow[17].

Ignoring the small dissolved oxygen component, we can define an estimated cerebral oxygen delivery ($ecDO_2$) as:

$$ecDO_2 = k \times VMCA(1.39 \times Hb \times SaO_2) \qquad \textit{Eqn 5.2}$$

k = individual specific constant.

Assuming constant arterial haemoglobin concentration during the study, percentage change in $\Delta ecDO_2$ is calculated as percentage change from baseline of SaO_2 × VMCA. This analysis technique was not applied to data from the hyperoxia phase of the study as one would expect this to be associated with significant changes in the quantity of dissolved oxygen present in arterial blood[18].

Statistical analysis was carried out using SAS software (v9.1, SAS Institute, USA) and p values <0.05 were considered significant. Group changes were compared with baseline using non-parametric ANOVA and *post hoc* pairwise comparisons.

Correlations between variables were assessed by applying Spearman rank correlation to data from the 17 time points, with Bonferoni corrected two tailed tests of significance.

5.3 Results

5.3.1 BBS Stability

Change in attenuation over the three hour period of the phantom study is shown in figure 5.1. The mean change in attenuation across the wavelength range was 0.004 OD. The group mean change in attenuation between baseline and the nadir of hypoxaemia also shown for comparison on figure 5.1.

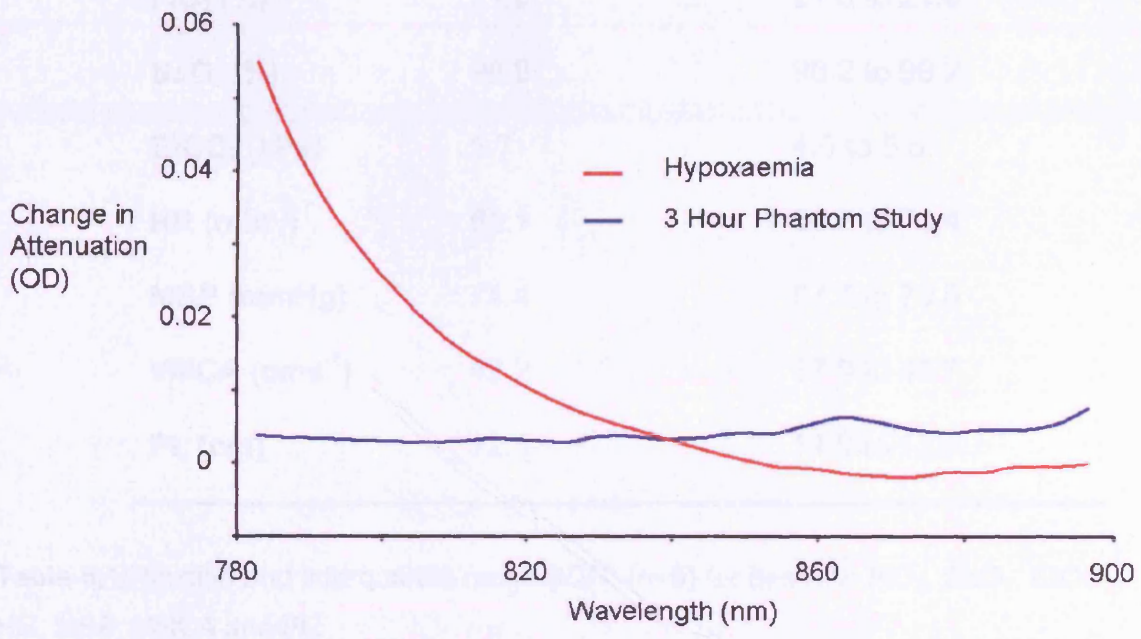

Figure 5.1: Change in attenuation during three hour phantom study compared to group mean change in attenuation from baseline to nadir of hypoxaemia.

5.3.2 Human Studies

Table 5.1 shows baseline data for the subject group. There were no significant changes in PL during any of the phases of the study ($p>0.05$).

5.3.2.1 Hypoxaemia

The median time of hypoxia required to achieve arterial oxygen saturation of 80% was 4.7 minutes (range 3 – 12 minutes). The length of each recovery period was fixed at 5 minutes for all subjects.

Figure 5.2 shows data for a single subject, demonstrating the experimental time course. Assessment of the data during both hypoxaemia and recovery revealed a significant correlation between $\Delta ecDO_2$ and Δ[oxCCO] ($r=0.78$ $p<0.001$), but

no correlation between $\Delta ecDO_2$ and Δ[Hbdiff] (r=0.49 p=0.145) or between $\Delta ecDO_2$ and Δ[HbT] (r=-0.33 p=0.584).

	Median	*IQR*
FiO_2 (%)	21.0	21.0 to 21.0
SaO_2 (%)	98.6	98.2 to 99.2
$EtCO_2$ (kPa)	5.7	4.9 to 5.8
HR (min^{-1})	61.1	56.7 to 70.4
MBP (mmHg)	74.4	67.7 to 79.8
VMCA (cms^{-1})	43.2	37.9 to 49.7
PL (cm)	12.5	11.9 to 12.7

Table 5.1: Median and interquartile range (IQR) (n=8) for baseline FiO_2, SaO_2, $EtCO_2$, HR, MBP, VMCA and PL.

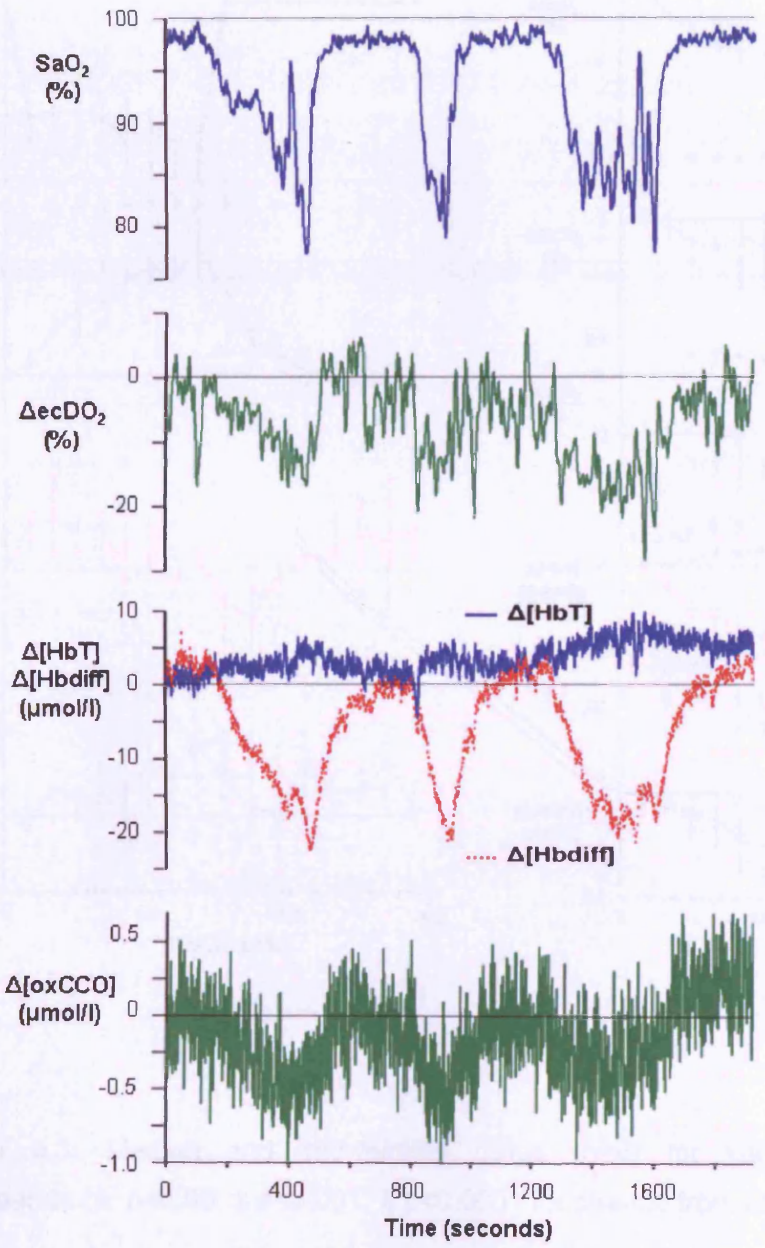

Figure 5.2: SaO_2, $\Delta ecDO_2$, Δ[Hbdiff], Δ[HbT] and Δ[oxCCO] for single subject during three cycles of hypoxaemia.

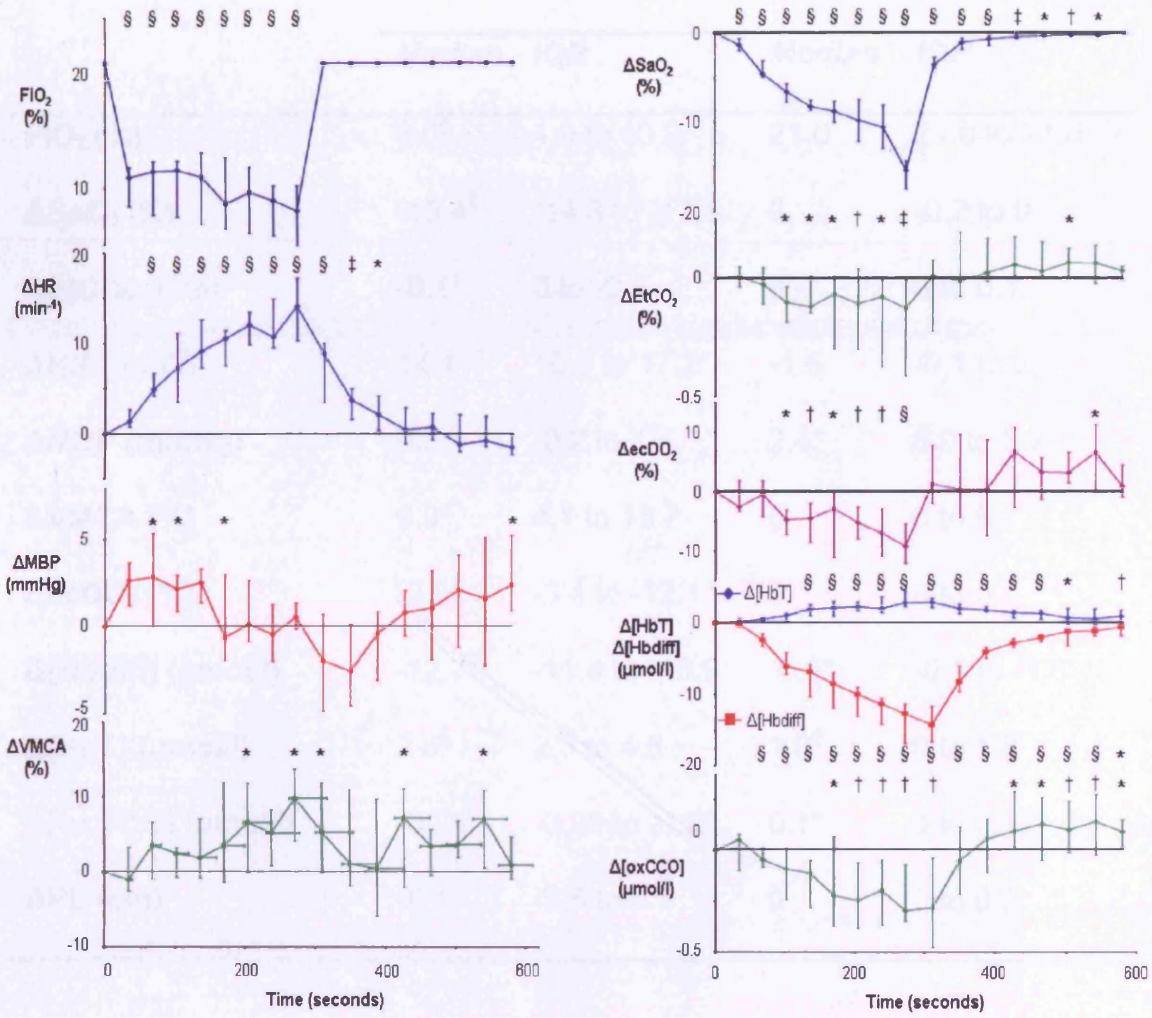

Figure 5.3: Median and interquartile range (n=8) for variable values during hypoxaemia (✶ $p<0.05$, ‡ $p<0.001$, § $p<0.0001$ for change from baseline).

	Hypoxaemia		*Recovery*	
	Median	***IQR***	***Median***	***IQR***
FiO_2 (%)	8.0§	4.9 to 10.2	21.0	21.0 to 21.0
ΔSaO_2 (%)	-15.4§	-14.3 to -17.5	0	-0.2 to 0
$\Delta EtCO_2$ (kPa)	-0.1‡	0 to -0.4	0	0 to 0.1
ΔHR (min^{-1})	14.1§	10.3 to 17.2	-1.5	-0.1 to 2.4
ΔMBP (mmHg)	0.5	-0.2 to 1.4	2.4*	0.9 to 5.2
ΔVMCA (%)	9.9*	4.1 to 13.7	0	0 to 0
$\Delta ecDO_2$ (%)	-9.2§	-5.4 to -12.1	0	0 to 0
Δ[Hbdiff] (µmol/l)	-12.7§	-11.4 to -16.9	-0.6*	-0.1 to -1.8
Δ[HbT] (µmol/l)	2.8§	2.3 to 4.5	1.0†	0 to 1.8
Δ[oxCCO] (µmol/l)	-0.24†	-0.28 to -0.06	0.1*	0 to 0.12
ΔPL (cm)	-0.1	-0.5 to 0.1	0	0 to 0.2

Table 5.2: Median and interquartile range (IQR) (n=8) for changes from baseline to nadir of hypoxaemia, and end of recovery period for measured variable values (* $p<0.05$, † $p<0.01$, ‡ $p<0.001$, § $p<0.0001$ for change from baseline).

5.3.2.2 Hyperoxia

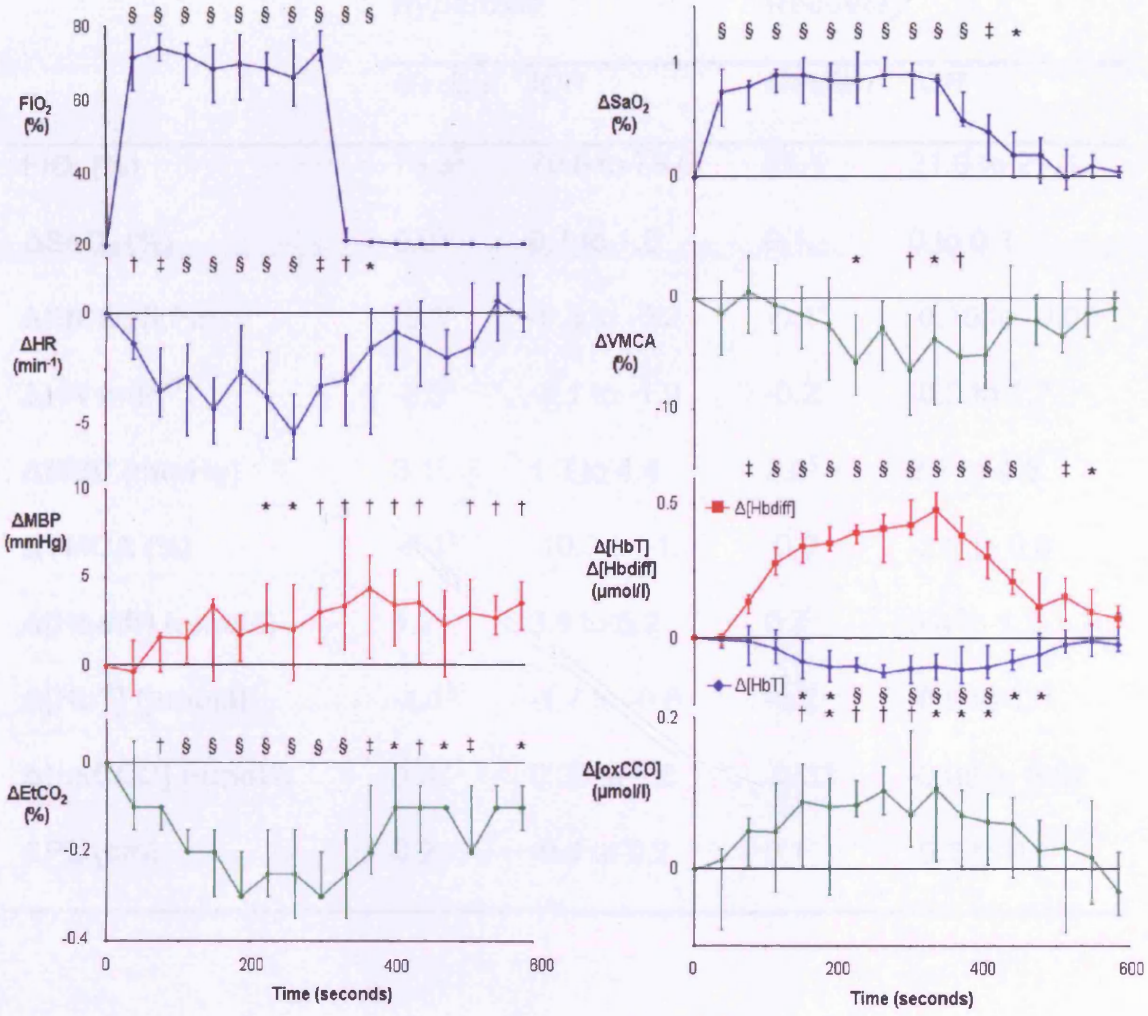

Figure 5.4: Median and interquartile range (n=8) for variable values during hyperoxia (⋆ $p<0.05$, † $p<0.01$, ‡ $p<0.001$, § $p<0.0001$ for change from baseline).

	Hyperoxia		*Recovery*	
	Median	***IQR***	***Median***	***IQR***
FiO_2 (%)	73.3§	70.5 to 78.6	21.1	21.0 to 21.3
ΔSaO_2 (%)	0.9§	0.7 to 1.0	0.1	0 to 0.1
Δ$EtCO_2$ (kPa)	-0.3§	-0.3 to -0.2	-0.1*	-0.15 to -0.05
ΔHR (min^{-1})	-3.3‡	-5.1 to -1.9	-0.2	-0.9 to 1.7
ΔMBP (mmHg)	3.1†	1.3 to 4.4	3.6†	2.1 to 4.8
ΔVMCA (%)	-6.4†	-10.3 to -1.4	-0.9	-2.0 to 0.6
Δ[Hbdiff] (µmol/l)	4.2§	3.9 to 5.2	0.7	0.4 to 1.2
Δ[HbT] (µmol/l)	-1.1§	-1.7 to -0.6	-0.2	-0.5 to 1.0
Δ[oxCCO] (µmol/l)	0.07†	0.03 to 1.8	-0.03	-0.06 to 0.02
ΔPL (cm)	0.2	-0.4 to 0.2	0.1	-0.2 to 0.1

Table 5.3: Median and interquartile range (IQR) (n=8) for changes from baseline to nadir of hyperoxia, and end of recovery period for measured variable values (* $p<0.05$, † $p<0.01$, ‡ $p<0.001$, § $p<0.0001$ for change from baseline).

5.3.2.3 Hyperventilation

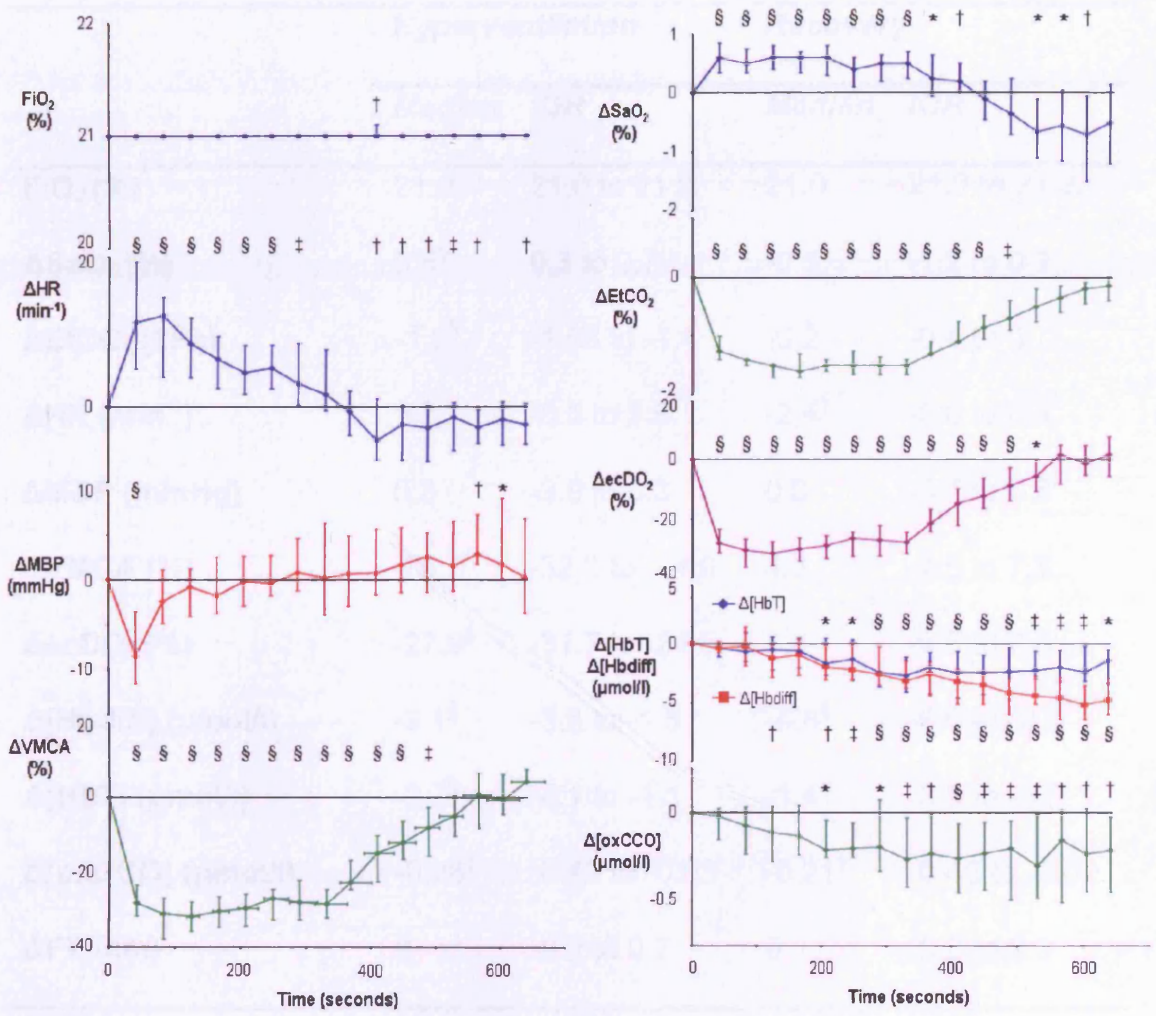

Figure 5.5: Median and interquartile range (n=20) for variable values during hyperventilation (* p<0.05, † p<0.01, ‡ p<0.001, § p<0.0001 for change from baseline).

	Hyperventilation		*Recovery*	
	Median	***IQR***	***Median***	***IQR***
FiO_2 (%)	21.0	21.0 to 21.0	21.0	21.0 to 21.2
ΔSaO_2 (%)	0.5§	0.3 to 0.7	-0.5	-1.2 to 0.2
$\Delta EtCO_2$ (kPa)	-1.5§	-1.65 to -1.4	-0.2	-0.4 to 0
ΔHR (min^{-1})	1.7	-0.5 to 7.6	-2.4†	-5.0 to 0.4
ΔMBP (mmHg)	0.3	-3.0 to 6.3	0.3	-3.7 to 6.8
ΔVMCA (%)	-28.5§	-32.2 to -24.6	4.3	-4.6 to 7.5
$\Delta ecDO_2$ (%)	-27.9§	-31.7 to -24.5	1.8	-5.5 to 7.8
Δ[Hbdiff] (µmol/l)	-3.1§	-3.8 to -1.5	-4.8§	-6.0 to -2.9
Δ[HbT] (µmol/l)	-2.7§	-4.1 to -1.1	-1.4*	-3.3 to -0.5
Δ[oxCCO] (µmol/l)	-0.26‡	-0.42 to -0.03	-0.21†	-0.45 to -0.02
ΔPL (cm)	0	-0.2 to 0.2	0	-0.3 to 0.3

Table 5.4: Median and interquartile range (IQR) (n=20) for changes from baseline to nadir of hyperventilation, and end of recovery period for measured variable values (* $p<0.05$, † $p<0.01$, ‡ $p<0.001$, § $p<0.0001$ for change from baseline).

During hyperventilation there were no correlations between $\Delta ecDO_2$ and Δ[oxCCO] (r=-0.31 p=0.69) or $\Delta ecDO_2$ and Δ[HbT] (r=-0.25 p=0.96) but $\Delta ecDO_2$ correlated with Δ[Hbdiff] (r=-0.68 p=0.008).

5.3.2.4 Hypercapnoea

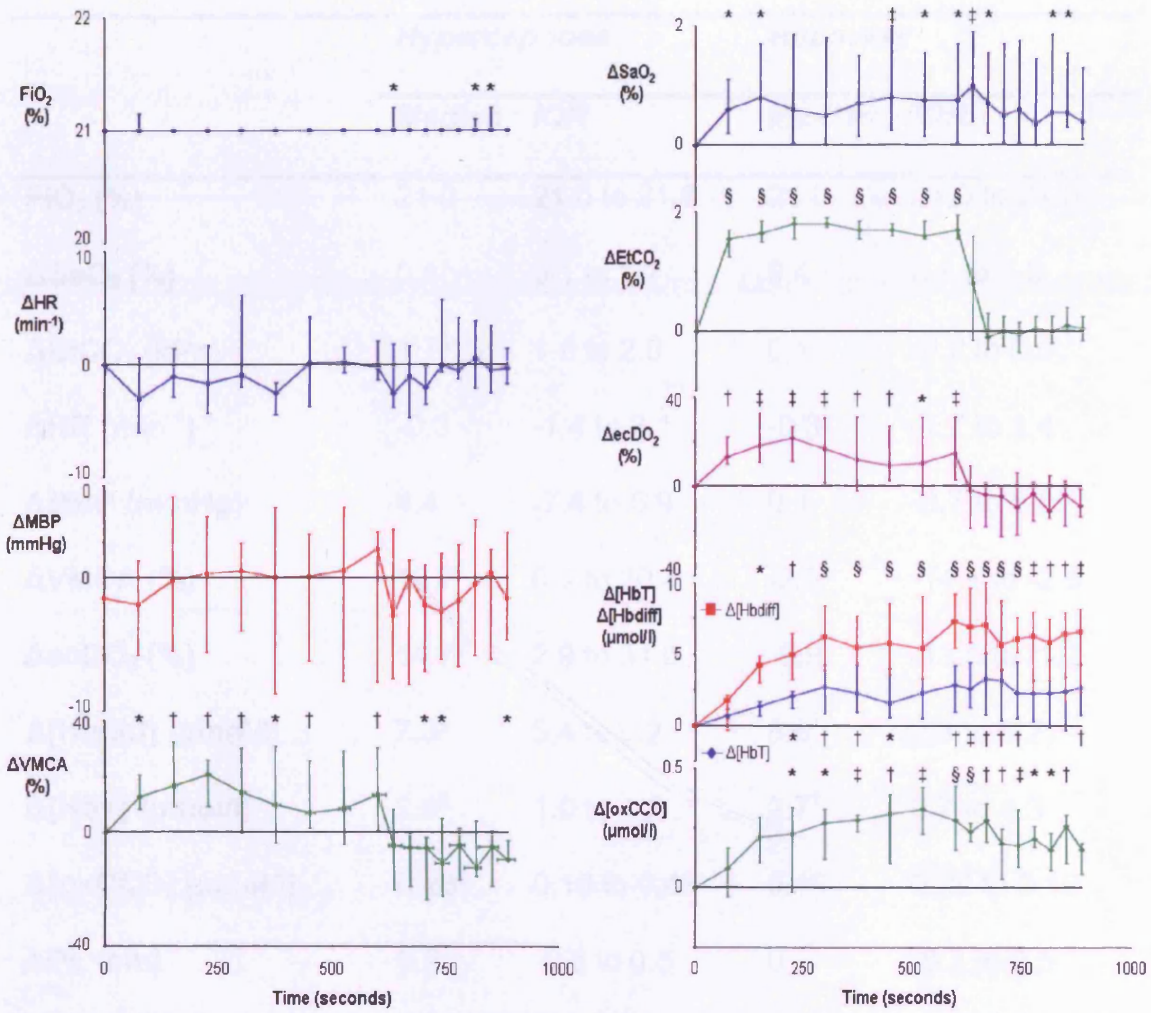

Figure 5.6: Median and interquartile range (n=8) for variable values during hypercapnoea (✶ $p<0.05$, † $p<0.01$ for change from baseline).

	Hypercapnoea		*Recovery*	
	Median	***IQR***	***Median***	***IQR***
FiO_2 (%)	21.0	21.0 to 21.0	21.0	21.0 to 21.0
ΔSaO_2 (%)	0.8*	0.1 to 1.7	0.4	0.1 to 1.3
$\Delta EtCO_2$ (kPa)	1.7§	1.6 to 2.0	0.1	-0.2 to 0.3
ΔHR (min^{-1})	-0.3	-1.4 to 2.1	-0.3	-1.7 to 1.4
ΔMBP (mmHg)	4.4	-7.4 to 5.9	0.1	-3.7 to 5.9
ΔVMCA (%)	13.7†	0.9 to 30.4	-9.3*	-14.4 to -2.5
$\Delta ecDO_2$ (%)	14.7‡	2.9 to 31.0	-8.9	-13.5 to -1.3
Δ[Hbdiff] (µmol/l)	7.3§	5.4 to 9.2	6.6‡	2.3 to 8.2
Δ[HbT] (µmol/l)	2.9†	1.0 to 4.2	2.7†	0.7 to 4.3
Δ[oxCCO] (µmol/l)	0.28§	0.16 to 0.43	0.16	0.06 to 0.19
ΔPL (cm)	0.2	-0.5 to 0.5	0	-0.2 to 0.5

Table 5.5: Median and interquartile range (IQR) (n=8) for changes from baseline to nadir of hypercapnoea, and end of recovery period for measured variable values (* $p<0.05$, † $p<0.01$, ‡ $p<0.001$, § $p<0.0001$ for change from baseline).

During hypercapnoea there were no correlations between $\Delta ecDO_2$ and Δ[oxCCO] ($r=0.37$ $p=0.414$), $\Delta ecDO_2$ and Δ[HbT] ($r=-0.28$ $p=0.76$) or $\Delta ecDO_2$ and Δ[Hbdiff] ($r=-0.37$ $p=0.42$).

5.3.2.5 Moderate Hyperventilation

	Hypercapnoea		*Recovery*	
	Median	***IQR***	***Median***	***IQR***
FiO_2 (%)	21.0	21.0 to 21.0	21.0	21.0 to 21.0
ΔSaO_2 (%)	0.3†	0.2 to 0.5	0.0	-0.4 to 0.2
$\Delta EtCO_2$ (kPa)	-0.6§	-0.6 to -0.4	0	-0.2 to 0.3
Δ[Hbdiff] (µmol/l)	-1.4	-1.6 to -0.5	-1.2	-2.1 to -0.2
Δ[HbT] (µmol/l)	-0.8	-1.9 to -0.2	0.8	-1.0 to 1.8
Δ[oxCCO] (µmol/l)	0.05	-0.06 to 0.10	-0.02	-0.06 to 0.12
ΔPL (cm)	-0.3	-0.4 to 0.6	1.0	-0.1 to 1.2

Table 5.6: Median and interquartile range (IQR) (n=9) for changes from baseline to nadir of hyperventilation, and end of recovery period during moderate graded hyperventilation study for measured variable values († $p<0.01$, § $p<0.0001$ for change from baseline).

5.4 Discussion

Changes in cerebral [oxCCO] measured using BBS in adult humans during changes in oxygenation and $EtCO_2$ are shown. These results demonstrate the potential of this instrumentation to make non-invasive measurements of changes in mitochondrial redox in the adult brain. Measured optical pathlength did not change significantly during any of these studies suggesting that large changes in light scattering which would invalidate the assumptions of the MBLL did not occur. Signal to noise ratio for the calculation of optical pathlength using second differential spectroscopy has been estimated using Monte Carlo simulation[19]. From this data we would estimate the predicted accuracy of our pathlength calculation to be in the region of 5.2%.

5.4.1 Phantom Study

The results from the stability study show a small change in NIR light attenuation across the course of a three hour data collection period. This change in attenuation can be considered an instrumentation artefact as one would not expect any changes in the optical characteristics of the epoxy phantom over this time scale. However the magnitude of the attenuation change during the phantom study is negligible compared to that measured during hypoxaemia and in addition the spectrum of this artefactual attenuation change is very near to being flat and will have a minimal effect on the chromophore fitting procedure. We can therefore conclude that the stability of the BBS system is adequate for studies of the duration we describe and that the cerebral chromophore changes measured are not a product of instrumentation artefact.

5.4.2 Hypoxaemia

We describe significant changes in cerebral [oxCCO] measured during hypoxaemia to an SaO_2 of 80%. We found distinct differences between the measured CCO and haemoglobin signals. Figure 5.3 shows Δ[HbT] rising during the hypoxaemic challenge before gradually returning towards, but not reaching, baseline values after five minutes of normoxic recovery. This infers an increase in cerebral blood volume during hypoxaemia probably as a result of hypoxaemic vasodilatation. Δ[Hbdiff] provides an assessment of changes in the balance of $\Delta[HbO_2]$ and Δ[HHb] and is usually assumed to be a measure of changes in the balance of regional cerebral oxygen delivery and utilisation. Although its interpretation is complicated by volume changes within the various vascular compartments, Δ[Hbdiff] has been used to define thresholds for critical ischaemia in patients undergoing neurovascular procedures[16]. In this study we show Δ[Hbdiff] decreasing during hypoxaemia and then returning towards, but not reaching, baseline values after five minutes of normoxic recovery. Δ[oxCCO] decreases during hypoxaemia and returns to baseline before Δ[Hbdiff] with a subsequent increase above baseline during the normoxic recovery period. Increased cerebral Δ[oxCCO] during the recovery period after hypoxaemia has been demonstrated in animal models[20] and has not been

fully explained but may be related to $ecDO_2$ rising above baseline during the recovery period.

Calculation of the correlation between $\Delta ecDO_2$ and Δ[Hbdiff], Δ[HbT] and Δ[oxCCO] was performed on the data from both the hypoxaemic and recovery phases of the study to assess the ability of the three measures to detect both decreased and increased $ecDO_2$. Both Δ[Hbdiff] and Δ[HbT] did not rise above, or drop below, baseline respectively in response to the increase in $ecDO_2$ during recovery and this results in the lack of significant correlations. There was a significant correlation between $\Delta ecDO_2$ and Δ[oxCCO], inferring that this NIRS measurement has clinical relevance as a measure of changes in cerebral oxygen delivery. We therefore suggest that Δ[oxCCO] provides a more reliable assessment of changes in cerebral oxygen delivery during hypoxaemia than either Δ[Hbdiff] or Δ[HbT].

Hampson *et al* investigated changes in the CCO *signal* in response to hypoxaemia in healthy volunteers and demonstrated reduction of CCO during reductions of SaO_2 to 70%, although they were not able to calculate chromophore concentration changes. However, the light attenuation conversion algorithm used in Hampson's study, known as the Duke-P algorithm, has been criticised, because it produces a high degree of crosstalk between the HbO_2 and CCO signals and, furthermore, when applied to animal datasets, has produced Δ[oxCCO] in excess of total CCO concentration measured in brain homogenates[6].

Edwards *et al* investigated Δ[oxCCO] in neonates using a commercial six wavelength NIRO 1000 spectrometer. They found no Δ[oxCCO] during alterations in SaO_2 between 85-99%[21]. Our previous work in patients with obstructive sleep apnoea demonstrated a reduction in Δ[oxCCO] during severe desaturation[10], but this clinical paradigm did not allow for controlled SaO_2 manipulation and cellular and cerebrovascular responses in this patient group, who are exposed to repeated severe hypoxic episodes, may not reflect those of healthy individuals.

In an attempt to investigate the effect of an isolated hypoxaemia on Δ[oxCCO] we used an $EtCO_2$ feedback loop to minimise changes in $PaCO_2$. Despite this, we found a small but significant median reduction in $EtCO_2$ of 0.1 kPa at the nadir of hypoxemia. However the moderate graded hyperventilation protocol results demonstrate that a slow reduction in $EtCO_2$ of 0.5 kPa does not produce a significant reduction in Δ[oxCCO] and it is therefore unlikely that the 0.1 kPa reduction in $EtCO_2$ during hypoxaemia is unlikely to be of clinical relevance to the Δ[oxCCO] results.

Controversy exists over how readily CCO becomes reduced following reduced oxygen tension. Several different algorithms exist for the conversion of light attenuation to chromophore concentration changes and the choice of algorithm can affect the results[6]. Some animal studies suggest that CCO reduction only occurs during extreme reduction in cerebral oxygen delivery[20,22,23], whilst others have found a gradual reduction in CCO during hypoxaemia[24]. These variations may relate to the experimental challenges, which comprised graded hypoxia[24], anoxia[20,23] or induced hypotension[22]. Some investigators have observed a 20-25 second delay between changes in haemoglobin concentrations and CCO redox state following anoxia and have interpreted this as evidence that CCO reduction does not occur during moderate hypoxaemia[20,23]. Yet we also observed a temporal delay between the first significant drops in Δ[Hbdiff] and Δ[oxCCO] during a moderate hypoxaemia paradigm and the instigation of anoxia may be too swift a challenge to allow full investigation of the relationship between CCO redox state and oxygen delivery. In addition, these studies used animals initially ventilated with supra-normal concentrations of oxygen, resulting in baseline arterial oxygen tensions between 14.7 and 65 kPa[20,22-24]. Elevated baseline values might further delay the onset of changes in CCO redox during hypoxaemia leading to the conclusion that CCO reduction only occurs after severe reduction in oxygen delivery. These comparisons are further complicated by the fact that some studies have been performed in perfluorocarbon (PFC) exchanged animals[24] with resultant greatly decreased tissue oxygen delivery compared to the blooded animal for a given arterial oxygen tension.

For the measurement of Δ[oxCCO] to be a useful clinical marker of reduced cerebral oxygen delivery, changes from baseline must be observed before irreparable cerebral hypoxic injury occurs. We show that in the healthy human brain, gradual CCO reduction takes place during moderate hypoxaemia in healthy volunteers. This result indicates that BBS measurement of CCO redox state has the potential to monitor the adequacy of cerebral mitochondrial oxygen delivery and therefore merits evaluation as a patient monitor.

5.4.3 Hyperoxia

The responses of HR, MBP, and $EtCO_2$ to hyperoxia were similar to those discussed in chapter 4 and are not discussed further. We observed a reduction in [HbT] during hyperoxia demonstrating the vasoconstrictive affect with subsequent reduction in cerebral blood volume and this then returned to baseline during the recovery period. Hyperoxia has competing effects on cerebral oxygen delivery consisting of increased arterial oxygen content but reduced cerebral blood flow. In our study [Hbdiff] increased during hyperoxia despite the reduction in VMCA, and hence CBF, as measured by TCD. Assuming no large changes in $CMRO_2$ this implies that the combined effect of hyperoxia is to increase cerebral oxygen delivery. Δ[oxCCO] also increased during hyperoxia and then returned to baseline by the end of the study. This suggests that cerebral CCO is not fully oxidised at normoxic normocapnoea and that changes in mitochondrial redox state can be induced by normobaric hyperoxygenation. Other investigators have shown positive Δ[oxCCO] either in the recovery period after anoxia or in response to changes in $PaCO_2$ and oxidation of CCO has also been demonstrated in response to visual stimulation[25] . Evidence therefore exists to suggest that increases in baseline CCO oxidation state occur during physiological challenges, but, to our knowledge, this is the first report of positive Δ[oxCCO] during hyperoxia. The resting oxidation state of CCO has been investigated using BBS in animal models. Springett *et al* compared the drop in Δ[oxCCO] during anoxia at either normocapnoea or hypercapnoea in the piglet brain. Full reduction of CCO during anoxia and full oxidation of CCO in the hyperaemic period after anoxia at hypercapnoea were assumed and hence a baseline CCO oxidation state of

67.3 ± 18.3% oxidised was derived[20]. Cooper *et al* compared the reduction in Δ[oxCCO] during anoxia with the reported total CCO concentration in the adult rat brain and assuming full reduction during anoxia derived a baseline oxidation of 82.0 ± 16.6% oxidised. Both these values are likely to be approximations: the assumption of complete CCO oxidation in the recovery period after hypercapnoeic anoxia as used by Springett *et al* may be erroneous and the comparison of NIRS data with CCO concentration measured in brain homogenates as carried out by Cooper *et al* makes no allowance for the multilayered anatomy of the rat brain with differing CCO concentrations in the various layers[26]. Both these studies suggest that CCO is not fully oxidised at normoxia and normocapnoea and our data are consistent with these findings.
Conversely Inagaki and Tamura used a dual-wavelength spectrophotometer in the blood free isolated rat head to study Δ[oxCCO] and found no further oxidation from baseline during increased oxygen tension. They therefore concluded that CCO was >95% oxidised at baseline. This study used a PFC perfused rat head which had been isolated from the body and this has some advantages in that the effects on light attenuation by changes in haemoglobin oxygenation are negligible. However this model is far from physiological as oxygen transfer to the brain tissue in the PFC perfused animal differs markedly from that found in the blood perfused animal and, in this study, cerebral perfusion was maintained by a non-pulsatile pump rather than the heart. These findings may therefore not be indicative of physiological responses in the healthy brain.

Our data present the intriguing possibility that it is possible to increase oxidation in the mitochondrial electron transfer chain by the simple technique of increasing FiO_2 and demonstrates the potential of BBS to measure the induced changes. Increased oxidation of CCO suggests an increase in aerobic metabolism and therefore ATP production increased FiO_2 might be a therapeutic option in conditions associated with cell death related energy failure. This possibility is investigated in chapter 7.

5.4.4 Hyperventilation

The haemodynamic and CBF responses to hyperventilation have been discussed in chapter 4. VMCA returned to baseline by the end of the study but Δ[HbT], which reflects arteriolar vasoconstriction, remained significantly below baseline at the end of the study, and a similar trend was observed in Δ[Hbdiff]. The predominant mechanism for this reduction in Δ[Hbdiff] is reduced CBF, which will tend to increase oxygen extraction and hence reduce venous oxyhaemoglobin saturation, and reduced arterial CBV producing a decrease in AVR. The reduced pCO_2 will cause a reduction in pH and this will induce a left shift in the oxygen-haemoglobin dissociation curve increasing the affinity for oxygen and tending to oppose the increased oxygen extraction. Δ[Hbdiff] remains below baseline at the end of the study and given that VMCA has returned to baseline by this stage, this is likely to be related to the persistence of reduced arterial CBV and AVR.

Δ[oxCCO] reduced during hyperventilation and did not return to baseline by the end of the study. The median drop in Δ[oxCCO] during hyperventilation was 0.26 μM and this compares with a median drop of 0.24 μM during hypoxaemia. It is interesting to note that the median estimated change in DO_2 during hyperventilation was 27.9% and this is much greater than that observed during hypoxaemia (9.2%). The estimated change in DO_2 during hypoxaemia will be an underestimate as there will also be a reduction in the quantity of dissolved oxygen but this effect is unlikely to be clinically significant. The Δ[Hbdiff] changes associated with the two challenges also vary markedly (-12.7 μM during hypoxaemia and -3.1 μM during hyperventilation) and this finding is at odds with the $\Delta ecDO_2$ response.

It may be that the reduced oxygen delivery during hyperventilation is responsible for the observed drop in Δ[oxCCO], however CCO oxidation state is affected by other factors other than oxygen tension for example electron flux through the enzyme, pH changes and changes in ADP concentration[27]. Changes in $PaCO_2$ will have metabolic effects beyond changes in oxygen delivery most notably to cause a decrease in pH and this reduction in pH will

tend to further reduce the CCO oxidation state[28,29]. This does not fully explain our results as one might therefore expect hyperventilation to be associated with a greater drop in Δ[oxCCO] than hypoxaemia. It appears that CCO redox state might be affected by a range of metabolic processes as yet incompletely understood. This may explain why we found no correlation between $\Delta ecDO_2$ and Δ[oxCCO] in this part of the study.

5.4.5 Hypercapnoea

In many ways the responses we observed in the BBS variables during hypercapnoea appear to be a continuation of those seen during hyperventilation. VMCA increased during hypercapnoea and returned to baseline by the end of the study, whereas Δ[HbT] and Δ[Hbdiff] increased with hypercapnoea and remained elevated above baseline values at the end of the study. Δ[oxCCO] also increased during hyperventilation and similarly to the discussion in 5.4.3 this may relate to increases in CBF and hence oxygen delivery or the metabolic effect of decreased pH. Similar to the results of the hyperventilation study we found no correlation between $\Delta ecDO_2$ and Δ[oxCCO] during this paradigm.

Oxidation in CCO during hypercapnoea has been observed in human neonates using a commercial six wavelength NIRS system and also in piglets using a BBS system[21,23]. The piglet study by Quaresima *et al* is particular notable as similar Δ[oxCCO] were found in the blooded and bloodless PFC exchanged animal suggesting that this finding is not related to crosstalk artefact or changes in light scattering.

5.5 Conclusion

We describe quantification of cerebral Δ[oxCCO] during hypoxaemia in healthy adults and show that this measurement provides a marker of reduced cellular oxygen availability in healthy humans. Hyperoxia induces increases in Δ[oxCCO] and oxidation in cerebral mitochondrial redox in disease states might be possible by the simple and cheap intervention of increasing FiO_2. Changes in $EtCO_2$ also induce Δ[oxCCO], and these changes may be related to changes

in DO_2 or metabolic effects. Further work both *in vitro* and *in vivo* is required to determine the relative contributions of these processes.

Although NIRS measured haemoglobin concentrations reflect intravascular oxygenation, the CCO signal indicates changes in *mitochondrial* oxygen delivery and utilisation. In health there is likely to be a close relationship between intravascular and mitochondrial oxygen delivery. However, in pathological situations, this relationship may be altered by tissue oedema, which reduces oxygen diffusion from capillary to mitochondrion. In addition, mitochondrial dysfunction, which reduces the ability to metabolise oxygen, may occur. It is anticipated that in these situations the mitochondrial CCO signal will yield different information to the intravascular haemoglobin signal, and will provide clinicians with a bedside tool with which to ensure adequate mitochondrial oxygen delivery and thus potentially preserve cell function.

The clinical relevance of cerebral Δ[oxCCO] has been demonstrated by NIRS measurements in adult patients undergoing cardiac surgery, where cerebral Δ[oxCCO] correlates with neurological outcome[9,30]. Other patient groups exist who are at risk of critically reduced cerebral oxygen delivery and one example of such a group is patients who have suffered TBI. The use of BBS monitoring in patients with TBI will be examined in chapter 7.

References

1. Richter OM, Ludwig B. Cytochrome c oxidase--structure, function, and physiology of a redox-driven molecular machine. *Rev Physiol Biochem Pharmacol* 2003;147:47-74.
2. Cooper CE, Matcher SJ, Wyatt JS, Cope M, Brown GC, Nemoto EM, Delpy DT. Near-infrared spectroscopy of the brain: relevance to cytochrome oxidase bioenergetics. *Biochem Soc Trans* 1994;22:974-980.
3. Cooper CE, Springett R. Measurement of cytochrome oxidase and mitochondrial energetics by near-infrared spectroscopy. *Philos Trans R Soc Lond B Biol Sci* 1997;352:669-676.
4. Ferrari M, Hanley DF, Wilson DA, Traystman RJ. Redox changes in cat brain cytochrome-c oxidase after blood-fluorocarbon exchange. *Am J Physiol* 1990;258:H1706-H1713.
5. Jöbsis FF. Noninvasive, infrared monitoring of cerebral and myocardial oxygen sufficiency and circulatory parameters. *Science* 1977;198:1264-1267.
6. Matcher SJ, Elwell CE, Cooper CE, Cope M, Delpy DT. Performance comparison of several published tissue near-infrared spectroscopy algorithms. *Anal Biochem* 1995;227:54-68.
7. Springett RJ, Wylezinska M, Cady EB, Hollis V, Cope M, Delpy DT. The oxygen dependency of cerebral oxidative metabolism in the newborn piglet studied with 31P NMRS and NIRS. *Adv Exp Med Biol* 2003;530:555-563.
8. Tsuji M, Naruse H, Volpe J, Holtzman D. Reduction of cytochrome aa3 measured by near-infrared spectroscopy predicts cerebral energy loss in hypoxic piglets. *Pediatr Res* 1995;37:253-259.
9. Kakihana Y, Matsunaga A, Tobo K, Isowaki S, Kawakami M, Tsuneyoshi I, Kanmura Y, Tamura M. Redox behavior of cytochrome oxidase and neurological prognosis in 66 patients who underwent thoracic aortic surgery. *Eur J Cardiothorac Surg* 2002;21:434-439.
10. McGown AD, Makker H, Elwell C, Al Rawi PG, Valipour A, Spiro SG. Measurement of changes in cytochrome oxidase redox state during obstructive sleep apnoea using near-infrared spectroscopy. *Sleep* 2003;26:710-716.

11. Cooper CE, Cope M, Springett R, Amess PN, Penrice J, Tyszczuk L, Punwani S, Ordidge R, Wyatt J, Delpy DT. Use of mitochondrial inhibitors to demonstrate that cytochrome oxidase near-infrared spectroscopy can measure mitochondrial dysfunction noninvasively in the brain. *J Cereb Blood Flow Metab* 1999;19:27-38.
12. Cope M. Specific extinction spectra of tissue chromophores. http://www.medphys.ucl.ac.uk/research/borl/research/NIR_topics/spectra/spectra.htm. 1991.
13. Essenpreis M, Cope M, Elwell C, Arridge S, van der Zee P, Delpy D. Wavelength dependence of the differential pathlength factor and the log slope in time-resolved tissue spectroscopy. *Adv Exp Med Biol* 1993;333:9-20.
14. Matcher SJ, Cooper CE. Absolute quantification of deoxyhaemoglobin concentration in tissue near infrared spectroscopy. *Phys Med Biol* 1994;39:1295-1312.
15. Woodard H, White D. The composition of body tissues. *B J Radiol* 1986;59:1209-1219.
16. Kirkpatrick PJ, Lam J, Al-Rawi P, Smielewski P, Czosnyka M. Defining thresholds for critical ischemia by using near-infrared spectroscopy in the adult brain. *J Neurosurg* 1998;89:389-394.
17. Valdueza JM, Balzer JO, Villringer A, Vogl TJ, Kutter R, Einhaupl KM. Changes in blood flow velocity and diameter of the middle cerebral artery during hyperventilation: assessment with MR and transcranial Doppler sonography. *Am J Neuroradiol* 1997;18:1929-1934.
18. Alves OL, Daugherty WP, Rios M. Arterial hyperoxia in severe head injury: a useful or harmful option? *Curr Pharm Des* 2004;10:2163-2176.
19. Matcher SJ, Cope M, Delpy DT. Use of the water absorption spectrum to quantify tissue chromophore concentration changes in near-infrared spectroscopy. *Phys Med Biol* 1994;39:177-196.
20. Springett R, Newman J, Cope M, Delpy DT. Oxygen dependency and precision of cytochrome oxidase signal from full spectral NIRS of the piglet brain. *Am J Physiol Heart Circ Physiol* 2000;279:H2202-H2209.
21. Edwards AD, Brown GC, Cope M, Wyatt JS, McCormick DC, Roth SC, Delpy DT, Reynolds EO. Quantification of concentration changes in

neonatal human cerebral oxidized cytochrome oxidase. *J Appl Physiol* 1991;71:1907-1913.

22. Cooper CE, Delpy DT, Nemoto EM. The relationship of oxygen delivery to absolute haemoglobin oxygenation and mitochondrial cytochrome oxidase redox state in the adult brain: a near-infrared spectroscopy study. *Biochem J* 1998;332:627-632.
23. Quaresima V, Springett R, Cope M, Wyatt JT, Delpy DT, Ferrari M, Cooper CE. Oxidation and reduction of cytochrome oxidase in the neonatal brain observed by in vivo near-infrared spectroscopy. *Biochim Biophys Acta* 1998;1366:291-300.
24. Stingele R, Wagner B, Kameneva MV, Williams MA, Wilson DA, Thakor NV, Traystman RJ, Hanley DF. Reduction of cytochrome-c oxidase copper precedes failing cerebral O2 utilization in fluorocarbon-perfused cats. *Am J Physiol* 1996;271:H579-H587.
25. Heekeren HR, Kohl M, Obrig H, Wenzel R, von PW, Matcher SJ, Dirnagl U, Cooper CE, Villringer A. Noninvasive assessment of changes in cytochrome-c oxidase oxidation in human subjects during visual stimulation. *J Cereb Blood Flow Metab* 1999;19:592-603.
26. Drabkin DL. Metabolism of the Hemin Chromoproteins. *Physiol Rev* 1951;31:345-431.
27. Cooper CE, Springett RJ, Panagiotopoulou A, Penrice J. Near infrared spectroscopy of nitrosyl haemoglobin--relevance to in vivo detection of nitric oxide. *Biochem Soc Trans* 1996;24:448S.
28. Cooper CE, Matcher SJ, Wyatt JS, Cope M, Brown GC, Nemoto EM, Delpy DT. Near-infrared spectroscopy of the brain: relevance to cytochrome oxidase bioenergetics. *Biochem Soc Trans* 1994;22:974-980.
29. Thornstrom PE, Brzezinski P, Fredriksson PO, Malmstrom BG. Cytochrome c oxidase as an electron-transport-driven proton pump: pH dependence of the reduction levels of the redox centers during turnover. *Biochemistry* 1988;27:5441-5447.
30. Nollert G, Mohnle P, Tassani-Prell P, Uttner I, Borasio GD, Schmoeckel M, Reichart B. Postoperative neuropsychological dysfunction and cerebral oxygenation during cardiac surgery. *Thorac Cardiovasc Surg* 1995;43:260-264.

Chapter 6

Investigation of the presence of crosstalk between cytochrome c oxidase and haemoglobin signals during hypoxaemia

It has been suggested that NIRS measured Δ[oxCCO] might simply be an artefact of light conversion algorithms which are not able to adequately separate the CCO and haemoglobin signals. This is a complex area, yet the data collected during the studies described in this thesis provide an opportunity to investigate this issue.

In this chapter the presence of crosstalk is addressed through the application of two separate analysis techniques to the data recorded during the hypoxaemia part of the healthy volunteer studies (chapter 5). Firstly the relationship between the CCO and haemoglobin signals during the hypoxaemic and recovery phases of the study is investigated. Secondly, algorithms which either include or exclude the fitting of the oxidised-reduced CCO spectrum are compared.

The aim of this analysis is to investigate whether the CCO signal we are recording using BBS can be explained as merely be an artefact of the HbO_2 and HHb signals. If the CCO signal is explicable as an artefact then it is unlikely to provide information above that provided by the haemoglobin signals or be of clinical use.

6.1 Analysis of relationship between CCO and haemoglobin signals during hypoxaemia

6.1.1 Introduction

The specific extinction coefficients of the oxidised-reduced CCO difference spectrum in the near infrared region are similar in magnitude to those of oxy- and deoxy-haemoglobin[1], but the concentration of CCO in the brain is approximately one order of magnitude less than these other two chromophores[2]. This makes the separation of haemoglobin and CCO signals theoretically prone to crosstalk and raises the possibility that NIRS measured

changes in Δ[oxCCO] might be subject to artefacts resulting from measurement algorithms[3,4].

However, data collected using BBS systems and the UCLn algorithm during experimental protocols utilising mitochondrial inhibitors and perfluorocarbon-blood exchange in animals have shown that Δ[oxCCO] measurements are stable during large contemporaneous changes in [HbO_2] and [HHb][5,6]. If significant crosstalk were present then one might expect these changes in haemoglobin concentrations to produce spurious Δ[oxCCO]. Furthermore, data from human visual stimulation studies and from primary autonomic patients during periods of posture induced orthostatic hypotension suggest that cerebral Δ[oxCCO] is not merely crosstalk artefact[7,8].

In order to show that crosstalk is minimal it is necessary to show that Hb and HbO_2 (or any two non-collinear combinations) can be varied without affecting the CCO signal[9]. When using human subjects it is difficult to devise ethical experimental paradigms with which to test the presence or absence of crosstalk as it is not clear whether a particular change in haemoglobin oxygenation will affect CCO redox and there does not exist an alternative 'gold standard' with which to measure CCO redox without removing cerebral tissue. The main factor likely to affect CCO redox state is mitochondrial oxygen tension and this in turn will be predominantly affected by haemoglobin oxygenation. It is therefore unlikely that we will be able to produce wholly independent changes in haemoglobin oxygenation and CCO redox. However, if Δ[oxCCO] was merely a spurious artefact of the light conversion algorithm and no significant changes in light scattering occur, we might expect there to be a constant relationship between Δ[oxCCO] and the haemoglobin concentration changes. Conversely, if we do not observe a constant relationship between Δ[oxCCO] and the haemoglobin concentration changes then it is unlikely that measured Δ[oxCCO] is merely crosstalk artefact. When analysing the data from the hypoxaemia part of the healthy volunteer studies described in section 5.3.2.1 it became apparent that the CCO and haemoglobin signals showed different responses with Δ[oxCCO] returning to baseline values early in the hyperaemic recovery period

and subsequently rising above baseline levels whereas Δ[Hbdiff] and Δ[HbT] remain below and above baseline levels respectively. This suggested the there might be separation of the CCO and haemoglobin and signals and provided an ideal opportunity to investigate their inter-relationship.

6.1.2 Methods

The data used for this analysis were those collected during the hypoxaemia phase of the healthy volunteer studies as detailed in section 5.3.2.1. Briefly a BBS system was used to collect NIR spectra during alterations in FiO_2 though optodes placed on the heads of healthy volunteers. Spectra were collected at 1 Hz and converted into Δ[HbO_2], Δ[HHb] and Δ[oxCCO] using the UCL*n* algorithm. 10 second means of changes in chromophore concentrations were produced at nine equally spaced points during the hypoxaemia phase and nine equally spaced points during the recovery phase, thus splitting each phase into eight sections as shown in figure 4.4.

A multiple linear regression model was produced from the hypoxaemic period data (time points 1 to 9) for all subjects with Δ[oxCCO] as the dependent variable, and Δ[HbO_2] and Δ[HHb] as the independent variables. This analysis characterises the relationship between the Δ[oxCCO], and Δ[HbO_2] and Δ[HHb] during the hypoxaemic phase. A predicted Δ[oxCCO] ($\Delta[oxCCO]_{pred}$) for the recovery period was derived from the recovery period Δ[HbO_2] and Δ[HHb] using the multiple linear regression model results and $\Delta[oxCCO]_{pred}$ and $\Delta[oxCCO]_{meas}$ for the recovery period were compared. If Δ[oxCCO] was merely crosstalk artefact then the relationship between Δ[oxCCO], and Δ[HbO_2] and Δ[HHb] should remain constant during the two phases and $\Delta[oxCCO]_{pred}$ and $\Delta[oxCCO]_{meas}$ would be identical.

Statistical analysis was carried out using SAS software (v9.1, SAS Institute, USA) and p values <0.05 were considered significant. $\Delta[oxCCO]_{pred}$ and $\Delta[oxCCO]_{meas}$ for the recovery period were compared using a mixed model analysis to account for the repeated measures within each subject.

6.1.3 Results

There were no changes in optical pathlength during the study ($p>0.05$). Multiple linear regression of the group data from the hypoxaemic period revealed:

$$\Delta[oxCCO] = 0.0422 \times \Delta[HbO_2] + 0.0652 \times \Delta[HHb] - 0.0173 \qquad \textit{Eqn 6.1}$$

$p<0.0001$ $r=0.51$

Equation 6.1 was used to derive $\Delta[oxCCO]_{pred}$ for the recovery period. $\Delta[oxCCO]_{pred}$ and $\Delta[oxCCO]_{meas}$ differed significantly ($p=0.01$) (figure 6.1).

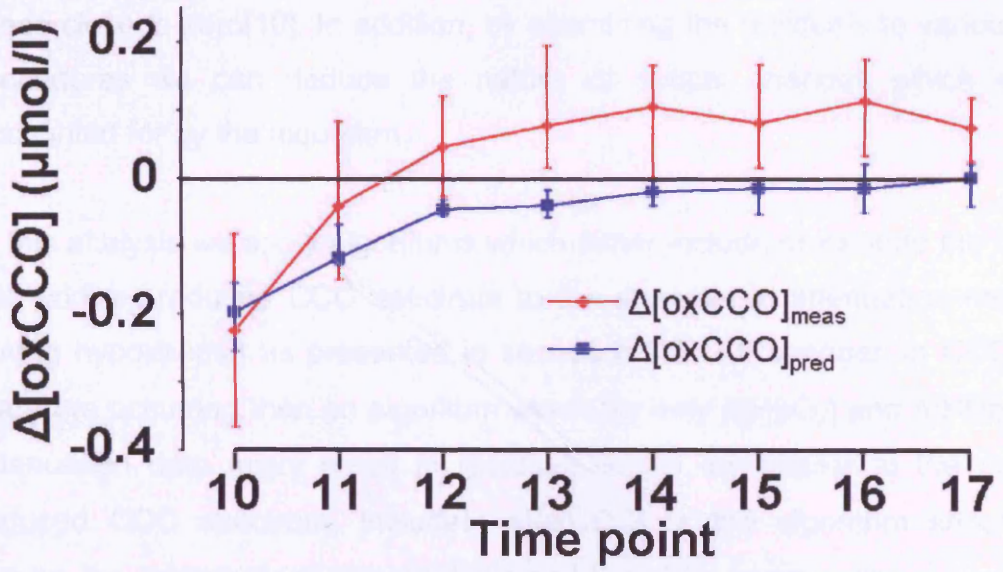

Figure 6.1: Comparison of measured and predicted Δ[oxCCO] during the recovery phase of the healthy volunteer hypoxaemia study.

6.1.4 Discussion

The fact that there were no significant changes in mean optical pathlength during the study, and that $\Delta[oxCCO]_{pred}$ and $\Delta[oxCCO]_{meas}$ were different (figure 6.1), suggests that $\Delta[oxCCO]_{meas}$ is not merely a crosstalk artefact resulting from the large changes in $\Delta[HbO_2]$ and $\Delta[HHb]$.

6.2 Analysis of residuals from fitting chromophore concentrations to near infrared data

6.2.1 Introduction

The UCL*n* BBS algorithm is a multiple regression technique which produces a 'best fit' between the attenuation data and the chromophore spectra. This fitting procedure may produce residuals due to changes in light scattering, changes in concentrations of chromophores not included in the algorithm or imperfect chromophore spectra. In order to verify the validity of the regression technique the residuals to the regression analysis must satisfy a number of assumptions: they must be normally distributed, heteroscedastic and independent with a mean close to zero[10]. In addition, by examining the residuals to various fitting procedures we can deduce the nature of optical changes which are not accounted for by the algorithm.

In this analysis we apply algorithms which either include or exclude the fitting of the oxidised-reduced CCO spectrum to the changes in attenuation measured during hypoxaemia as presented in section 5.3.2.1. If changes in CCO redox state are occurring then an algorithm which fits only $\Delta[HbO_2]$ and Δ[HHb] to the attenuation data might result in residuals which are similar to the oxidised-reduced CCO spectrum. Including Δ[oxCCO] in the algorithm should then reduce the magnitude of the residuals and therefore improve the regression fit. Conversely if the changes in attenuation can be accounted for solely by $\Delta[HbO_2]$ and Δ[HHb] then including Δ[oxCCO] in the algorithm will not improve the fit and might increase the magnitude of the residuals.

6.2.2 Methods

The data used for this analysis were those collected during the hypoxaemia phase of the healthy volunteer studies and summarised in section 6.1.2. The points just prior to the start of each hypoxaemia (baseline), and at the nadir of each hypoxaemia (hypoxaemia) were identified manually using the SaO_2 data. At each of the two points the mean of the preceding ten seconds of data was calculated. Data from the three experimental cycles were averaged to give mean values for SaO_2 and NIR light intensity at baseline and hypoxaemia for

each subject. Optical pathlength was calculated using second differential analysis of the 740nm water feature as previously discussed[11]. Change in NIR attenuation between baseline and hypoxaemia was then calculated from:

$$\Delta A = \log_{10}\left(\frac{I_{hypox}}{I_{base}}\right) \qquad \textit{Eqn 6.2}$$

where ΔA=change in attenuation, I_{base}=light intensity at baseline and I_{hypox}=light intensity at hypoxaemia (OD).

The UCL*n* algorithm[12] was used to fit chromophore extinction coefficients, corrected for the wavelength dependence of the optical pathlength[13], to the group mean change in attenuation, using 120 wavelengths between 780 and 900 nm. Chromophore specific extinction coefficients were downloaded from the medical physics UCL website[14]. First, only HbO_2 and HHb spectra (2 component fit – equation 6.3) and then HbO_2, HHb and the oxidised-reduced CCO difference spectra (3 component fit – equation 6.4) were fitted to the group mean change in attenuation. After interpolation of the residuals to the spectral resolution of the BBS system, the sums of the squares of the residuals from these two analyses were calculated, and the distributions of the two sets of residuals were compared.

$$\begin{pmatrix}\Delta[HbO_2]\\ \Delta[HHb]\end{pmatrix} = \frac{1}{PL}\begin{pmatrix}\varepsilon_{HbO_2}(\lambda_i) & \varepsilon_{HHb}(\lambda_i)\\ \vdots & \vdots\\ \varepsilon_{HbO_2}(\lambda_j) & \varepsilon_{HHb}(\lambda_j)\end{pmatrix}^{-1}\begin{pmatrix}\Delta A(\lambda_i)\\ \vdots\\ \Delta A(\lambda_j)\end{pmatrix} \qquad \textit{Eqn 6.3}$$

$$\begin{pmatrix}\Delta[HbO_2]\\ \Delta[HHb]\end{pmatrix} = \frac{1}{PL}\begin{pmatrix}\varepsilon_{HbO_2}(\lambda_i) & \varepsilon_{HHb}(\lambda_i) & \varepsilon_{oxCCO}(\lambda_i)\\ \vdots & \vdots & \vdots\\ \varepsilon_{HbO_2}(\lambda_j) & \varepsilon_{HHb}(\lambda_j) & \varepsilon_{oxCCO}(\lambda_j)\end{pmatrix}^{-1}\begin{pmatrix}\Delta A(\lambda_i)\\ \vdots\\ \Delta A(\lambda_j)\end{pmatrix} \qquad \textit{Eqn 6.4}$$

PL=pathlength (cm), ε = specific extinction coefficient of the subsequent chromophore (OD/μM/cm) and ΔA =change in attenuation, at wavelengths λ_i to λ_j.

A simulated attenuation spectrum was then calculated using assumed Δ[HHb], Δ[HbO_2] and Δ[oxCCO] and their respective specific extinction coefficients (equation 6.5): for this purpose attenuation changes due to other chromophore concentration changes were ignored.

$$\Delta A(\lambda_i) = PL\{\Delta[HbO_2] \times \varepsilon_{HbO_2}(\lambda_i) + \Delta[HbO_2] \times \varepsilon_{HHb}(\lambda_i) + \Delta[HbO_2] \times \varepsilon_{oxCCO}(\lambda_i)$$

Eqn 6.5

A 2 component model was fitted to this spectrum and the resultant residuals were compared with the residuals from the 2 component fit to the measured group mean change in attenuation between baseline and hypoxaemia. 2 component fits to the experimental and simulated data for each individual were then compared.

Statistical analysis was carried out using SAS software (v9.1, SAS Institute, USA) and p values <0.05 were considered significant. Group changes between baseline and hypoxaemia were compared using Wilcoxon signed rank test, distributions of the residuals from the various fitting procedures were compared using a 2 sample Siegel-Tukey test[15] and normality of residuals was assessed using the Shapiro-Wilk test. Exact two tailed tests of significance were used throughout.

6.2.3 Results

Results are presented as median (interquartile range). During the study SaO_2 fell from a baseline value of 98.6% (98.2 to 99.2) to 82.9% (81.7 to 84.7) at the end of hypoxaemia (p=0.008). Due to the ten second averaging window this median SaO_2 is higher than the 80% target which triggered then end of hypoxaemia phase. There was no change in optical pathlength between baseline and hypoxaemia (p=0.31) with median (IQR) of 12.6cm (11.6 to 12.8) at baseline and 11.9cm (11.4 to 12.3) at the end of hypoxaemia. Group mean change in attenuation from baseline to hypoxaemia is shown in figure 6.2.

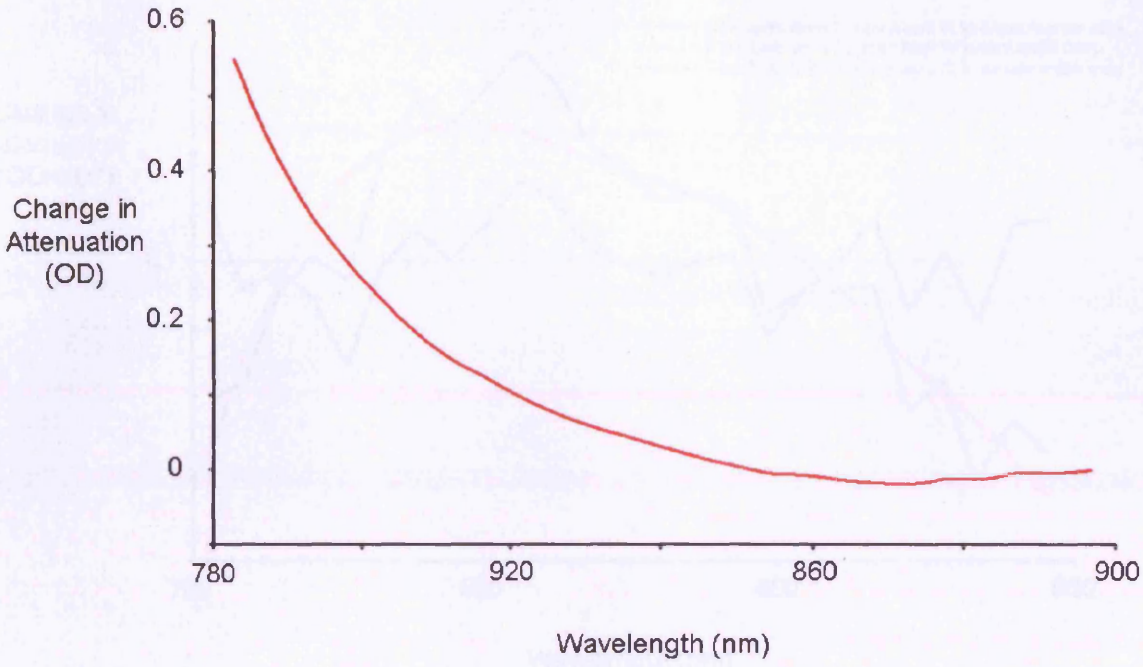

Figure 6.2: Group mean change in attenuation between baseline and hypoxaemia.

The residuals from the 2 and 3 component fits to the group mean experimental spectrum differed from each other ($p<0.0001$) (figure 6.3). The sum of the squares of the residuals was 9.6×10^{-6} OD^2 for the 2 component fit to the experimental spectrum and 1.2×10^{-6} OD^2 for the 3 component fit to the experimental spectrum. The residual mean was 1.6×10^{-5} OD for the 2 component fit and 2.6×10^{-8} OD for the 3 component fit. The residuals for both the 2 and 3 component fits showed no significant departure from normality (2 component $p=0.39$, 3 component $p=0.92$). Heteroscedasticity of the residuals was tested by plotting predicted changes in attenuation against residuals (figure 6.4). The 2 component fit produced residuals that were clearly heteroscedastic whereas those produced by the 3 component fit were more homoscedastic. There was no difference between the residuals from the 2 component fits to the experimental and simulated spectra ($p=0.49$) (figure 6.3).

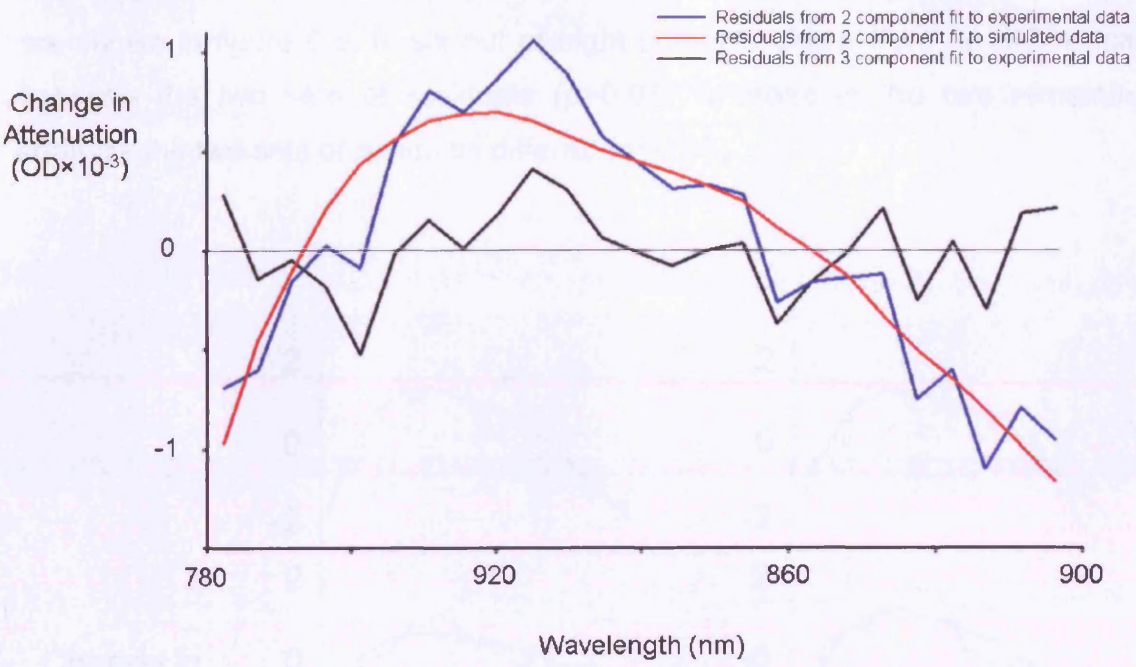

Figure 6.3: Residuals from 2 and 3 component fits to group mean change in near infrared attenuation between baseline and hypoxaemia and 2 component fit to simulated 3 component spectrum.

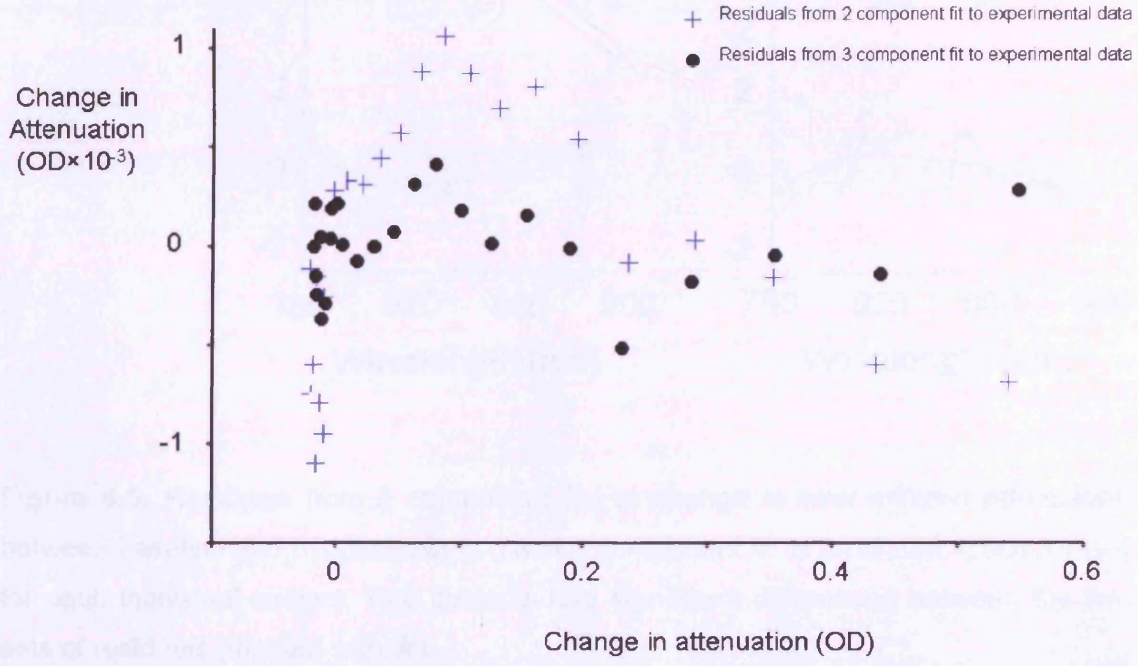

Figure 6.4: Graphical test for heteroscedasticity plotting residuals of regression against change in attenuation predicted by regression results for 2 and 3 component fits.

The 2 component fits to the experimental and simulated data for each subject are shown in figure 6.5. In six out of eight subjects, there were no differences between the two sets of residuals ($p>0.05$) whereas in the two remaining subjects the two sets of residuals differed ($p<0.05$).

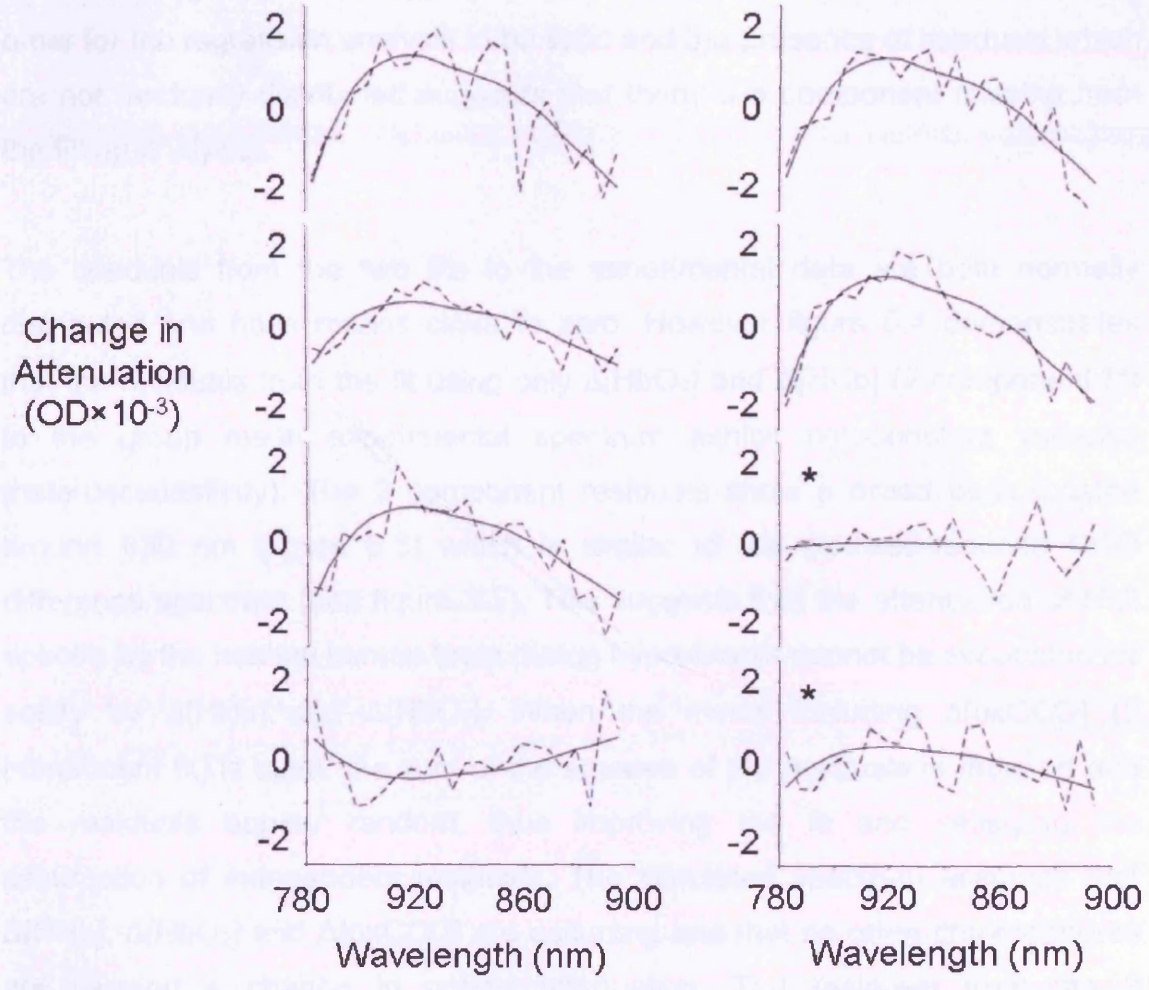

Figure 6.5: Residuals from 2 component fits to change in near infrared attenuation between baseline and hypoxaemia (- -) and 2 component fit to simulated spectrum (—) for each individual subject. Two subjects had significant differences between the two sets of residuals (marked with ✶).

6.2.4 Discussion

The quality of a multiple regression fit can be determined by assessing the residuals of the fitting procedure. The better the fit the smaller will be the sum of the square of the residuals, with the perfect theoretical fit having residuals all equal to zero. Regression analysis assumes that any residuals which are present should be randomly distributed around zero, normally distributed and exhibit homogenous variance[10]. These assumptions must all be satisfied in order for the regression analysis to be valid and the presence of residuals which are not randomly distributed suggests that there is a component missing from the fitting analysis.

The residuals from the two fits to the experimental data are both normally distributed and have means close to zero. However figure 6.4 demonstrates that the residuals from the fit using only $\Delta[HbO_2]$ and $\Delta[HHb]$ (2 component fit) to the group mean experimental spectrum exhibit non-constant variance (heteroscedasticity). The 2 component residuals show a broad peak located around 830 nm (figure 6.3) which is similar to the oxidised-reduced CCO difference spectrum (see figure 3.5). This suggests that the attenuation of NIR spectra by the healthy human brain during hypoxaemia cannot be accounted for solely by $\Delta[HHb]$ and $\Delta[HbO_2]$. When the model including $\Delta[oxCCO]$ (3 component fit) is used, the sum of the squares of the residuals is reduced and the residuals appear random, thus improving the fit and satisfying the assumption of independent residuals. The simulated spectrum assumes that $\Delta[HHb]$, $\Delta[HbO_2]$ and $\Delta[oxCCO]$ are occurring and that no other chromophores are causing a change in optical attenuation. The residuals from the 2 component fit to this spectrum are those that would be expected from the 2 component fit to the experimental data if $\Delta[HHb]$, $\Delta[HbO_2]$ and $\Delta[oxCCO]$ were occurring in the brain during this hypoxaemic challenge. The residuals from the 2 component fit to the experimental spectrum do not differ from those resulting from the 2 component fit to the simulated spectrum. This strongly suggests that $\Delta[oxCCO]$ is occurring and accounts for the distribution of the residuals from the 2 component fit to the experimental data.

There is no statistical difference between the individual 2 component fits to the experimental and simulated data in six out of eight of the individual subjects. This demonstrates the optical effect of Δ[oxCCO] at the individual as well as the group level. In the two subjects who exhibited differences between the residuals to the experimental and simulated data, the residuals to the simulated data are close to zero. This results in a very low dispersion in the residuals to the simulated data. It is possible that in these two individuals the physiological challenge was insufficient to produce a significant change in Δ[oxCCO]. In one case the plot of the 2 component fit to the simulated spectrum is concave downwards rather than concave upward as shown by all the other subjects. This implies that we measured an increase in Δ[oxCCO] in this subject. This is unlikely to be a physiological response to hypoxaemia. Re-examining the individual data during this study suggests that this finding might relate to artefactual changes in light attenuation which may be caused by inadequate optode fixation of subject movement.

This analysis adds further weight to our conclusion that real changes in cerebral CCO signal occur during moderate hypoxaemia by demonstrating that Δ[oxCCO] measured using our BBS system and the UCL*n* algorithm is not merely crosstalk artefact and that we can detect these changes using non-invasive BBS.

6.3 General Discussion

Many techniques including *in vivo*, *in vitro* and *in silico* experiments have been used to investigate crosstalk in the context of measurement of Δ[oxCCO]. Matcher *et al* applied various light conversion algorithms to a simulated data set consisting of a time series of absolute attenuation spectra generated using analytical diffusion theory[12]. They combined *in vitro* spectra of HbO_2 and HHb representing concentration changes of between 0 and 40 μM for Δ[HHb] and 20 and 60 μM for Δ[HbO_2] and excluded any change in the CCO signal so that any Δ[oxCCO] derived by the algorithms would be a spurious artefact. Six different published algorithms were compared and it was found that the UCL*n* algorithm produced the smallest spurious Δ[oxCCO] with a magnitude of 0.06 μM. This

study highlights the fact that different instrumentation and algorithms will affect the presence and degree of crosstalk experienced and re-iterates that non-broadband NIRS systems may be unsuitable for measuring Δ[oxCCO][5]. When interpreting this finding it is important to realise that the magnitude of the haemoglobin concentration changes used to produce the simulated spectra for this modelling study are at least an order of magnitude greater than those we measured during hypoxaemia in healthy volunteers. This study also demonstrates that using multiple wavelengths within the conversion algorithm significantly reduces the spurious Δ[oxCCO]. Further modelling studies have suggested that algorithm accuracy for Δ[oxCCO] significantly increases with number of wavelengths used up to approximately 10 wavelengths[16].

A similar study using a NIRO 300 spectrometer has been performed *in vitro* using human blood, intralipid and water in a tissue phantom with the oxyhaemoglobin concentration varied using oxygen bubbling and yeast and a spurious Δ[oxCCO] of 1% of the Δ[HbO_2] was found[17]: we would expect our BBS system, which uses multiple wavelengths to produce a smaller artefact than the four wavelength NIRO 300.

Cooper *et al* took a different but complementary approach in a study using a BBS system to investigate CCO redox changes in the neonatal pig[5]. The CCO redox state was fixed using cyanide and then large changes in haemoglobin oxygenation were induced. Δ[oxCCO] was found to be stable during the large contemporaneous haemoglobin concentration changes and it was concluded that BBS is able to accurately measure changes in the cerebral CCO redox state. Quaresima *et al* used a similar neonatal pig model to investigate changes in cerebral CCO redox state during episodes of anoxia[6]. They found very similar Δ[oxCCO] responses in both the blooded animals and those who had 80% of their haemoglobin replaced by a perfluorocarbon blood substitute. These findings again suggest that we are able to measure Δ[oxCCO] against a background of changing haemoglobin concentration without producing significant artefactual Δ[oxCCO].

Conversely Sakamoto *et al* reported crosstalk between the CCO and HHb signals in the piglet brain when using a BBS system[3]. They fixed the CCO redox state using cyanide and then used haemodilution to reduce the haematocrit from 35 to 5%. A linear drop in Δ[oxCCO] × PL during haemodilution was found and it was concluded that the CCO signal is highly dependent on haematocrit. However in this study PL was directly measured using second differential spectroscopy and a linear decrease in PL with haemodilution was found. The results for the CCO redox state are presented as chromophore concentration multiplied by PL and are therefore uncorrected for the changes in PL. One is therefore left unsure whether the dependence of the CCO signal change on haematocrit would remain once the effect of changes in PL had been incorporated. Nevertheless large changes in haematocrit are extremely unlikely during the types of physiological challenges described in this thesis and within this context we feel the effect of haematocrit on our measured Δ[oxCCO] is negligible.

Evidence for crosstalk has also been sought in studies using human subjects. Skov *et al* used a four wavelength Radiometer spectrometer to measure changes in cerebral haemoglobin and oxCCO concentrations in children undergoing cardiac surgery[4]. They reported the possibility of crosstalk between the CCO and haemoglobin signals and concluded that NIRS measurement of the CCO redox state required further validation. An interesting series of papers has investigated the issue of crosstalk artefact within a paradigm of visual stimulation in the adult human. This group initially reported changes in CCO redox state in the occipital cortex during visual stimulation[18] and later used a Monte Carlo simulation to show that their initial results might simply represent crosstalk artefact[19]. They then modified their experimental paradigm in order to minimise global haemodynamic effects and subsequently reported that they were not able to model the measured Δ[oxCCO] as a crosstalk artefact and concluded that actual changes in CCO redox state were occurring during visual stimulation[7].

The situation during functional activation paradigms is more complex than that found during hypoxaemia as Δ[oxCCO] would be expected to occur within discrete cortical regions and more work is clearly required to further elucidate this important issue. Findings may not be easily transferable between species as the variations in optical geometry will affect the light transfer and several of the *in silico* studies do not take account of the multi-layered structure of the human head and the varying concentration of CCO within these layers.

The data presented in this chapter provides some evidence that the Δ[oxCCO] we measure is not merely a crosstalk artefact. This analysis is clearly insufficient to definitively discount the issue of crosstalk and additional modelling and experimental studies are required to further investigate the use of the NIRS algorithms to detect changes in the CCO signal in multi-layered systems. We plan to address this issue using a combination of continuous wave and phase resolved spectroscopy together with knowledge of the CCO concentrations in the various cranial layers and their respective optical characteristics.

These findings increase confidence in the ability of the BBS system to detect real changes in Δ[oxCCO] and therefore support the use of this equipment to make clinical measurements of CCO redox changes.

References

1. Cooper CE, Matcher SJ, Wyatt JS, Cope M, Brown GC, Nemoto EM, Delpy DT. Near-infrared spectroscopy of the brain: relevance to cytochrome oxidase bioenergetics. *Biochem Soc Trans* 1994;22:974-980.
2. Brown GC, Crompton M, Wray S. Cytochrome oxidase content of rat brain during development. *Biochem Biophys Acta* 1991;1057:273-275.
3. Sakamoto T, Jonas RA, Stock UA, Hatsuoka S, Cope M, Springett RJ, Nollert G. Utility and limitations of near-infrared spectroscopy during cardiopulmonary bypass in a piglet model. *Pediatr Res* 2001;49:770-776.
4. Skov L, Greisen G. Apparent cerebral cytochrome aa3 reduction during cardiopulmonary bypass in hypoxaemic children with congenital heart disease. A critical analysis of in vivo near-infrared spectrophotometric data. *Physiol Meas* 1994;15:447-457.
5. Cooper CE, Cope M, Springett R, Amess PN, Penrice J, Tyszczuk L, Punwani S, Ordidge R, Wyatt J, Delpy DT. Use of mitochondrial inhibitors to demonstrate that cytochrome oxidase near-infrared spectroscopy can measure mitochondrial dysfunction noninvasively in the brain. *J Cereb Blood Flow Metab* 1999;19:27-38.
6. Quaresima V, Springett R, Cope M, Wyatt JT, Delpy DT, Ferrari M, Cooper CE. Oxidation and reduction of cytochrome oxidase in the neonatal brain observed by in vivo near-infrared spectroscopy. *Biochim Biophys Acta* 1998;1366:291-300.
7. Uludag K, Steinbrink J, Kohl-Bareis M, Wenzel R, Villringer A, Obrig H. Cytochrome-c-oxidase redox changes during visual stimulation measured by near-infrared spectroscopy cannot be explained by a mere cross talk artefact. *Neuroimage* 2004;22:109-119.
8. Tachtsidis I, Tisdall M, Leung T, Cooper C, Delpy D, Smith M, Elwell C. Investigation of in vivo measurement of cerebral cytochrome-c-oxidase redox changes using near-infrared spectroscopy in patients with orthostatic hypotension. *Physiol Meas* 2007;28:199-211.
9. Springett R, Newman J, Cope M, Delpy DT. Oxygen dependency and precision of cytochrome oxidase signal from full spectral NIRS of the piglet brain. *Am J Physiol Heart Circ Physiol* 2000;279:H2202-H2209.

10. Kirkwood B, Sterne JAC (2003) *Essential Medical Statistics*, 2nd ed. Massachusetts: Blackwell Science Ltd.
11. Matcher SJ, Cope M, Delpy DT. Use of the water absorption spectrum to quantify tissue chromophore concentration changes in near-infrared spectroscopy. *Phys Med Biol* 1994;39:177-196.
12. Matcher SJ, Elwell CE, Cooper CE, Cope M, Delpy DT. Performance comparison of several published tissue near-infrared spectroscopy algorithms. *Anal Biochem* 1995;227:54-68.
13. Essenpreis M, Cope M, Elwell CE, Arridge SR, van der Zee P, Delpy DT. Wavelength dependence of the differential pathlength factor and the log slope in time-resolved tissue spectroscopy. *Adv Exp Med Biol* 1993;333:9-20.
14. Cope M. Specific extinction spectra of tissue chromophores. http://www.medphys.ucl.ac.uk/research/borl/research/NIR_topics/spectra/spectra.htm. 1991.
15. Siegel S, Castellan NJ Jr (1988) *Nonparametric Statistics for the Behavioural Sciences*, 2nd ed. Singapore: McGraw-Hill.
16. Van Huffel S, Casaer P, Van Mele P, Willems G (1995) TLS regression , wavelength and chromophore selection analysis in NIRS data quantification. pp 743-754
17. Suzuki S, Takasaki S, Ozaki T, Kobayashi Y. A tissue oxygenation monitor using NIR spatially resolved spectroscopy. *SPIE Proc* 1999;3597:582-592.
18. Heekeren HR, Kohl M, Obrig H, Wenzel R, von Pannwitz W, Matcher SJ, Dirnagl U, Cooper CE, Villringer A. Noninvasive assessment of changes in cytochrome-c oxidase oxidation in human subjects during visual stimulation. *J Cereb Blood Flow Metab* 1999;19:592-603.
19. Uludag K, Kohl M, Steinbrink J, Obrig H, Villringer A. Cross talk in the Lambert-Beer calculation for near-infrared wavelengths estimated by Monte Carlo simulations. *J Biomed Opt* 2002;7:51-59.

Chapter 7

Changes in cerebral cellular and mitochondrial redox state during normobaric hyperoxia in patients with traumatic brain injury

This chapter describes a study to investigate changes in cerebral metabolism during normobaric hyperoxia (NBH) in patients with TBI. TBI is associated with depressed aerobic metabolism and mitochondrial dysfunction and although NBH has been suggested as a treatment for TBI, human studies have produced equivocal results. This study utilises a wide range of invasive and non-invasive monitoring modalities including BBS, brain tissue oxygen tension ($PbrO_2$) measurement and cerebral microdialysis to study the effects of NBH after TBI and to investigate changes in cellular and mitochondrial redox state, as measured by brain tissue lactate:pyruvate ratio (LPR) and change in [oxCCO] respectively.

7.1 Introduction

TBI describes a heterogenous set of injury mechanisms and pathologies, but there appear to be common metabolic pathways leading to depressed aerobic metabolism, reduced cellular ATP production, inability to maintain ionic homeostasis and ultimately cell death[1-4]. The exact aetiology of this cellular energy failure is poorly understood but both reduced substrate delivery and impaired mitochondrial substrate utilisation appear to be implicated. Efficient cellular ATP production requires oxygen availability within mitochondria, yet Alves *et al* demonstrated using a cerebral fluid percussion insult in the cat that TBI induces cerebral hypoxia despite unchanged arterial oxygen tension and MBP and so reduced ATP production after TBI may be in part related to mitochondrial hypoxia[3]. As discussed in section 2.3, it is well established that hypotension and hypoxaemia, which reduce cerebral oxygen delivery, are associated with poor functional outcome after TBI[5-10] and so, within the context of attempting to minimise secondary injury after TBI it appears vital to ensure adequate oxygen delivery to cerebral mitochondria, particularly in the early stages post TBI when reduced cerebral blood flow increases the risk of cerebral hypoxia[11].

This concept appears straightforward, yet it is far from simple to assess or even to define 'adequate mitochondrial oxygen delivery'. Values of *in vivo* mitochondrial oxygen tension either in health or disease are not yet established, but a delayed fluorescence technique for measuring mitochondrial oxygen tension in cell cultures has recently been described and this has the potential to make *in vivo* measurements[12]. It is possible to measure $PbrO_2$ using commercially available invasive probes, yet although it has been demonstrated that reduced $PbrO_2$ is associated with poor outcome after TBI, the threshold for tissue ischaemia is not well established and concentrations between 0.7 and 2.7 kPa have been suggested[13-16]. It is unlikely that, even at the mitochondrial level, there will exist a well defined ischaemic threshold for oxygen tension as this will depend on factors such as the degrees of mitochondrial dysfunction and pharmacological sedation, both of which might decrease oxygen requirements. Given the potential for, and the detrimental effects of, hypoxia after TBI, a monitoring tool is needed which is able to assess the adequacy of mitochondrial oxygen tension in an individual and time specific manner. This might allow targeted treatment aimed at maintaining ATP production and avoiding cellular energy failure. This might prove beneficial after TBI.

Animal models assessing CCO activity using histopathological techniques indicate that CCO mediated oxidative metabolism is decreased after TBI and that this effect may last up to 10 days post injury[17]. We have shown in chapter 5 that BBS can measure non-invasively changes in CCO redox state and that when $PaCO_2$ is stable these changes correlate with changes in cerebral oxygen delivery. BBS would therefore appear to be an ideal technique for assessing the reactivity of CCO redox state to changes in mitochondrial oxygen delivery in patients with TBI.

In light of the risk of cerebral hypoxia, hyperoxia has been investigated as a potential treatment strategy for increasing aerobic metabolism after TBI. In particular, hyperbaric hyperoxia (HBH) has shown beneficial effects in both animals and humans after TBI[18-20]. However chambers capable of delivering HBH to critically ill patients are expensive and availability is severely limited.

Interest has therefore grown in the use of NBH which is extremely cheap and simple to administer. Studies investigating the use of NBH in adults after TBI have consistently shown increases in $PbrO_2$ and reductions in microdialysis measured brain tissue lactate concentration[21-23]. Interpretation of these findings is however controversial with some investigators concluding that the reduction in microdialysate lactate concentrations supports a beneficial role for NBH[21] while others suggest that the lack of changes in microdialysate LPR and glucose indicates that glucose oxidation might be impaired during NBH[22]. Cerebral microdialysis is a routine part of multimodality monitoring on the NCU and has been discussed in section 2.4.1. Raised microdialysate lactate concentration is associated with tissue hypoxemia and poor outcome after TBI. However it reflects not only the degree of anaerobic metabolism but also the global glycolytic rate [24]. Lactate:pyruvate ratio (LPR) is considered a superior marker of anaerobic metabolism and is a measure of cellular redox state[25]. It has the added advantage of being independent of *in vivo* catheter recovery and is the most widely monitored microdialysis variable after TBI. To date, NBH studies in humans after TBI have shown no changes in LPR and this has contributed to the controversy surrounding interpretation of the resulting data.

We hypothesise that NBH will induce oxidation in cerebral redox state in adult patients in the early period post TBI.

7.2 Methods

This study was approved by the Joint Research Ethics Committee of the National Hospital for Neurology and Neurosurgery and the Institute of Neurology and, as all patients were unconscious at the time of the study, written assent was obtained from their personal representatives. Inclusion criteria were a diagnosis of TBI requiring sedation and ventilation on the NCU. Exclusion criteria were the expectation of death or weaning of sedation within 24 hours of injury, a baseline FiO_2 ≥60% or more than 48 hours elapsing between the time of injury and the start of the study.

11 adult patients were enrolled into the study (10 male, 1 female). The median age was 42 years (range 17 to 68) and the median time between the injury and the start of the study was 25 hours (range 15-47).

7.2.2 Monitored Variables

Multimodality monitoring and protocolised ICP and CPP directed care was instigated. As part of routine care, invasive intracranial pressure (Microsensor, Codman, MA, USA), $PbrO_2$ (Licox PMO, Integra Neurosciences, NJ, USA) and cerebral microdialysis (CMA 70 or 71, CMA/Microdialysis, Solna, Sweden) catheters were inserted into the brain interstitium through a three divergent lumen skull bolt (Technicam Ltd, Newton Abbott, UK). Microdialysis catheter positioning followed the recommendations of the consensus meeting on microdialysis in neurointensive care[26] with catheters targeted to the pericontusional tissue in the case of focal lesions, or the right frontal lobe in the case of diffuse injury. The microdialysis catheters were perfused with Perfusion Fluid CNS (CMA/Microdialysis), at a rate of 0.3 µl/min. No data were collected in the first 4 hours after catheter placement to avoid insertion artefacts and catheter positioning was confirmed with subsequent radiological imaging. Microdialysate glucose, lactate and pyruvate concentrations were measured at the bedside using a CMA 600 analyser (CMA/Microdialysis).

For the purposes of this study, broadband spectrometer optodes were placed 3.5 cm apart in a black plastic holder, and fixed to the upper forehead in the midpupillary line ipsilateral to the invasive cerebral monitoring. The BBS instrumentation was identical to that described in section 5.2 and spectra were acquired at a frequency of 1 Hz. A peak intensity greater than 1500 photons was considered adequate and in one patient the sampling exposure time was increased in order to obtain this.

The source-detector optode pair for each channel of the NIRO 300 was placed in a black plastic holder with a source-detector separation of 5cm. One channel was fixed to the right hand side of the forehead and the other to the left hand side of the forehead in the midpupillary line with the channel laterality allocated randomly. Within each pair the source fibres were positioned medially and the

detector optodes laterally in order to minimise the transmission of light from the channel 1 source to the channel 2 detector and vice versa. A bandage and a light absorbing cloth were placed over the optode holders to eliminate stray light and prevent optode movement. SRS and MBBL data was collected at 6 Hz.

VMCA ipsilateral to the NIRS optodes was measured using 2 MHz transcranial Doppler ultrasonography (Nicolet, UK), as a surrogate of cerebral blood flow[27]. The side of the brain containing the invasive monitoring and over which the BBS optodes and TCD probe were placed was that which showed the most evidence of cerebral injury on CT and is termed the 'most injured hemisphere': the side of the brain with the least evidence of injury is termed the 'least injured hemisphere'.

7.2.2 Study Protocol

All patients received local protocol-guided therapy, based on Joint Section of Neurotrauma and Critical Care of the American Association of Neurological Surgeons[28] and European Brain Injury Consortium guidelines[29]. After 30 minutes of baseline data collection, the FiO_2 was increased to 60% for 60 minutes and then to 100% for 60 minutes before being returned to baseline for a further 30 minutes. Cerebral microdialysate specimens were collected and analysed at intervals of 15 minutes and ABG analysis was performed at intervals of 30 minutes, commencing 15 minutes after the start of the baseline period. There is an inherent delay associated with cerebral microdialysis monitoring which relates to diffusion of metabolites into the extracellular space and across the catheter membrane, and the time taken to collect the microdialysate. Therefore, a final microdialysis sample was collected 75 minutes after the FiO_2 was returned to baseline. A schematic of the study protocol is shown in figure 7.1.

7.2.3 Data Analysis

All monitored variables were collected to PC and synchronised. Absolute Δ[oxCCO], Δ[Hbdiff] and Δ[HbT] calculated from the BBS measured changes in light attenuation as described in section 5.2.4. While analysing the data it became apparent that small changes in optical pathlength were occurring

during the study and changes in chromophore concentration measured using the BBS were therefore continuously corrected for optical pathlength calculated using second differential analysis of the 740 nm water feature[30]. Bilateral TOI and ΔCBV were calculated from the NIRO 300 data as described in section 4.2.3. Summary data were produced for the four phases of the study: baseline, 60%, 100% and return to baseline FiO_2. For the initial and final baseline periods 15 minute means for each variable were calculated, centred on the time of ABG sampling within that phase. For the 60% and 100% FiO_2 phases, means of the data between the two ABG samples within that phase were calculated (figure 7.1).

Statistical analysis was carried out using SAS software (v9.1, SAS Institute, USA) and p values <0.05 were considered significant. Group changes were compared with baseline using non-parametric ANOVA and *post hoc* pairwise comparisons. Correlations between variables were assessed using Spearman rank correlation analysis with Bonferoni corrected two-tailed tests of significance.

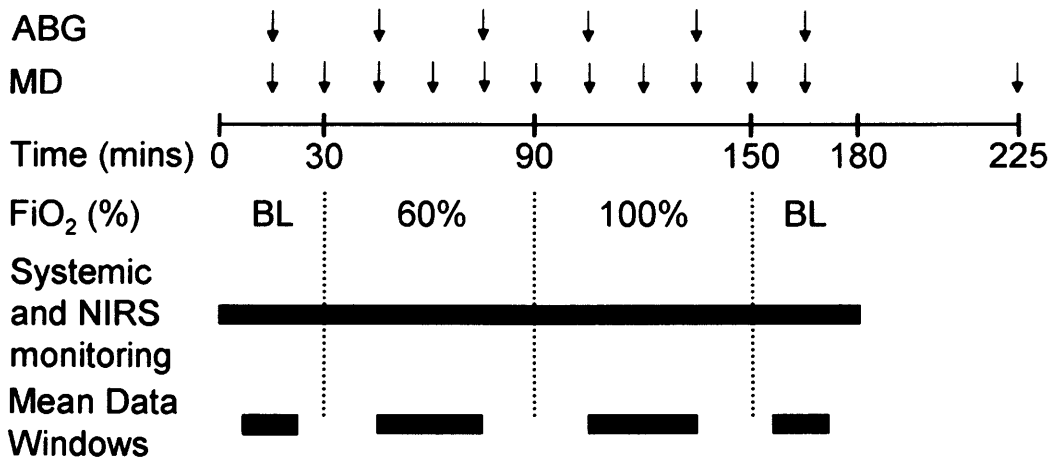

Figure 7.1: Study and analysis protocol for study of TBI patients during NBH. ABG - arterial blood gas sampling, MD - microdialysate sampling, BL - baseline.

7.3 Results

Patient demographics and details of presenting pathology are shown in table 7.1. Computed tomography scans of the heads of the recruited patients are shown in figure 7.2.

Patient	*Age*	*Sex*	*Injury Mechanism*	*Pathology*	*Initial GCS*	*Outcome*	*Time (hrs)*	*Treatment*
1	42	M	Assault	EDH	7	Survived	25	Surgical
2	17	M	RTA	ASDH	3	Survived	27	Surgical
3	57	F	RTA	SAH	10	Died	15	Medical
4	61	M	Fall	Contusions	8	Died	24	Medical
5	45	M	Fall	ASDH/SAH	7	Died	47	Medical
6	22	M	Assault	ASDH	11	Survived	22	Surgical
7	68	M	Fall	ASDH/ICH	14	Survived	37	Surgical
8	44	M	Fall	Contusions	7	Died	25	Surgical
9	27	M	Unknown	EDH/SAH	8	Died	24	Surgical
10	20	M	RTA	EDH	7	Survived	25	Surgical
11	34	M	Fall	ASDH	4	Survived	43	Medical

Table 7.1: Demographic data and details of presenting pathology for patient group. Time- time from injury to start of NBH study. GCS-Glasgow Coma Score, EDH-extradural haematoma, ASDH-acute subdural haematoma, SAH-subarachnoid haemorrhage.

During the study on patient 3, movement of the NIRS optodes caused gross changes in light attenuation and during the study on patient 7 a power failure led to total loss of NIR data. These two patients were excluded from further analysis. Data from the remaining patients were analysed, but there was some data loss in some patients. Specifically $PbrO_2$ monitoring was not possible in patient 10 due to inadvertent catheter removal prior to the study; SRS data collection failed in patients 6 and 10 due to software malfunction; BBS optode movement in patient 2 caused gross artefacts and subsequent data removal and microdialysis perfusate pump failure in the same patient prevented collection of the final microdialysate sample. Gross artefact was defined as measured changes in chromophore concentration in excess of total

physiological concentrations or a linear trend in measured chromophore concentration changes throughout the study with no return towards baseline.

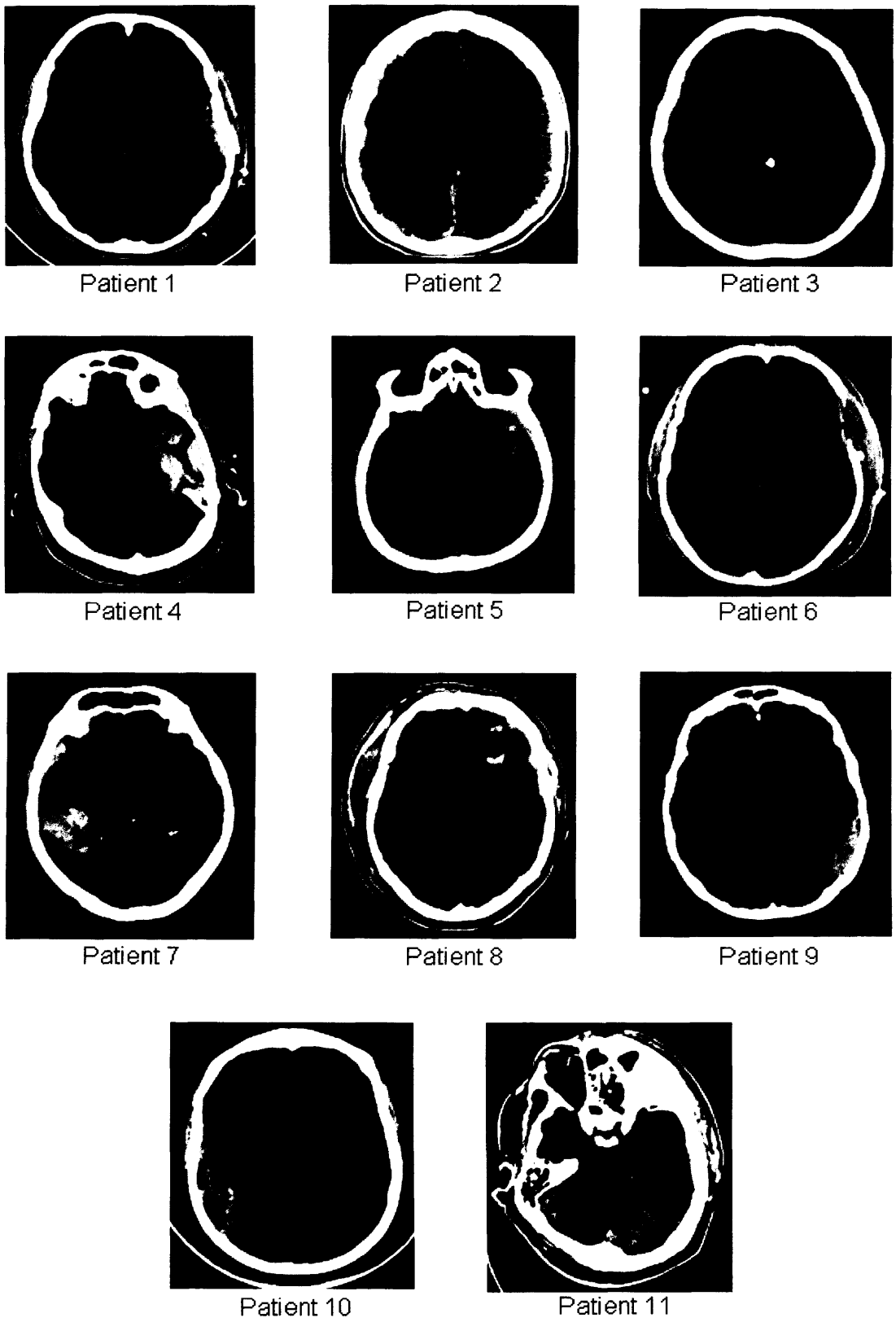

Figure 7.2: CT scans of patients recruited to study of NBH after TBI.

Table 7.2 shows baseline values of measured variables. Table 7.3 shows variable values during the baseline and 100% FiO_2 phases for individual patients. Table 7.4 shows group changes in monitored variable values from the initial baseline to the 60% and 100% FiO_2 and the final baseline phases.
Group changes for measured variables are shown in figures 7.3 and 7.4.

	FiO_2 (%)	*SaO_2 (%)*	*PaO_2 (kPa)*	*$PbrO_2$ (kPa)*	*$PaCO_2$ (kPa)*	*ICP (mmHg)*	*CPP (mmHg)*	*VMCA (cm/s)*
Median	28.5	99.0	14.00	1.57	4.46	16.6	66.1	40.8
Q1	25.9	97.7	11.90	1.22	4.40	10.2	64.6	38.8
Q3	34.0	99.1	14.80	2.90	4.52	24.0	68.4	46.0

	A[Gluc] (mmol/l)	*MD[Gluc] (mmol/l)*	*MD[Lac] (mmol/l)*	*MD LPR*	*PL (cm)*	*TOIinj (%)*	*TOIuninj (%)*
Median	5.80	2.83	3.09	19.8	12.1	74.9	72.6
Q1	5.70	1.86	2.15	16.7	11.9	71.7	55.6
Q3	7.20	3.03	3.95	25.9	13.0	79.1	77.0

Table 7.2: Median and interquartiles for baseline values of measured variables in patients with TBI.

There was no difference in baseline TOI between the two cerebral hemispheres but changes in TOI measured over the most (ΔTOIinj) and least (ΔTOIuninj) injured cerebral hemispheres were significantly different from each other during both the 60% (ΔTOI 1.8% higher on the injured side p=0.02) and 100% FiO_2 phases (ΔTOI 1.1% higher on the more injured side p=0.02). There were no differences between the changes in CBV measured over the two hemispheres during any phase of the study.

Change in $PbrO_2$ correlated with change in [oxCCO] (r_s=0.57 p=0.005) and change in [oxCCO] correlated with change in LPR (r_s=-0.53 p=0.006) but change in $PbrO_2$ did not correlate with LPR (r_s=-0.41 p= 0.06).

Patient	*Epoch*	*BrpO_2* *(kPa)*	*MD[Lac]* *(mmol/l)*	*MD LPR*	*Δ[Hbdiff]* *(μmol/l)*	*Δ[HbT]* *(μmol/l)*	*Δ[oxCCO]* *(μmol/l)*
1	Baseline	0.95	3.95	16.0	0.00	0.00	0.00
	100%	8.65	3.53	13.8	3.57	-0.76	0.39
2	Baseline	1.31	2.12	18.2			
	100%	7.27	2.15	17.2			
4	Baseline	2.79	2.15	25.6	0.00	0.00	0.00
	100%	9.94	2.02	24.5	5.69	-0.19	0.12
5	Baseline	1.84	5.49	25.9	0.00	0.00	0.00
	100%	13.29	5.44	24.3	3.91	-3.83	0.13
6	Baseline	3.35	3.09	19.8	0.00	0.00	0.00
	100%	4.70	2.17	18.1	6.83	-0.31	0.13
8	Baseline	1.00	6.28	28.6	0.00	0.00	0.00
	100%	4.33	6.33	25.9	3.72	-5.92	0.28
9	Baseline	5.89	1.72	16.7	0.000	0.00	0.00
	100%	30.56	1.32	16.0	14.62	5.60	3.06
10	Baseline		2.76	30.4	0.00	0.00	0.00
	100%		2.22	23.3	12.51	-2.37	0.34
11	Baseline	1.34	3.63	15.5	0.00	0.00	0.00
	100%	6.99	3.86	17.2	7.37	1.81	-2.37

Table 7.3: Variable values during the baseline and 100% FiO_2 phases for individual patients. Note data loss for patients 2 and 10 relating to technical issues described in section 7.3.

Epoch	*FiO_2* *(%)*	*ΔSaO_2* *(%)*	*ΔPaO_2* *(kPa)*	*$\Delta PbrO_2$* *(kPa)*	*$\Delta PaCO_2$* *(kPa)*	*ΔICP* *(mmHg)*	*ΔCPP* *(mmHg)*
60%	57.3 §	1.0 ‡	15.70 §	1.78 §	0.09	-0.4	1.6
100%	97.2 §	1.0 §	41.55 §	6.55 §	0.16	0.1	-1.3
Final Baseline	29.2 §	-0.7	-1.00	0.57 §	0.08	0.1	-2.3 *

Epoch	*ΔVmca* *(%)*	*ΔTOIinj* *(%)*	*ΔTOIuninj* *(%)*	*ΔCBVinj* *(ml/100g)*	*ΔCBVuninj* *(ml/100g)*	*ΔA[Gluc]* *(mmol/l)*	*ΔPL* *(cm)*
60%	0.4	3.8 †	0.5	0	-0.01	0.15	0.1
100%	1.4	4.0 §	3.9 §	-0.03	-0.08	-0.10	0.3 †
Final Baseline	3.5	2.4 †	0.9	0.04	-0.05	-1.3	0.2

Epoch	*ΔMD[Gluc]* *(mmol/l)*	*ΔMD[Lac]* *(mmol/l)*	*ΔMD LPR*	*Δ[Hbdiff]* *(μmol/l)*	*Δ[HbT]* *(μmol/l)*	*Δ[oxCCO]* *(μmol/l)*
60%	-0.08	-0.32	-1.5	2.13 §	-0.15	0.10
100%	-0.09	-0.13 *	-1.5 *	6.45 §	-0.56	0.21 ‡
Final Baseline	-0.12	-0.34 †	-2.0 †	2.27 ‡	0.45	0.06

Table 7.4: Changes in variable values from baseline to 60% and 100% FiO_2 phases for patients with TBI during NBH (* $p<0.05$, † $p<0.01$, ‡ $p<0.001$, § $p<0.0001$).

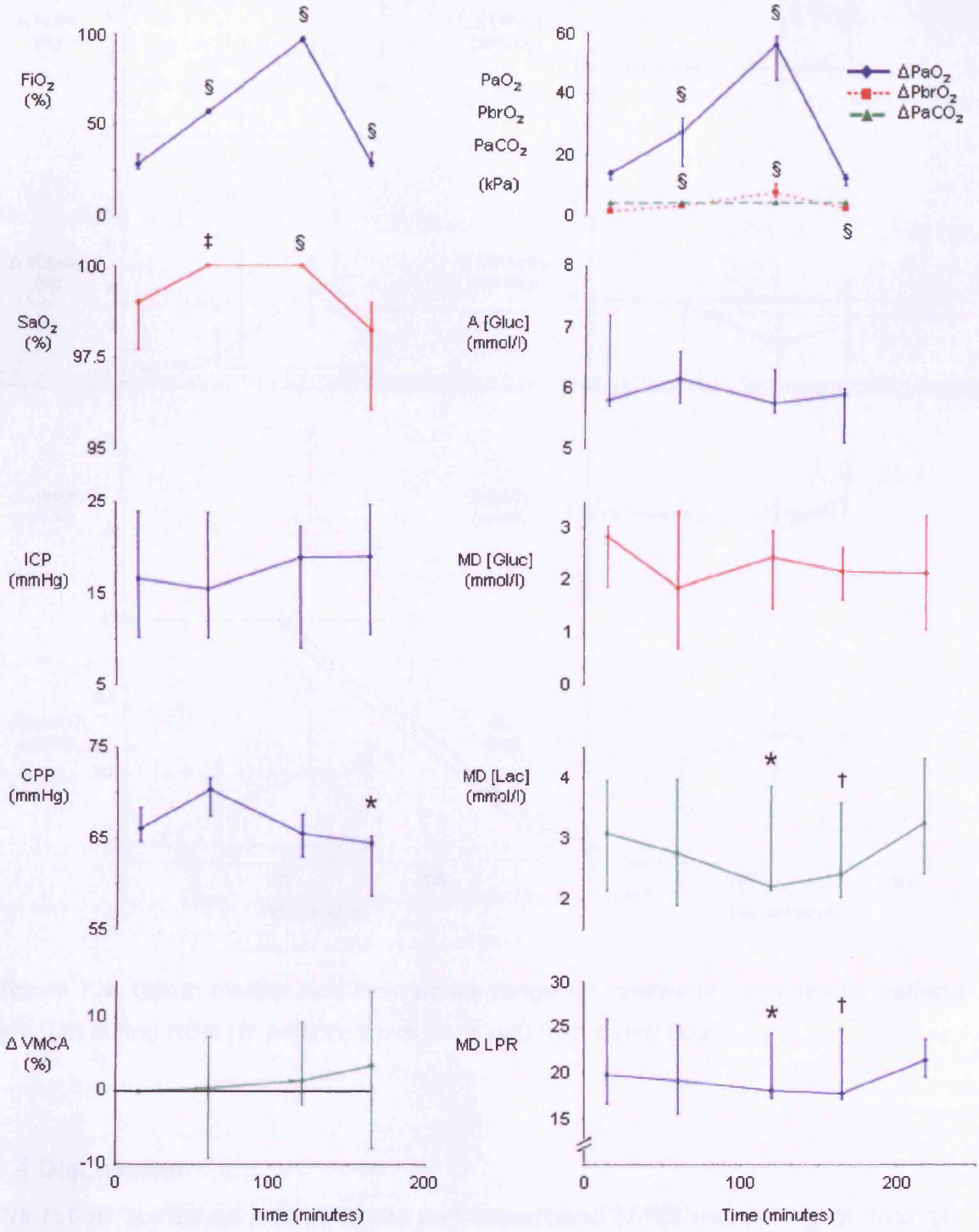

Figure 7.3: Group median and interquartile range for measured variables for patients with TBI during NBH. In the plot of changes in gas tensions there were no significant changes in $PaCO_2$ (★ $p<0.05$, † $p<0.01$, ‡ $p<0.001$, § $p<0.0001$).

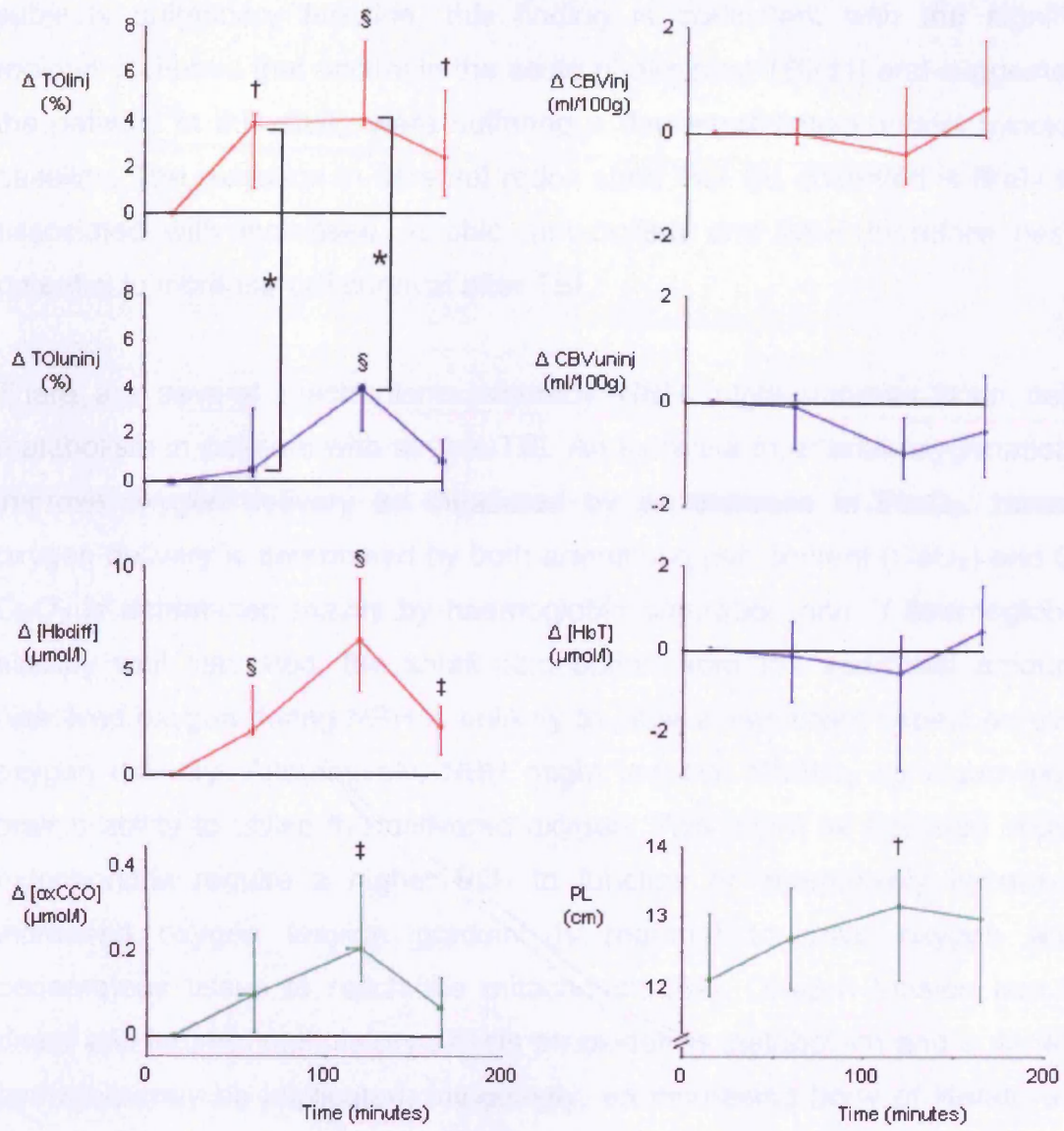

Figure 7.4: Group median and interquartile range for measured variables for patients with TBI during NBH (★ p<0.05, † p<0.01, ‡ p<0.001, § p<0.0001).

7.4 Discussion

We report combined microdialysis and broadband NIRS monitoring of changes in cerebral redox state in patients with TBI. Our results demonstrate oxidation in cerebral cellular and mitochondrial redox state during NBH in the first 48 hours post injury. The magnitude of the changes in [oxCCO] during NBH was greater in the TBI cohort (median 0.21 µmol/l) than the healthy volunteers (median 0.07 µmol/l, section 5.3.2) and although this comparison is complex to interpret as the challenges were not matched in terms of methods of ventilation and the

subjects pulmonary function, this finding is consistent with the significant regional ischemia that occurs in the acute phase post TBI[31] and suggests that the patients in this study were suffering a degree of mitochondrial hypoxia at baseline. The oxidation in cerebral redox state that we observed is likely to be associated with increased aerobic metabolism and NBH therefore has the potential to increase cell survival after TBI.

There are several mechanisms whereby NBH might improve brain cellular metabolism in patients with severe TBI. An increase in arterial oxygenation will improve oxygen delivery as measured by an increase in $PbrO_2$. However, oxygen delivery is determined by both arterial oxygen content (CaO_2) and CBF. CaO_2 is determined mainly by haemoglobin saturation and, if haemoglobin is already well saturated, the small contribution from the additional amount of dissolved oxygen during NBH is unlikely to have a significant impact on overall oxygen delivery. Alternatively, NBH might improve $CMRO_2$ by improving the brain's ability to utilise the delivered oxygen. This might be because impaired mitochondria require a higher PO_2 to function or alternatively because an increased oxygen tension gradient is required to drive oxygen across oedematous tissue to reach the mitochondria[32]. Oxygen tension has both direct and indirect modulatory effects on oxidative metabolism and a variety of pathways may be implicated. Intriguingly, an increasing body of literature has demonstrated the ability of NO, which is implicated in the pathobiology of TBI, to inhibit oxygen binding to CCO, and hence its subsequent reduction, by competing for the oxygen binding site in a reversible manner[33]. Raised cerebral NO levels are present after TBI and might therefore contribute to mitochondrial dysfunction[1]. It is possible that elevated mitochondrial oxygen tension might antagonise the effects of NO and therefore favour the binding of oxygen and its subsequent reduction, but this mechanism remains hypothetical at present.

$PbrO_2$ reflects the balance between *tissue* oxygen delivery and utilisation[3]. In agreement with several other investigators we found that $PbrO_2$ increased during NBH, indicating increased cerebral oxygen availability[16,23,34]. Δ[Hbdiff] represents changes in the balance between arterial oxygen delivery

and oxygen offloading to tissue in the context of stable CBF and CBV. As we observed no changes in VMCA or [HbT] during NBH, it can be assumed that cerebral haemodynamics were stable during the study period. The increase in Δ[Hbdiff] during NBH therefore suggests improvement in the balance between oxygen delivery and demand and this is further supported by the associated increase in $PbrO_2$.

There were no significant changes in NIRO 300 measured CBV over either hemisphere, and no difference in CBV response between the two sides. TOI increased significantly in both hemispheres reflecting the increased oxygen delivery and the increase was greater in the in the most injured hemisphere during both the 60% and 100% FiO_2 phases. There are several possible interpretations of this finding. VMCA in the more injured hemisphere was unchanged during NBH yet in the healthy volunteers we found a significant reduction in VMCA during hyperoxia (section 5.3.2). Significant intra-patient heterogeneity exists after TBI[31] and regional differences in the vascular response to hyperoxia might exist. If hyperoxic vasoconstriction occurred predominantly in the least injured hemisphere then the reduction in arterial blood volume in this hemisphere would translate to a less marked rise in TOI during NBH. Although CBV was unchanged, the altered cerebral compliance after TBI makes it difficult to predict the relative changes in arterial and venous volume and these may differ from those found in the healthy brain. Alternatively there might be differences in the baseline AVR between the two sides. A decreased baseline AVR in the most injured hemisphere would cause a relatively larger increase in TOI on this side as the change in saturation occurs predominantly in the venous circulation. However this theory is not supported by the finding of similar baseline TOI values recorded over the two hemispheres and we have previously shown that changes in AVR have a relatively small effect on changes in TOI (section 4.3.5). It is also important to consider differences in the optical characteristics of the two hemispheres. Several of the patients in this study had asymmetrical haemorrhage overlying or within the cerebral tissue and some were operated on prior to the NIR data collection. Although TOI does not require correction for total optical pathlength, differences in the optical characteristics between the two hemispheres might influencing the

tissue interrogated by the NIR light and cause variation in partial optical pathlengths in the various cranial layers. These findings again underline the complexities in interpreting TOI data. Bilateral VMCA recording would allow further investigation of NBH induced changes in haemodynamics and modelling studies will be required to address the changes in tissue optical characteristics found after TBI.

The decrease in microdialysate lactate concentration that we observed is similar in direction and magnitude to that found by other workers and is likely to represent improvement in tissue hypoxia during NBH[21-23]. Microdialysate LPR is a marker of cellular redox state and reflects the NAD to reduced-NAD ratio, and the degree of aerobic metabolism[4]. In contrast to previous studies, we observed a significant reduction in microdialysate LPR during NBH, suggesting an increase in aerobic metabolism. The changes in microdialysate variables that we report are small and it is not possible to ascertain their clinical significance from these data. Nevertheless this pilot study protocol utilised a relatively short (2 hour) period of NBH and similar changes in microdialysate lactate concentration during NBH have been associated with improved outcome after TBI[21]. There was no change in arterial or microdialysate glucose concentrations during the study. However, in contrast to the arterial measurements, there was a trend toward reduced microdialysate glucose concentration during NBH and this might represent increased cerebral glucose utilisation.

We observed an increase in Δ[oxCCO] during NBH that returned to baseline by the end of the study. There was a positive correlation between Δ[oxCCO] and change in $PbrO_2$ and a negative correlation between Δ[oxCCO] and change in LPR. These changes in cellular and mitochondrial redox state during NBH indicate an increase in electron transfer from CCO to oxygen, thus favouring increased flux through the mitochondrial electron transfer chain and increased aerobic metabolism. In combination with the Δ[Hbdiff], these data suggest that increased arterial and tissue oxygen delivery is driving an increase in oxygen

utilisation and ATP production. However, simultaneous measurements of $CMRO_2$ and ATP concentration are needed to confirm this hypothesis.

Δ[oxCCO] in the human brain has not previously been compared with other markers of cellular redox state. The correlation between non-invasive regional (NIRS), and invasive focal (cerebral MD), measures of changes in cerebral redox state suggest that the NIRS changes that we are recording are related to cellular metabolism. The time course of the microdialysate data appears to differ from that of the $PbrO_2$ and NIRS data. This may contribute to the correlation between change in $PbrO_2$ and change in LPR failing to reach significance after the Bonferoni correction and influence the strength of the relationship between changes in $PbrO_2$ and [oxCCO].

HBH has been shown to improve cerebral metabolism and outcome, but studies of NBH have produced variable results. In a fluid percussion injury model in rats, HBH alleviated injury-induced reduction in mitochondrial redox and increased cerebral oxygen consumption[19]. In a randomized controlled clinical trial, Rockswold *et al* found that HBH reduced mortality after TBI without increasing the number of patients with favourable outcome[20]. In a further study by the same group, HBH reduced CSF lactate concentrations and this effect lasted for six hours after the end of the treatment period[18]. However, CSF pyruvate was not measured in this study so LPR could not be calculated. In the clinical situation of TBI, NBH has been more widely investigated. Menzel *et al* reported reduced microdialysate lactate levels in TBI patients treated with NBH[23]. In a later study, the same group confirmed reduced microdialysate lactate concentrations but found no significant change in LPR during a 24 hour period of 100% FiO_2 commenced within the first 6 hours post injury, with patients acting as their own controls[21]. In this study NBH resulted in decreased mortality compared to historic controls. Magnoni *et al* also reported reduced microdialysate lactate and no significant changes in LPR after NBH in patents with TBI, but interestingly found no change in cerebral arterio-venous oxygen difference[22]. These findings were interpreted by the authors as indicating no change in oxidative glucose metabolism during NBH.

Our study differs from others in several respects. Firstly we positioned our microdialysis catheters in the more affected cerebral hemisphere, and targeted the pericontusional brain tissue[26]. In the study by Tolias *et al* microdialysis catheters were placed in the least affected hemisphere[21] whereas in the study by Magnoni *et al* the catheter positioning is unclear[22]. Oxidative depression after TBI is primarily restricted to the ipsilateral cerebral cortex[17] and positioning of microdialysis catheters has a critical effect on metabolite microdialysate concentrations[35]. Secondly there are differences in the timing of the studies and the duration of NBH treatments. In particular, the study by Magnoni *et al* enrolled patients up to 79 hours post injury and studied them for several subsequent days[22]. The potential for cerebral hypoxia is most likely early after TBI[11] and there may be a critical time window for NBH treatment. In our patient group all studies commenced less than 48 hours post injury.

If hyperoxia improves mitochondrial function and cerebral aerobic metabolism, $CMRO_2$ will increase. We did not measure $CMRO_2$ so are unable to comment further on this issue in relation to our study. However, in a previous study investigating the impact of HBH (100% oxygen at 1.5 atm) on cerebral metabolism, there was a modest improvement in global $CMRO_2$ in the 15% of patients with reduced CBF prior to treatment[18]. In contrast to findings in HBH, current evidence reporting the effect of NBH on $CMRO_2$ after TBI is inconclusive. In their study, Magnoni *et al* reported a non-significant reduction in arterio-venous oxygen content difference during NBH[22], but interpretation of these findings is difficult because CBF was not measured and venous oxygen content was assessed using jugular bulb venous oximetry, which provides a global measure and may miss important regional effects. Conversely animal studies reveal increased $CMRO_2$ in response to NBH after TBI[36]. More recently, Diringer *et al* examined the direct effect of NBH on cerebral metabolism, assessed using positron emission tomography, in five patients with severe TBI[37]. This study seems to indicate that there is no role for NBH after TBI. However, this study measured global $CMRO_2$ and regional changes might have been missed. Nortje *et al* used similar methodology combined with cerebral microdialysis and also found no changes in global cerebral metabolism. However they demonstrated increased $CMRO_2$ in areas of low

baseline $CMRO_2$ and although these findings were not replicated in the tissue surrounding the microdialysis catheter they also found reductions in LPR during NBH[38]. These findings of regional improvements in cerebral metabolism are consistent with our own. It is also possible that NBH might improve outcome in severe TBI through mechanisms not reflected in a measurable increase in $CMRO_2$[39]. Further clinical research is therefore needed in larger numbers of patients to establish whether NBH is of therapeutic value after TBI.

In the normal brain, at least, hyperoxia is generally believed to cause vasoconstriction but we found no changes in VMCA, CBV or ICP during NBH in our study. Although there was a statistically significant reduction in CPP during the baseline return phase, we do not believe that this was clinically significant and, in any case, the lowest CPP lay within the range allowed by our management protocols. Simple explanations for the lack of evidence of cerebral vasoconstriction in our study are the placement of the microdialysis and NIRS monitors to target the more injured areas of brain, with our findings being consistent with impaired autoregulation within the regions of interest. Alternatively the slight increase in $PaCO_2$ that we recorded, which in isolation would tend to cause vasodilatation and increase in ICP, might have counteracted any effects of hyperoxic vasoconstriction. However, the absence of evidence of vasoconstriction in our study is also likely to be related to the complex response of the injured brain to NBH[3]. Tolias *et al* reported a reduction in ICP during NBH in patients with TBI[21] but Rockswold *et al* found that CBF and ICP were only decreased during NBH in those with elevated baseline CBF and that CBF increased during HBH in patients in whom CBF was reduced or normal prior to treatment[18]. Once again, when interpreting these data, it is important to bear in mind the significant metabolic heterogeneity that exists after TBI.

Microdialysis provides a hyperfocal measurement of brain tissue biochemistry but does not identify metabolic changes in tissue distant from the catheter. As the perfusate is not static there is insufficient time for equilibrium to occur across the membrane and the concentration of metabolites in the microdialysate therefore only represents a fraction of the true brain tissue

concentration. This fraction is termed the relative recovery. Relative recovery has been calculated for the metabolites analyzed in our study and has been shown to be equivalent for the CMA 70 and 71 catheters used in this study[40]. As lactate and pyruvate have similar molecular weights, LPR is not affected by changes in relative recovery and this is one advantage of this measurement over other microdialysis variables. In common with other investigators we demonstrated a prolonged effect of NBH on microdialysate variables, lasting beyond the period of NBH. There is an inherent delay involved in microdialysis monitoring of cellular redox state and although we applied a timing correction to account for the time taken for perfusate to pass along the catheter tubing the metabolite concentrations measured represent an average over the time of sampling. A delay may also exist related to the diffusion distance between the cellular and extracellular spaces. However, in our study microdialysate lactate concentration and LPR were not significantly different from baseline values by 75 minutes after the end of the hyperoxygenation period.

The clinical application of NIRS measurement of Δ[oxCCO] has been identified by studies correlating Δ[oxCCO] with post-operative neurological dysfunction in patients undergoing cardiac surgery[41] and during deep saturations associated with sleep apnea[42]. We show an oxidation in CCO during NBH and this implies that CCO is not fully oxidised in the resting state after TBI. Similarly oxidation in CCO above the resting state has been shown in healthy animals[43] and humans[44] in the recovery period following hypoxemia and in healthy humans during NBH (section 5.3.2).

NBH has potentially toxic effects on the lungs, eyes and central nervous system and, although the doses and duration of treatment required to produce these affects are not clearly defined and are likely to vary between individuals, oxygen toxicity is unlikely to occur when breathing 100% FiO_2 for less than 24 hours[3]. There is evidence to suggest increased free radical production when breathing air at high pressure (3 atmosphere) but none showing increased free radical levels at 1.5 atmosphere or less[19]. Whilst hyperoxygenation has the theoretical capacity to increase free radical production, it is also possible that by promoting electron flux through the electron transfer chain, it might prevent the

formation of free radicals produced by build up of reducing equivalents. Oxygen toxicity is extremely unlikely following the regime applied during this study but further work is required to investigate the potential risks of longer periods of NBH after TBI.

This pilot study has several limitations. We studied only a small number of TBI patients and further data collection in a large cohort of patients is required to validate these findings. VMCA is a surrogate marker of CBF and relies on there being no significant changes in middle cerebral artery calibre during the study. Continuous bedside measurement of absolute CBF, in conjunction with measurements of arterial and venous oxygen content difference and calculation of $CMRO_2$, would aid further investigation of NBH. In this study patients acted as their own controls and it is possible that the changes that we observed might have been influenced by the natural course of TBI. However, we do not believe this is the case as all measured variables returned towards, or reached, baseline values by the end of the study. Furthermore, changes in cerebral metabolism unrelated to our interventions are likely to have been minimal as systemic variables were stable over the time course of this study. The significant disease heterogeneity that exists within the diagnosis of TBI makes it extremely difficult, if not impossible, to identify control cohorts adequately matched for disease type and severity within a dataset of the size that we present.

In summary we show oxidation in cerebral cellular and mitochondrial compartments during NBH in patients with TBI using two independent monitoring techniques. Cerebral microdialysis and NIRS monitoring provide complementary information which can further our understanding of TBI pathophysiology. It might also be possible to use these techniques to guide targeted treatment strategies. Our results suggest that NBH has the potential to improve outcome after TBI and further investigation is warranted.

References

1. Zauner A, Daugherty W, Bullock M, Warner D. Brain oxygenation and energy metabolism: part I-biological function and pathophysiology. *Neurosurgery* 2002;51:289-302.
2. Zauner A, Clausen T, Alves O, Rice A, Levasseur J, Young H, Bullock R. Cerebral metabolism after fluid-percussion injury and hypoxia in a feline model. *J Neurosurg* 2002;97:643-649.
3. Alves OL, Daugherty WP, Rios M. Arterial hyperoxia in severe head injury: a useful or harmful option? *Curr Pharm Des* 2004;10:2163-2176.
4. Siesjo B (1978) *Brain energy metabolism*, 1st ed. Chichester: John Wiley and Sons,
5. Miller JD, Becker DP. Secondary insults to the injured brain. *J Royal Coll Surg (Edinburgh)* 1982;27:298.
6. Miller JD, Sweet RC, Narayan R, Becker DP. Early insults to the injured brain. *JAMA* 1978;240:439-442.
7. Miller JD, Butterworth JF, Gudeman SK, Faulkner JE, Choi SC, Selhorst JB, Harbison JW, Lutz HA, Young HF, Becker DP. Further experience in the management of severe head injury. *J Neurosurg* 1981;54:289-299.
8. Chesnut RM. Secondary brain insults after head injury: clinical perspectives. *New Horiz* 1995;3:366-375.
9. Chesnut RM, Marshall LF, Klauber MR, Blunt BA, Baldwin N, Eisenberg HM, Jane JA, Marmarou A, Foulkes MA. The role of secondary brain injury in determing outcome from severe head injury. *J Trauma* 1993;34:216-222.
10. Jones PA, Andrews PJD, Midgley S, Anderson SI, Piper IR, Tocher JL, Housley AM, Corrie JA, Slattery J, Dearden NM, Miller JD. Measuring the burden of secondary insults in head-injured patients during intensive care. *J Neurosurg Anesth* 1994;6:4-14.
11. Bouma GJ, Muizelaar JP, Stringer WA, Choi SC, Fatouros P, Young HF. Ultra-early evaluation of regional cerebral blood flow in severely head-injured patients using xenon-enhanced computerized tomography. *J Neurosurg* 1992;77:360-368.

12. Mik E, Stap J, Sinaasappel M, Beek J, Aten J, van Leeuwen T, Ince C. Mitochondrial PO2 measured by delayed fluorescence of endogenous protoporphyrin IX. *Nat Methods* 2006;3:939-945.
13. Kiening KL, Unterberg AW, Bardt TF, Schneider GH, Lanksch WR. Monitoring of cerebral oxygenation in patients with severe head injuries: brain tissue PO2 versus jugular vein oxygen saturation. *J Neurosurg* 1996;85:751-757.
14. Valadka AB, Gopinath SP, Contant CF, Uzura M, Robertson CS. Relationship of brain tissue PO2 to outcome after severe head injury. *Crit Care Med* 1998;26:1576-1581.
15. van den Brink WA, van Santbrink H, Steyerberg EW, Avezaat CJ, Suazo JA, Hogesteeger C, Jansen WJ, Kloos LM, Vermeulen J, Maas AI. Brain oxygen tension in severe head injury. *Neurosurgery* 2000;46:868-876.
16. van Santbrink H, Maas AI, Avezaat CJ. Continuous monitoring of partial pressure of brain tissue oxygen in patients with severe head injury. *Neurosurgery* 1996;38:21-31.
17. Hovda DA, Yoshino A, Kawamata T, Katayama Y, Becker DP. Diffuse prolonged depression of cerebral oxidative metabolism following concussive brain injury in the rat: a cytochrome oxidase histochemistry study. *Brain Res* 1991;567:1-10.
18. Rockswold SB, Rockswold GL, Vargo JM, Erickson CA, Sutton RL, Bergman TA, Biros MH. Effects of hyperbaric oxygenation therapy on cerebral metabolism and intracranial pressure in severely brain injured patients. *J Neurosurg* 2001;94:403-411.
19. Daugherty WP, Levasseur JE, Sun D, Rockswold GL, Bullock MR. Effects of hyperbaric oxygen therapy on cerebral oxygenation and mitochondrial function following moderate lateral fluid-percussion injury in rats. *J Neurosurg* 2004;101:599-604.
20. Rockswold GL, Ford SE, Anderson DC, Bergman TA, Sherman RE. Results of a prospective randomized trial for treatment of severely brain-injured patients with hyperbaric oxygen. *J Neurosurg* 1992;76:929-934.

21. Tolias CM, Reinert M, Seiler R, Gilman C, Scharf A, Bullock MR. Normobaric hyperoxia--induced improvement in cerebral metabolism and reduction in intracranial pressure in patients with severe head injury: a prospective historical cohort-matched study. *J Neurosurg* 2004;101:435-444.
22. Magnoni S, Ghisoni L, Locatelli M, Caimi M, Colombo A, Valeriani V, Stocchetti N. Lack of improvement in cerebral metabolism after hyperoxia in severe head injury: a microdialysis study. *J Neurosurg* 2003;98:952-958.
23. Menzel M, Doppenberg EMR, Zauner A, Soukup J, Reinert MM, Bullock R. Increased inspired oxygen concentration as a factor in improved brain tissue oxygenation and tissue lactate levels after severe human head injury. *J Neurosurg* 1999;91:1-10.
24. Tisdall MM, Smith M. Cerebral microdialysis: research technique or clinical tool. *Br J Anaesth* 2006;97:18-25.
25. Persson L, Valtysson J, Enblad P, Warme PE, Cesarini K, Lewen A, Hillered L. Neurochemical monitoring using intracerebral microdialysis in patients with subarachnoid hemorrhage. *J Neurosurg* 1996;84:606-616.
26. Bellander BM, Cantais E, Enblad P, Hutchinson P, Nordstrom CH, Robertson C, Sahuquillo J, Smith M, Stocchetti N, Ungerstedt U, Unterberg A, Olsen NV. Consensus meeting on microdialysis in neurointensive care. *Intensive Care Med* 2004;30:2166-2169.
27. Valdueza J, Balzer J, Villringer A, Vogl T, Kutter R, Einhaupl K. Changes in blood flow velocity and diameter of the middle cerebral artery during hyperventilation: assessment with MR and transcranial Doppler sonography. *Am J Neuroradiol* 1997;18:1929-1934.
28. Bullock R, Chesnut RM, Clifton G, Ghajar J, Marion DW, Narayan RK, Newell DW, Pitts LH, Rosner MJ, Wilberger JW. Guidelines for the management of severe head injury. Brain Trauma Foundation. *Eur J Emerg Med* 1996;3:109-127.
29. Maas AI, Dearden M, Teasdale GM, Braakman R, Cohadon F, Iannotti F, Karimi A, Lapierre F, Murray G, Ohman J, Persson L, Servadei F, Stocchetti N, Unterberg A. EBIC-guidelines for management of severe head injury in adults. European Brain Injury Consortium. *Acta Neurochir (Wien)* 1997;139:286-294.

30. Matcher SJ, Cooper CE. Absolute quantification of deoxyhaemoglobin concentration in tissue near infrared spectroscopy. *Phys Med Biol* 1994;39:1295-1312.
31. Coles JP. Regional ischemia after head injury. *Curr Opin Crit Care* 2004;10:120-125.
32. Menon DK, Coles JP, Gupta AK, Fryer TD, Smielewski P, Chatfield DA, Aigbirhio F, Skepper JN, Minhas PS, Hutchinson PJ, Carpenter TA, Clark JC, Pickard JD. Diffusion limited oxygen delivery following head injury. *Crit Care Med* 2004;32:1384-1390.
33. Moncada S, Bolanos JP. Nitric oxide, cell bioenergetics and neurodegeneration. *J Neurochem* 2006;97:1676-1689.
34. McLeod AD, Igielman F, Elwell C, Cope M, Smith M. Measuring cerebral oxygenation during normobaric hyperoxia: a comparison of tissue microprobes, near-infrared spectroscopy, and jugular venous oximetry in head injury. *Anesth Analg* 2003;97:851-856.
35. Engstrom M, Polito A, Reinstrup P, Romner B, Ryding E, Ungerstedt U, Nordstrom CH. Intracerebral microdialysis in severe brain trauma: the importance of catheter location. *J Neurosurg* 2005;102:460-469.
36. Levasseur J, Alessandri B, Reinert M, Clausen T, Zhou Z, Altememi N, Bullock M. Lactate, not glucose, up-regulates mitochondrial oxygen consumption both in sham and lateral fluid percussed rat brains. *Neurosurgery* 2006;59:1122-1130.
37. Diringer MN, Aiyagari V, Zazulia AR, Videen TO, Powers WJ. Effect of hyperoxia on cerebral metabolic rate for oxygen measured using positron emission tomography in patients with acute severe head injury. *J Neurosurg* 2007;106:526-529.
38. Nortje J, Coles JP, Timofeev I, Fryer T, Aigbirhio F, Smielewski P, Outtrim J, Chatfield D, Pickard J, Hutchinson P, Gupta A, Menon D. Effect of hyperoxia on regional oxygenation and metabolism after severe traumatic brain injury: preliminary findings. *Crit Care Med* 2008;36:273-281.
39. Fehlings MG, Baker A. Is there a role for hyperoxia in the management of severe traumatic brain injury? *J Neurosurg* 2007;106:525.

40. Hutchinson PJ, O'Connell MT, Nortje J, Smith P, Al-Rawi PG, Gupta AK, Menon DK, Pickard JD. Cerebral microdialysis methodology--evaluation of 20 kDa and 100 kDa catheters. *Physiol Meas* 2005;26:423-428.
41. Kakihana Y, Matsunaga A, Tobo K, Isowaki S, Kawakami M, Tsuneyoshi I, Kanmura Y, Tamura M. Redox behavior of cytochrome oxidase and neurological prognosis in 66 patients who underwent thoracic aortic surgery. *Eur J Cardiothorac Surg* 2002;21:434-439.
42. McGown AD, Makker H, Elwell C, Al Rawi PG, Valipour A, Spiro SG. Measurement of changes in cytochrome oxidase redox state during obstructive sleep apnoea using near-infrared spectroscopy. *Sleep* 2003;26:710-716.
43. Springett R, Newman J, Cope M, Delpy DT. Oxygen dependency and precision of cytochrome oxidase signal from full spectral NIRS of the piglet brain. *Am J Physiol Heart Circ Physiol* 2000;279:H2202-H2209.
44. Tisdall M, Tachtsidis I, Leung T, Ewell C, Smith M. Near infrared spectroscopic quantification of changes in the concentration of oxidized cytochrome oxidase in the healthy human brain during hypoxemia. *J Biomed Opt* 2007;12:024002.

Chapter 8
Concluding remarks and future work

8.1 Summary

This thesis investigates the use of near infrared spectroscopy as a tool for monitoring the adult human brain. Initially, detailed studies are performed using healthy volunteers. Within this cohort the spectroscopic responses we measure are likely to be representative of global cerebral changes. We use spatially resolved spectroscopy to measure TOI over the frontal lobes during changes in cerebral oxygenation, blood flow and volume induced by isocapnoeic hypoxaemia and hyperoxia, and normoxic hyperventilation and hypercapnoea. TOI appears to be an attractive clinical measurement as it provides an absolute measure of tissue oxyhaemoglobin saturation presented in the accessible format of a percentage. However, wide variability in absolute TOI values within and between subjects exists. This variability may limit the use of absolute TOI as a clinical marker of the adequacy of cerebral oxygen delivery and may explain why TOI has not found wide clinical applicability thus far. Multiple regression techniques are used to show that TOI response is affected by changes in arterial oxyhaemoglobin saturation, end tidal carbon dioxide tension, cerebral blood volume and mean arterial blood pressure. However, the effect of changes in cerebral blood volume and mean blood pressure is minimal compared to the other two variables. The predominant effects of changes in end tidal carbon dioxide tension in the brain are changes in cerebral blood volume and flow. The regression technique we use controls for changes in cerebral blood volume and so we can conclude that changes in TOI are predominantly affected by changes in arterial oxyhaemoglobin saturation and cerebral blood flow: both of which are directly linked to cerebral oxygen delivery. We suggest that change in TOI may be clinically useful as a marker of changes in cerebral oxygen delivery.

Broadband spectroscopy is used to measure changes in [oxCCO] in the healthy brain. Few studies of this measurement in adult humans have been reported. We present changes in [oxCCO] during a series of physiological challenges and demonstrate induced increases and decreases in [oxCCO]. In agreement with

several animal studies we conclude that cerebral CCO is not fully oxidised in the resting state. During hypoxaemia we show that changes in [oxCCO] correlate with estimated changes in cerebral oxygen delivery despite there being no correlation between estimated changes in cerebral oxygen delivery and changes in either [Hbdiff] or [HbT]. NBH induces increases in [oxCCO] and this demonstrates that NBH had potential as a therapeutic tool for inducing changes in mitochondrial redox state and thus the rate of aerobic metabolism.

We then analyse then measured CCO signal more closely by examining the BBS data from the volunteer hypoxaemia studies. NIRS measured changes in [oxCCO] have been viewed with scepticism by some within the biomedical optics community and one of the main debates concerns the ability of measurement algorithms to adequately separate the CCO and haemoglobin signals. We provide evidence that the CCO signal is not merely a crosstalk algorithm arising from changes in the haemoglobin signals and then show that the raw optical attenuation we measure during hypoxaemia cannot be fully accounted for by only analysing changes in [HbO_2] and [HHb]. If these two chromophores alone are fitted to the optical data then the residual attenuation is not significantly different to that expected if changes in [oxCCO] are occurring. This suggests that real changes in CCO redox state are occurring during hypoxaemia.

Changes in [oxCCO] during normobaric hyperoxia in patients with TBI in the early hours post injury are then investigated. We demonstrate the feasibility of near infrared spectroscopic monitoring on the NCU. We compare non-invasive near infrared spectroscopic data with invasive cerebral monitoring tools. Using cerebral microdialysis and broadband spectroscopy we show oxidation in both cerebral cellular redox state (as measured by brain extracellullar fluid lactate pyruvate ratio) and cerebral mitochondrial redox state (as measured by changes in [oxCCO]), and present correlations between these two monitoring modalities. We conclude that normobaric hyperoxia, in the context of TBI, may increase aerobic metabolism and has the potential to improve patient outcome.

8.2 Future Work

This thesis suggests that measurement of changes in [oxCCO] in the adult head has potential as a cerebral monitoring tool. Based in large part on the data presented here, our group has obtained a £400 000 grant from the ESPRC to further investigate this measurement. We are constructing a new state-of-the-art two channel spectrometer which combines broadband and phase modulated spectroscopy. This will offer several advantages over the existing instrumentation. It will allow continuous and absolute measurement of the tissue scatter and absorption coefficients. We will therefore be able to determine if changes in light scatter are occurring and so verify whether or not the assumptions within the modified Beer-Lambert law can be applied during the types of studies presented in this thesis. This combined phase and broadband system will also allow us to make measurements of absolute [HbO_2], [HHb] and [oxCCO]. The prospect of making absolute measurements of [oxCCO] in patients with brain injury is particularly interesting. As previously noted, changes in [oxCCO] in animals correlate with MRS measured changes in ATP levels and it would be fascinating to compare absolute [oxCCO] with MRS measurements in brain injured patients. We plan to make bilateral measurements and examine differences in cerebral metabolism between the least and most injured cerebral hemispheres of patients with TBI.

We are also using a variety of techniques to address further the ability of our BBS algorithms to separate the CCO and haemoglobin signals. We are building multilayered phantoms with which to test the new spectroscopy system and to determine the sensitivity to changes in [oxCCO] occurring predominantly in the cerebral cortex. A parallel arm of work concerns the understanding of the CCO responses. We are developing computer based models in order to simulate CCO responses to cerebral physiology. The data presented here is crucial to this process and is vital for both model training and parameter setting.

The data presented here contribute to the current and ongoing debate surrounding the use of normobaric hyperoxia in patients with TBI. We add to the evolving body of literature suggesting that NBH may improve regional cerebral metabolism after TBI. This intervention is cheap and easily accessible and

certainly merits further investigation in randomised trials. Prior to this, further work is required to identify optimal dosing strategy and treatment windows. The history of randomised controlled trials of interventions in TBI is littered with negative results and to maximise the chance of identifying beneficial interventions it is vital to examine surrogate markers in pilot studies before advancing to large expensive multi-centre trials. The use of broadband spectroscopy to measure changes in [oxCCO] concentration may prove to be an ideal surrogate marker and work is required to examine the relationship between these changes and outcome after TBI.